Random Beamforming for Multi-cell Multi-Input Multi-Output (MIMO) Systems

HIEU DUY NGUYEN

(B. Eng. (First-Class Hons.), VNU)

A THESIS SUBMITTED FOR THE DEGREE OF

DOCTOR OF PHILOSOPHY

DEPARTMENT OF ELECTRICAL AND COMPUTER ENGINEERING

NATIONAL UNIVERSITY OF SINGAPORE

2013

To my beloved parents ...

Declaration

I hereby declare that this thesis is my original work and it has been written by me in its entirety. I have duly acknowledged all the sources of information which have been used in the thesis.

This thesis has also not been submitted for any degree in any university previously.

_____

Hieu Duy Nguyen

25 September 2013

Acknowledgments

I would like to express my sincere gratitude to my supervisor Assistant Professor Hon Tat Hui for his guidance and supervision during my Ph.D. candidature. He has supported me with enthusiastic encouragement and inspiration, without which I might not complete my degree on time.

I also would like to express my deepest appreciation to my co-supervisor Assistant Professor Rui Zhang, who has provided helpful discussions and insightful comments on my research topics. It is my pleasure to work closely with him and benefit by his profound knowledge.

Last but not least, I would like to acknowledge my parents, who always support and encourage me to achieve my goals.

Contents

Abstract

Random beamforming (RBF) is a practically favourable transmission scheme for multiuser multi-antenna downlink systems since it requires only *partial* channel state information (CSI) at the transmitter. Under the conventional single-cell setup, RBF is known to achieve the optimal sum-capacity scaling law as the number of users goes to infinity, thanks to the *multiuser diversity* enabled transmission scheduling that virtually eliminates the intra-cell interference. In this thesis, we extend the study of RBF to a more practical multi-cell downlink system with single/multi-antenna receivers subject to the additional inter-cell interference (ICI).

First, we consider the case of *finite* signal-to-noise ratio (SNR) at each receiver with one single antenna. We derive a closed-form expression of the achievable sum-rate with the multi-cell RBF, based upon which we show an asymptotic sum-rate scaling law as the number of users goes to infinity. Next, we consider the *high-SNR* regime and for tractable analysis assume that the number of users in each cell scales in a certain order with the per-cell SNR. Under this setup, we characterize the achievable degrees of freedom (DoF) (which is defined as the sum-rate normalized by the logarithm of the SNR as SNR goes to infinity) for the single-cell case with RBF. Then we extend the analysis to the multi-cell RBF case by characterizing the *DoF region*, which consists of all the achievable DoF tuples for all the cells subject to their mutual ICI. It is shown that the DoF region characterization provides useful guideline on how to design a *cooperative* multi-cell RBF system to achieve optimal throughput

tradeoffs among different cells. Furthermore, our results reveal that the multi-cell RBF scheme achieves the "interference-free" DoF region upper bound for the multi-cell system, provided that the per-cell number of users has a sufficiently large scaling order with the SNR. Our result thus confirms the optimality of multi-cell RBF in this regime even without the complete CSI at the transmitter, as compared to other full-CSI requiring transmission schemes such as *interference alignment*.

Furthermore, the impact of receive spatial diversity on the rate performance of RBF is not yet fully characterized even in a single-cell setup. We thus study a multi-cell multiple-input multiple-output (MIMO) broadcast system with RBF applied at each base station and either the minimum-mean-square-error (MMSE), matched filter (MF), or antenna selection (AS) based spatial receiver at each mobile terminal. We investigate the effect of different spatial diversity receivers on the achievable sum-rate of multi-cell RBF systems subject to both the intra- and inter-cell interferences. We first derive closed-form expressions for the distributions of the receiver signal-to-interference-plus-noise ratio (SINR) with different spatial diversity techniques, based on which we compare their rate performances at given SNRs. We then investigate the high-SNR regime and for a tractable analysis assume that the number of users in each cell scales in a certain order with the per-cell SNR. Under this setup, we characterize the DoF region for multi-cell MIMO RBF systems. Our results reveal that significant sum-rate DoF gains can be achieved by the MMSE-based spatial receiver as compared to the cases without spatial diversity receivers or with the suboptimal spatial receivers (MF or AS). This is in sharp contrast to the existing result that spatial diversity

receivers only yield marginal sum-rate gains in RBF, which was obtained in the regime of large number of users but fixed SNR per cell.

List of Figures

List of Algorithms

List of Acronyms

AS	Antenna Selection
AWGN	Additive White Gaussian Noise
BC	Broadcast Channel
BD	Block Diagonalization
BS	Base Station
CDF	Cumulative Distribution Function
CSCG	Circularly Symmetric Complex Gaussian
CSI	Channel State Information
DoF	Degrees of Freedom
DPC	Dirty-Paper Coding
GLPP	Grassmannian Line Packing Problem
IA	Interference Alignment
IC	Interference Channel
ICI	Inter-Cell Interference
IID	Independent and Identically Distributed
INR	Interference-to-Noise Ratio
MF	Matched Filter
MIMO	Multiple Input Multiple Output
MISO	Multiple Input Single Output
MMSE	Minimum-Mean-Square Error

MU	Multi-User
OBF	Orthogonal Beamforming
PDF	Probability Distribution Function
PFS	Proportional Fair Scheduling
RBF	Random Beamforming
RCRM	Rank Constrained Rank Minimization
RMT	Random Matrix Theory
SINR	Signal-to-Interference-plus-Noise Ratio
SISO	Single Input Single Output
SNR	Signal-to-Noise Ratio
SUD	Single User Detection
SVD	Singular Value Decomposition

List of Notations

$\mathbb{C}^{m\times n}$	Complex $m \times n$ matrices
$\mathcal{CN}(\mu, \sigma^2)$	Complex Gaussian random variable with mean μ and variance σ^2
$(.)^T, (.)^H$	Transpose and conjugate-transpose
$\boldsymbol{Tr}(\boldsymbol{X})$	Trace of the matrix $\boldsymbol{X}$
$E_X[.]$	Mean of random variable X (subscript dropped when obvious)
$\lvert\boldsymbol{X}\rvert$	Determinant of the matrix $\boldsymbol{X}$
$\boldsymbol{X}^{-1}$	Inverse transform of the matrix $\boldsymbol{X}$
span($\boldsymbol{X}$)	Space spanned by the column vectors of the matrix $\boldsymbol{X}$
rank($\boldsymbol{X}$)	Rank of the matrix $\boldsymbol{X}$
$\lvert\lvert\boldsymbol{x}\rvert\rvert$	(Vector) Euclidian norm, i.e., $\lvert\lvert\boldsymbol{x}\rvert\rvert^2 = \boldsymbol{x}^H\boldsymbol{x}$
$\lvert\lvert\boldsymbol{X}\rvert\rvert_2$	(Matrix) Spectral norm, i.e., the largest singular value of $\boldsymbol{X}$
$\lvert\lvert\boldsymbol{X}\rvert\rvert_*$	(Matrix) Nuclear norm, i.e., $\lvert\lvert\boldsymbol{X}\rvert\rvert_* = \boldsymbol{Tr}\big(\sqrt{\boldsymbol{X}^H\boldsymbol{X}}\big)$
$\lfloor.\rfloor, \{.\}$	Integer and fractional parts of a real number
$\boldsymbol{A} \succ \boldsymbol{0}$	Hermitian and positive definite matrix $\boldsymbol{A}$

Chapter 1

Introduction

1.1 Motivation

Wireless communication paradigm has evolved from single-user single-input single-output (SISO) and multiple-input multiple-output (MIMO) systems to multi-user (MU) MIMO counterparts, which are shown greatly improving the rate performance by transmitting to multiple users simultaneously. The sum-capacity and the capacity region of a single-cell MU MIMO downlink system or the so-called MIMO broadcast channel (MIMO-BC) can be attained by the nonlinear "Dirty Paper Coding (DPC)" scheme [9] [10] [74]. However, DPC requires a high implementation complexity due to the non-linear successive encoding/decoding at the transmitter/receiver, and is thus not suitable for real-time applications. Other studies have proposed to use alternative linear precoding schemes for the MIMO-BC, e.g., the block-diagonalization (BD) scheme [67], to reduce the complexity. More information on the key developments of

single-cell MIMO communication can be found in, for example, [5] [17] [55].

Moving to the multi-cell case, it is worth noting that the multi-cell downlink system with inter-cell interference (ICI) in general can be modelled as a Gaussian interference channel (IC). However, a complete characterization of the capacity region of the Gaussian IC, even for the two-user case, is still open [14]. An important recent development is the so-called "interference alignment (IA)" technique (see, e.g., [8] [19] [28] [54] and the references therein). With the aid of IA, the maximum achievable degrees of freedom (DoF), which is defined as the sum-rate normalized by the logarithm of the signal-to-noise ratio (SNR) as the SNR goes to infinity or the so-called "pre-log" factor, has been obtained for various IC models to provide useful insights on designing optimal transmission schemes for interference-limited MU systems.

Besides IA-based studies for the high-SNR regime, there is a vast body of works in the literature which investigated the multi-cell cooperative downlink precoding/beamforming at a given finite user's SNR. These results are typically categorized based on two different types of assumptions on the level of base stations' (BSs') cooperation. For the case of "fully cooperative" multi-cell systems with global transmit message sharing across all the BSs, a virtual MIMO-BC channel is equivalently formed. Therefore, existing single-cell downlink precoding techniques can be applied (see, e.g., [48] [81] [82] and the references therein) with a non-trivial modification to deal with the per-BS power constraints as compared to the conventional sum-power constraint for the single-cell MIMO-BC case. In contrast, if transmit messages are

only locally known at each BS, coordinated precoding/beamforming can be implemented among BSs to control the ICI to their best effort [12] [43] [57]. In [6] [62] [83], various parametrical characterizations of the Pareto boundary of the achievable rate region have been obtained for the multiple-input single-output (MISO) IC with coordinated transmit beamforming and single-user detection (SUD).

The most important point is that all such precoding schemes, for single- or multi-cell systems, rely on the assumption of perfect channel state information (CSI) at the transmitter, which may not be valid in practical cellular systems with a large number of users. Consequently, the study of quantized channel feedback has become an important and active area of research (see, e.g., [30] and the references therein).

In a landmark work [72], Viswanath *et al.* introduced a single-beam "opportunistic beamforming (OBF)" scheme for the MISO-BC, which exploits the multiuser diversity gain and requires only partial channel feedback to the BS. Since spatial multiplexing gain can be captured by transmitting with more than one random beams, the so-called "random beamforming (RBF)" scheme was also described in [72] and further investigated in [64]. The achievable sum-rate with RBF in a single-cell system has been shown in [64], [65], which scales identically to that with the optimal DPC scheme assuming perfect CSI as the number of users goes to infinity, for any given user's SNR. Essentially, this result implies that the intra-cell interference in a single-cell RBF system can be virtually eliminated when the number of users is sufficiently large, and an "interference-free" MU broadcast system is realizable.

Although substantial extensions of the single-cell RBF scheme have been pur-

sued, there is very limited work on the performance of the RBF scheme in a more realistic multi-cell system, where the ICI becomes a dominant factor. It is worth noting that since the universal frequency reuse is more favourable in future generation cellular systems, ICI becomes a more severe issue as compared to the traditional case with only a fractional frequency reuse. A notable work is [47], in which the sum-rate scaling law for the multi-cell system with RBF has been shown to be similar to the single-cell result in [64], [65] as the number of per-cell users goes to infinity, regardless of the ICI. This result, albeit appealing, does not provide any insight on how to practically design RBF in an ICI-limited multi-cell system.

Furthermore, the effect of *receive spatial diversity* on the rate performance of RBF with multi-antenna receivers is not yet fully characterized in the literature, even in the single-cell case. Note that some prior works have studied RBF under a single-cell MIMO setup, e.g., [64], [65]. Assuming that the number of users goes to infinity for any given SNR, it has been shown therein that RBF schemes with single- or multi-antenna receivers achieve the same sum-rate scaling law with the growing number of users. The conventional asymptotic analysis thus leads to some pessimistic results that receive spatial diversity provides only *marginal* gains to the achievable rate of RBF [64], [65].

In this thesis, we aim to characterize the achievable rate for the multi-cell RBF scheme by more judiciously analyzing the impacts of ICI on the system throughput, for both the finite-SNR and high-SNR regimes. We furthermore investigate the achievable rate of a multi-cell MIMO RBF system with different receive spatial di-

versity techniques under the *high-SNR* regime. Our newly obtained insights are in sharp contrast to the existing results in the literature. Particularly, it is revealed that intra- and inter-cell interference play a very important role in multi-cell RBF systems. Therefore, the optimal performance is achieved only by carefully allocating the number of transmit beams in each cell. It is also discovered that receive spatial diversity is significantly beneficial to the rate performance of multi-cell RBF systems. More details and discussions will be given in the subsequent chapters.

1.2 Performance Measures

There are many different measures which can be used to characterize the performance of wireless communication systems. In this section, we briefly summarize the key measures which will be considered throughout this thesis.

1.2.1 Output Signal-to-Noise Ratio and Signal-to-Interference-Plus-Noise Ratio

Consider a wireless communication system with either single or multiple antennas at the receiver/user. The receiver can employ spatial diversity techniques if there are multiple antennas at the receiver side. The output SNR is defined as

$$\text{SNR} = \frac{\text{Power of the desired signal at the output of the combiner}}{\text{Power of the noise at the output of the combiner}}. \tag{1.1}$$

In a wireless system, the channel is time-varying. The output SNR, which

depends explicitly on the channel, is thus a random quantity. It is obvious that the performance becomes better with a higher output SNR.

A relevant performance measure to the SNR is the output signal-to-interference-plus-noise ratio (SINR). In a multiuser and/or multicell system, the received signal is affected by intra-/inter-cell interference and noise. Again, if there are multiple antennas at the receiver side, the receiver can employ spatial diversity techniques to (presumably) improve the performance. The output SINR is defined as

$$\text{SINR} = \frac{\text{Power of the desired signal at the output of the combiner}}{\text{Total power of the interference plus noise at the output of the combiner}}. \tag{1.2}$$

The output SINR is also a random quantity, depending on both the direct- and cross-link channels of the desired user and interference, respectively.

1.2.2 Ergodic and Outage Capacity

In his landmark paper [63], Shannon *et. al.* defined the capacity as the maximum amount of information that can be transferred reliably across a communication channel. Mathematically, the capacity is defined as the maximum of the *mutual information* between the transmitter and the receiver.

Now consider an experiment represented by the probability space S. A stochastic process is defined by assigning to every outcome ψ a function of time t, i.e., $X(t, \psi)$. The ensemble of a stochastic process is the set of all possible time functions that can result from an experiment, i.e., the set $\Big\{X(t, \psi_1),\ \ldots,\ X(t, \psi_k),\ \ldots\ \Big\}$. $X(t, \psi)$ is

called ergodic if the ensemble average equals time average

$$\lim_{T\to\infty}\frac{1}{T}\int_{-T/2}^{T/2}X(t,\psi_k)dt=\mathbb{E}\Big\{X(t_n,\psi)\Big\}=\int_{-\infty}^{\infty}xf(x;t_n)dx, \tag{1.3}$$

$\forall k,n$, where $f(x;t_n)$ is the first order probability density function (PDF) of the random variable $X(t_n,\psi)$. That is, the time-averaged mean of $X(t,\psi)$ equals its probabilistic mean.

In a wireless communication system, the channels are often stochastic processes, depending on both the time and state of the channel. For *ergodic capacity*, the underlying assumption here is that the channel fading processes are ergodic, and the transmission time is long as to reveal the long-term ergodic properties of such processes.

Note that the ergodicity assumption, in general, might not be satisfied in some fading channels. When there is no significant channel variability during the whole transmission, it is possible that the Shannon capacity equals to 0. In such cases, the $q\%$ outage capacity C_{out} should be considered, which is defined as the channel capacity C which is guaranteed to be supported by $(100-q)\%$ of the channel realizations, required to provide a reliable service, i.e.,

$$Pr\big\{C\leq C_{out}\big\}\leq q\% \tag{1.4}$$

1.2.3 Rate Region

In a point-to-point communication system, the channel capacity is a single number that imposes the maximum data rate from the transmitter to the receiver. In a

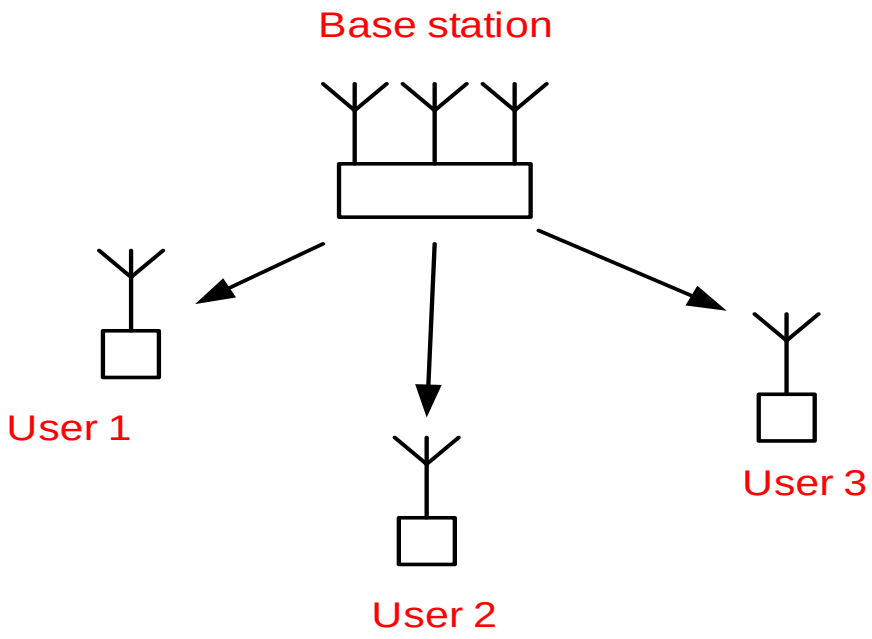

Figure 1.1: A broadcast channel with 3 users.

broadcast channel as shown in Fig. 1.1, the transmitter can simultaneously transmit to more than one user. Thus, we obtain a set of all simultaneously achievable rate vectors, often called the *rate region*. Similarly, the sum-rate region of a multi-cell system, such as shown in Fig. 1.2, is defined as the set of all the achievable sum-rate tuples for all the cells. Assume that we have C cells and K_c users in the c-th cell. The C-dimensional sum-rate region of the C-cell system is actually a projection of a $\left(\sum_{c=1}^{C} K_c\right)$-dimensional rate region, consisting of $\sum_{c=1}^{C} K_c$ rate vectors for all users in the system.

In real systems, there are several constraints on the transmit power, quality of service (QoS), etc., as the specifications for the networks. It is necessary to note that in those cases, the rate region should follow the specifications. Certainly, the rate

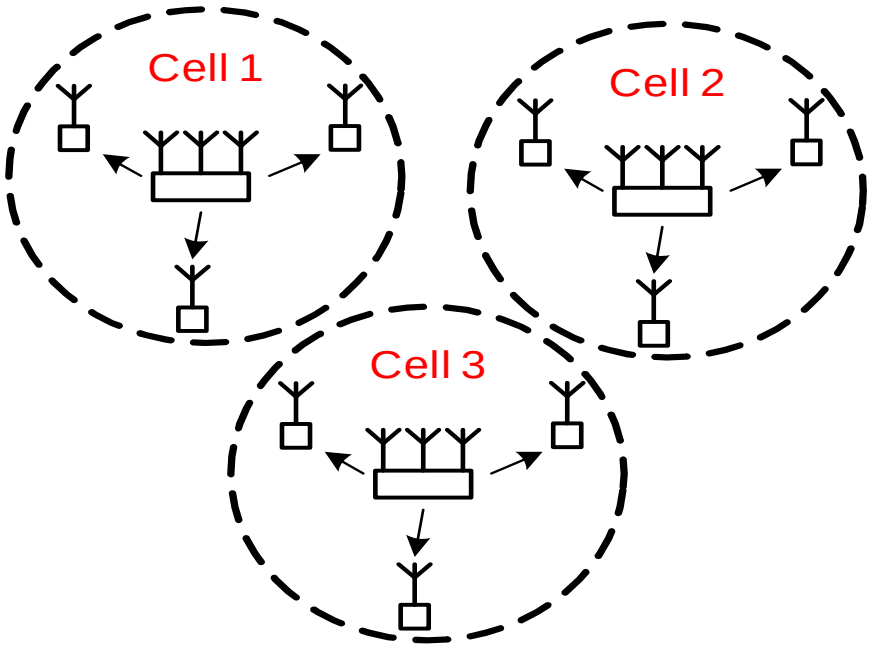

Figure 1.2: A three-cell downlink system.

regions under different setups might be different.

1.2.4 Degrees of Freedom (DoF) and DoF Region

The DoF, or the so-called "pre-log" factor, is a useful and widely-accepted metric for investigating the capacity/rate performance of wireless communication systems. Mathematically, the DoF is defined as the rate normalized by the logarithm of the SNR as the SNR goes to infinity

$$\text{DoF} = \lim_{\text{SNR}\to\infty} \frac{R(\text{SNR})}{\log_2(\text{SNR})}, \tag{1.5}$$

where $R(\text{SNR})$ is the throughput of the considered system, which is a function of the SNR.

As the DoF is a summary parameter for the rate/capacity, we also have the

DoF region which characterizes the rate region of multi-user systems. In particular, the DoF region of a multi-cell system is defined as follows [19] [28].

Definition 1.2.1 *(General DoF region) The DoF region of a C-cell downlink system is defined as*

$$\mathcal{D} = \Bigg\{ (d_1, d_2, \cdots, d_C) \in \mathbb{R}_+^C : \forall (\omega_1, \omega_2, \cdots, \omega_C) \in \mathbb{R}_+^C; \sum_{c=1}^{C} \omega_c d_c \leq \lim_{SNR \to \infty} \sup_{\boldsymbol{R} \in \mathcal{R}} \sum_{c=1}^{C} \omega_c \frac{R_c(SNR)}{\log_2(SNR)} \Bigg\}, \quad (1.6)$$

where SNR here means the per-cell SNR; ω_c, d_c, and $R_c(SNR)$ are the non-negative rate weight, the achievable DoF, and the sum-rate of the c-th cell, respectively; and the region $\mathcal{R}$ is the set of all the achievable sum-rate tuples for all the cells, denoted by $\boldsymbol{R}$ = ($R_1(SNR)$, $R_2(SNR)$, $\cdots$, $R_C(SNR)$.

1.3 Dissertation Overview and Major Contributions

1.3.1 Chapter 2 - Transmission Schemes for Single- and Multi-Cell Downlink Systems

The pioneering works of [15] [70] and [76] showed that MIMO techniques can lead to huge capacity improvements for point-to-point, or single-user, systems without increasing either power or bandwidth. The situation is considerably different for multi-user systems, where the inter-user/inter-cell interference exists and severely

affects the performance. In Chapter 2, we give a literature review on the precoder designing problem for single- and multi-cell downlink systems. For single-cell case, we introduce the optimal DPC and the linear BD schemes. Moving to the multi-cell/IC case, we describe the IA scheme which is asymptotically optimal for many types of IC under high-SNR regime.

1.3.2 Chapter 3 - Single-Cell MISO RBF

Since its introduction in the landmark paper [72], opportunistic communication has developed to a broad area with various constituent topics. In this chapter, we aim to present a succinct overview on the key developments of OBF/RBF, summarizing some of the most important results contributed to the field. Note that in the literature, virtually all the works consider the single-cell case. It is only quite recent that the rate performance of the multi-cell RBF is explored in our works [49] [50]. We therefore limit our survey to the single-cell OBF/RBF.

1.3.3 Chapter 4 - Multi-Cell MISO RBF

In this chapter, the achievable rates of the MISO RBF scheme in a multi-cell setup subject to the ICI are thoroughly investigated. Both finite-SNR and high-SNR regimes are considered. For the finite-SNR case, we provide closed-form expressions of the achievable average sum-rates for both single- and multi-cell RBF with a finite number of users per cell. We also derive the sum-rate scaling law in the conventional asymptotic regime, i.e., when the number of users goes to infinity with a fixed

SNR. Since the finite-SNR analysis has major limitations, we furthermore consider the high-SNR regime by adopting the DoF-region approach to characterize the optimal throughput tradeoffs among different cells in multi-cell RBF, assuming that the number of users per cell scales in a polynomial order with the SNR as the SNR goes to infinity. We show the closed-form expressions of the achievable DoF and the corresponding optimal number of transmit beams, both as functions of the user number scaling order or the user density, for the single-cell case. From this result, we obtain a complete characterization of the DoF region for the multi-cell RBF, in which the optimal boundary DoF point is achieved by BSs' cooperative assignment of their numbers of transmit beams according to individual cell's user densities. Finally, if the numbers of users in all cells are sufficiently large, we show that the multi-cell RBF, albeit requiring only partial CSI at transmitters, achieve the optimal DoF region even without the full transmitter CSI.

1.3.4 Chapter 5 - Multi-Cell MIMO RBF

The impact of receive spatial diversity on the rate performance of RBF is not fully characterized even in a single-cell setup. This chapter studies the achievable sum-rate in multi-cell MIMO RBF systems for the regime of both high SNR and large number of users per cell. We propose three RBF schemes for spatial diversity receivers with multiple antennas, namely, minimum-mean-square-error (MMSE), matched filter (MF), or antenna selection (AS). The SINR distributions in the multi-cell RBF with different types of spatial receiver are obtained in closed-form at any given finite SNR.

Based on these results, we characterize the DoF region achievable by different multi-cell MIMO RBF schemes under the assumption that the number of users per cell scales in a polynomial order with the SNR as the SNR goes to infinity. Our study reveals significant gains by using MMSE-based spatial receiver in the achievable sum-rate and DoF region in multi-cell RBF, which considerably differs from the existing result based on the conventional asymptotic analysis with fixed per-cell SNR. The results of this paper thus provide new insights on the optimal design of interference-limited multi-cell MIMO systems with only partial CSI at transmitters.

1.4 Publications

The following is the list of publications in referred journals and conference proceeding produced during my Ph.D. candidature.

1.4.1 Book Chapter

1. H. D. Nguyen, R. Zhang, and H. T. Hui, "Random beamforming in multi-user MIMO systems", to appear in *Recent Trends in Multiuser MIMO Communications*, InTech, ISBN: 980-953-307-459-2, 2013.

1.4.2 International Journal Papers

1. H. D. Nguyen, R. Zhang, and H. T. Hui, "Multi-cell random beamforming: achievable rates and degrees of freedom region," *IEEE Trans. Sig. Proc.*, vol. 61, no. 14,

pp. 3532-3544, July 2013 (Best Student Paper Award, 2nd NUS ECE Graduate Student Symposium, National University of Singapore, 2012).

2. H. D. Nguyen, R. Zhang, and H. T. Hui,"Effect of receive spatial diversity on the degrees of freedom region of multi-cell random beamforming," *submitted to IEEE Trans. Wireless Commun.*, May 2013.

1.4.3 International Conference Papers

1. H. D. Nguyen, X. Wang, and H. T. Hui, "Mutual coupling and transmit correlation: impact on the sum-rate capacity of the two-user MISO broadcast channels," *in Proc. IEEE International Symposium on Antennas and Propagation and USNC-URSI National Radio Science Meeting (APS/URSI '2011)*, pp. 63-66, Spokane, USA, July 2011.

2. X. Wang, H. D. Nguyen, and H. T. Hui, "Correlation coefficient expression by S-parameters for two omni-directional MIMO antennas," *in Proc. IEEE International Symposium on Antennas and Propagation and USNC-URSI National Radio Science Meeting (APS/URSI '2011)*, pp. 301-304, Spokane, USA, July 2011.

3. H. D. Nguyen, X. Wang, and H. T. Hui, "Keyhole and multi-keyhole MIMO channels: modeling and simulation," *in Proc. IEEE International Conference on Information, Communications and Signal Processing (ICICS '2011)*, pp. 1-5, Singapore, Dec. 2011.

4. C. P. Ho, H. D. Nguyen, X. Wang, and H. T. Hui, "A simple channel simulator for

multi-user MIMO broadcast channel systems," *in Proc. Progress in Electromagnetics Research Symposium (PIERS '2012)*, pp. 1317-1322, Kuala Lumpur, Malaysia, Mar. 2012.

5. H. D. Nguyen, R. Zhang, and H. T. Hui, "Degrees of freedom region in multi-cell random beamforming," *in Proc. IEEE International Conference on Acoustics, Speech, and Signal Processing (ICASSP '2012)*, pp. 2837-2840, Kyoto, Japan, Mar. 2012.

6. H. D. Nguyen, R. Zhang, and H. T. Hui, "Effect of receive spatial diversity on the degrees of freedom region in multi-cell random beamforming," *in Proc. IEEE Wireless Communications and Networking Conference (WCNC '2013)*, Shanghai, China, 2013.

Chapter 2

Transmission Schemes for Single- and Multi-Cell Downlink Systems

MIMO techniques have led to additional degrees of freedom which can be utilized to offer extra gains over conventional communication systems. The pioneering works of [15] [70] [76] and subsequent studies have shown significant improvements on the array, diversity, and multiplexing gains when MIMO techniques are employed in single-user, point-to-point scenarios. Further investigations have considered multi-user MIMO cases, where inter-user and inter-cell interferences become dominant factors. In this chapter, we summary the main results of the precoder designing problem for single- and multi-cell downlink systems.

2.1 Single-Cell MIMO BC

In this section, we describe the mathematical model of the single-cell MIMO downlink system. We then introduce the capacity-achieving scheme, i.e., DPC. It has been shown in [74] that the DPC scheme can achieve the capacity region of the single-cell MU MIMO downlink. The DPC scheme, however, is non-linear and requires a high implementation complexity at both the transmitter and receivers. On the other hand, linear precoding schemes are of low complexity but sub-optimal transmission techniques. We then briefly discuss the well-known BD scheme which is introduced in [67]. Finally, we present some asymptotic rate scaling laws for both the DPC and BD schemes.

2.1.1 Channel Model

We consider a MU MIMO BC with N_T antennas at the BS, and K users each with $N_{R,k}$ antennas. The received signal for the k-th user can be expressed as

$$\boldsymbol{y}_k = \boldsymbol{H}_k \boldsymbol{x} + \boldsymbol{n}_k, \tag{2.1}$$

where $\boldsymbol{n}_k \in \mathbb{C}^{N_{R,k}\times 1}$ and $\boldsymbol{H}_k \in \mathbb{C}^{N_{R,k}\times N_T}$ are the additive white Gaussian noise (AWGN) vector and the channel matrix associated with the k-th user, respectively; it is assumed that the components of the noise $\boldsymbol{n}_k$ are independent and identically distributed (i.i.d.) and each component is distributed as a circularly symmetric complex Gaussian (CSCG) variable with zero mean and unit variance, denoted as $\mathcal{CN}(0,1)$; $\boldsymbol{x} = \left[\boldsymbol{x}_1^T, \cdots, \boldsymbol{x}_K^T\right]^T$ is the aggregated transmit signal (column) vector where $\boldsymbol{x}_k$ is

the signal from the BS to user k. The BS is subjected to an average power constraint P_T, i.e., $\boldsymbol{Tr}(\boldsymbol{\Sigma_x}) \leq P_T$ where $\boldsymbol{\Sigma_x} = E[\boldsymbol{x}\boldsymbol{x}^H]$ is the transmit covariance matrix.

2.1.2 Dirty-Paper Coding

The DPC scheme approaches the precoder designing problem for single-cell MIMO BC from an information theoretical point of view. The objective is to maximize the weighted sum rate of all users. Note that the notion of DPC was first introduced in [10] in 1983. The fundamental idea is that when the CSI in the form of interference is present at the transmitter, the channel capacity is the same as that of a channel with no interference. This result has motivated the application of DPC to MIMO BC. It has been shown that the sum-capacity and the capacity region of a single-cell MU MIMO downlink system can be attained by the DPC scheme (see, e.g., [9] [10] [74]).

In the MU MIMO downlink system with K users, the DPC scheme is employed at the BS. At the k-th step, $k = 1, \ldots, K$, the BS chooses the codeword for user u_k. Since the BS knows the codewords of user $u_1, \ldots, u_{k-1}$, it can pre-subtract them. User u_k thus does not see the interferences from user $u_1, \ldots, u_{k-1}$. The transmit signal vector is

$$\boldsymbol{x} = \boldsymbol{x}_1 + \boldsymbol{x}_2 + \cdots + \boldsymbol{x}_K, \tag{2.2}$$

and the covariance matrix of user k is denoted as $\boldsymbol{\Sigma}_k = E[\boldsymbol{x}_k \boldsymbol{x}_k^H] \in \mathbb{C}^{N_T \times N_T}$. In this case, we have

$$\boldsymbol{\Sigma_x} = E[\boldsymbol{x}\boldsymbol{x}^H] = \boldsymbol{\Sigma}_1 + \boldsymbol{\Sigma}_2 + \cdots + \boldsymbol{\Sigma}_K. \tag{2.3}$$

The achievable rate for user u_k can be expressed as

$$R_{u_k} = \log_2 \frac{\left| \boldsymbol{I} + \boldsymbol{H}_{u_k} \left(\sum_{j \geq k} \boldsymbol{\Sigma}_{u_j} \right) \boldsymbol{H}_{u_k}^H \right|}{\left| \boldsymbol{I} + \boldsymbol{H}_{u_k} \left(\sum_{j > k} \boldsymbol{\Sigma}_{u_j} \right) \boldsymbol{H}_{u_k}^H \right|} \tag{2.4}$$

The rate region can be obtained by taking the convex hull of the union of all possible orderings $u_1, \ldots, u_K$ and all positive semidefinite matrices $\boldsymbol{\Sigma}_{u_1}, \ldots, \boldsymbol{\Sigma}_{u_K}$, subjected to $\sum_{k=1}^{K} \boldsymbol{Tr}\big(\boldsymbol{\Sigma}_{u_k}\big) \leq P_T$. It has been shown that the rate region of a MIMO-BC employing the DPC scheme coincides with the capacity region of this MIMO-BC channel (see [74]).

The sum capacity is defined as the maximum total rates, i.e.,

$$C_{sum} = \max_{\{\boldsymbol{\Sigma}_k\}_{k=1}^{K}, \sum_{k=1}^{K} \boldsymbol{Tr}\left(\boldsymbol{\Sigma}_k\right) \leq P_T} R_1 + R_2 + \cdots + R_K. \tag{2.5}$$

Note that (2.5) is neither a convex nor concave function of the covariance matrices. Thus, numerically finding the maximum is a nontrivial problem. Based on the notion of uplink-downlink duality for single-cell MIMO systems, it has been shown in [31] that (2.5) is equivalent to

$$C_{sum} = \max_{\{\boldsymbol{\Omega}_k\}_{k=1}^{K} : \boldsymbol{\Omega}_k \succeq \boldsymbol{0}, \sum_{k=1}^{K} \boldsymbol{Tr}\left(\boldsymbol{\Omega}_k\right) \leq P_T} \log_2 \left| \boldsymbol{I} + \sum_{k=1}^{K} \boldsymbol{H}_k^H \boldsymbol{\Omega}_k \boldsymbol{H}_k \right|. \tag{2.6}$$

Furthermore, Jindal *et. al.* introduced two algorithms to determine C_{sum}. We only present Algorithm 1 here since the second algorithm is similar but with some slight modifications.

Algorithm 1 [31]: Finding the sum capacity of a single-cell MIMO BC

Input: The power constraint P_T, number of iterations N, and K channel matrices: $\boldsymbol{H}_1, \ldots, \boldsymbol{H}_K$.

1. Initialize the covariance matrices $\boldsymbol{\Omega}_k^{(n)}$ such that $\sum_{k=1}^{K} \boldsymbol{Tr}\big(\boldsymbol{\Omega}_k^{(n)}\big) \leq P_T$, for $k = 1, \ldots, K$ and $n = -(K-2), \ldots, 0$. For example, we can choose $\boldsymbol{\Omega}_k^{(n)} = \frac{P_T}{KN}\boldsymbol{I}$.

2. Repeat the following steps N times.

for $n = 1$ to N **do**

2. a. Generate the auxiliary matrices

$$\boldsymbol{G}_k^{(n)} = \boldsymbol{H}_k \left(\boldsymbol{I} + \sum_{j=1}^{K-1} \boldsymbol{H}_{[k+j]_K}^H \boldsymbol{\Omega}_{[k+j]_K}^{(n-K+j)} \boldsymbol{H}_{[k+j]_K} \right)^{-1/2} \tag{2.7}$$

for $i = 1, \ldots, K$; where $[x]_K = \mod((x-1), K) + 1$.

2. b. Find the new covariance matrices $\left\{\boldsymbol{\Omega}_k^{(n)}\right\}_{k=1}^{K}$

$$\left\{\boldsymbol{\Omega}_k^{(n)}\right\}_{k=1}^{K} = \arg \max_{\{\boldsymbol{\Omega}_k\}_{k=1}^{K} : \boldsymbol{\Omega}_k \succeq \boldsymbol{0}, \sum_{k=1}^{K} \boldsymbol{Tr}(\boldsymbol{\Omega}_k) \leq P_T} \sum_{k=1}^{K} \log_2 \left| \boldsymbol{I} + \big(\boldsymbol{G}_k^{(n)}\big)^H \boldsymbol{\Omega}_k \boldsymbol{G}_k^{(n)} \right|. \tag{2.8}$$

Here we can use the water-filling algorithm with power constraint P_T.

end for

2.1.3 Block Diagonalization

The DPC scheme can achieve the sum capacity and the capacity region of a MU MIMO downlink system. However, the iterative nature of DPC typically results in a high computational cost and complexity at both the transmitter and receivers. In certain applications, such complexity might be forbidden especially at the receiver side, where the mobile users' devices are expected to be simple. Motivated by this limitation of the DPC scheme, Spencer *et. al.* has proposed the BD scheme in [67]. The BD scheme is a linear precoding technique which has low computational cost and complexity. We first describe the channel inversion (CI) technique for MU MIMO downlink systems with single-antenna users, which is the root of the BD scheme.

2.1.3.1 Channel Inversion for Single-Antenna Users

Consider (2.1) with $N_{R,k} = 1$ and $N_T \geq \sum_{k=1}^{K} N_{R,k}$. With only one antenna, each user cannot perform any interference cancellation technique. The objective is to design the precoder employed at the BS such that the inter-user interferences are minimized. In the CI scheme, the BS simply takes the inverse/pseudo-inverse of the channel matrix, thus completely eliminating the inter-user interference. The transmit signal can be expressed as

$$\boldsymbol{x} = \sqrt{\frac{P_T}{\boldsymbol{Tr}\left[\left(\boldsymbol{H}\boldsymbol{H}^H\right)^{-1}\right]}}\boldsymbol{H}^H\left(\boldsymbol{H}\boldsymbol{H}^H\right)^{-1}\boldsymbol{s}, \tag{2.9}$$

where $\boldsymbol{H} = \left[\boldsymbol{h}_1^T, \ldots, \boldsymbol{h}_K^T\right]^T$ is the aggregate channel matrix of K users and $\boldsymbol{s} = [s_1, s_2, \ldots, s_K]^T$ is the data signal vector intended to communicate to K users. Here,

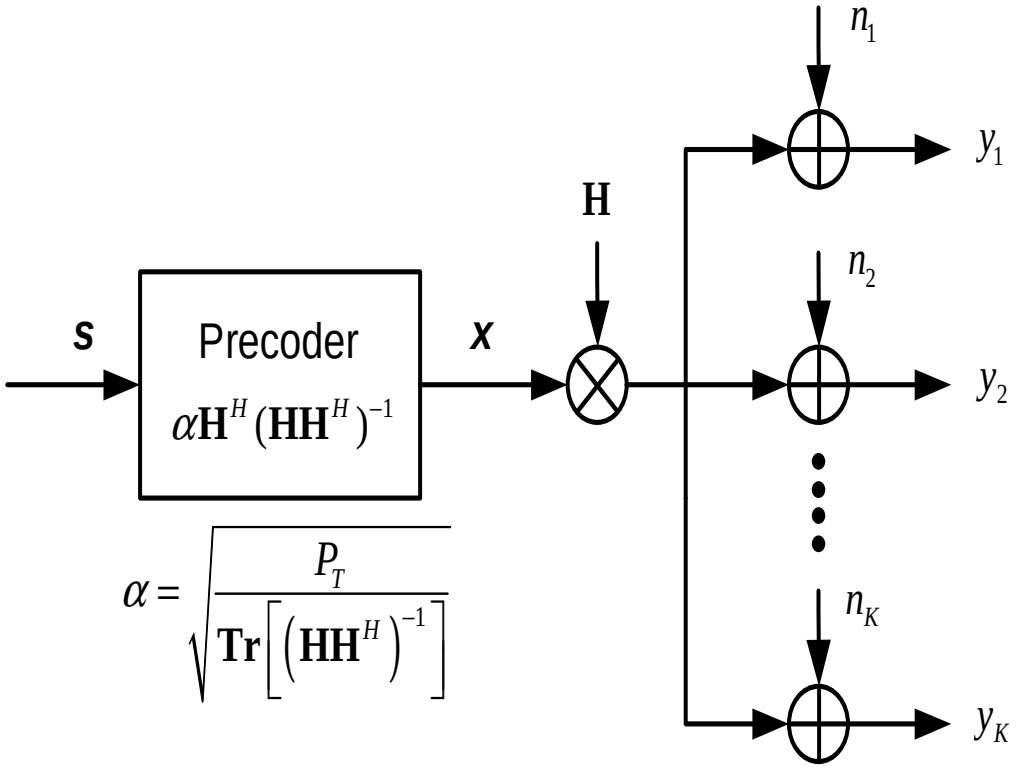

Figure 2.1: The channel inversion scheme for a MU MIMO downlink channel with single-antenna users.

the term $\sqrt{\frac{P_T}{\boldsymbol{Tr}\left[\left(\boldsymbol{H}\boldsymbol{H}^H\right)^{-1}\right]}}$ is due to the average transmit power constraint.

With this approach, all inter-user interference is canceled. We thus obtain K separate scalar channel. The received signal at the k-th user is

$$y_k = \sqrt{\frac{P_T}{\boldsymbol{Tr}\left[\left(\boldsymbol{H}\boldsymbol{H}^H\right)^{-1}\right]}} s_k + n_k. \tag{2.10}$$

The CI scheme is illustrated in Fig. 2.1.

2.1.3.2 Block Diagonalization for Multi-antenna Users

With multi-antenna at the receivers, the users in a MU MIMO downlink channel can apply receive spatial techniques to enhance the rate performance. Note that when the users have multiple antennas, the CI scheme can also be directly applied by considering each antenna as a separate user. In such cases, both the inter-user and inter-stream interferences are canceled out.

The BD scheme, rather than completely diagonalizing the channel, only block-diagonalizes it. The idea is to remove the inter-user interference only. Each receiver, however, needs to perform some types of signal processing to decode its data streams. The received signal at user k is

$$\boldsymbol{r}_k = \boldsymbol{B}_k \boldsymbol{H}_k \boldsymbol{A}_S \boldsymbol{s} + \boldsymbol{n}_k, \tag{2.11}$$

where $\boldsymbol{A}_S = \left[\boldsymbol{A}_1, \boldsymbol{A}_2, \cdots, \boldsymbol{A}_K\right]$ with $\boldsymbol{A}_k \in \mathbb{C}^{N_T \times N_{R,k}}$ and $\boldsymbol{s} = \left[\boldsymbol{s}_1^T, \cdots, \boldsymbol{s}_K^T\right]^T$ with $\boldsymbol{s}_k \in \mathbb{C}^{N_{R,k} \times 1}$ being, respectively, the precoding matrix and the transmit symbol of the k-th user, who is allocated $L_k \leq N_{R,k}$ transmit beams; $\boldsymbol{B}_k \in \mathbb{C}^{N_{R,k} \times N_{R,k}}$ is the receive decoder. The system model is illustrated in Fig. 2.2.

The goal is to find $\boldsymbol{A}_S$ such that

$$\boldsymbol{H}\boldsymbol{A}_S = \begin{bmatrix} \boldsymbol{M}_1 & \boldsymbol{0} & \dots & \boldsymbol{0} \\ \boldsymbol{0} & \boldsymbol{M}_2 & \dots & \boldsymbol{0} \\ \vdots & \vdots & \ddots & \vdots \\ \boldsymbol{0} & \boldsymbol{0} & \dots & \boldsymbol{M}_K \end{bmatrix} \tag{2.12}$$

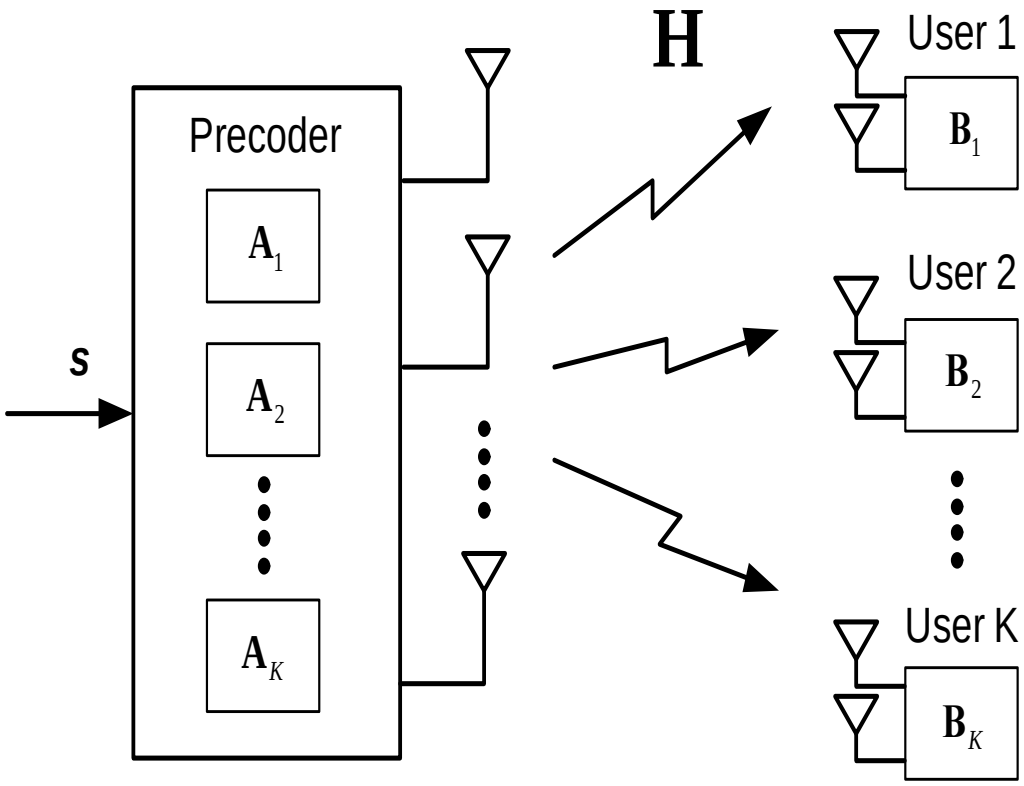

Figure 2.2: The block diagonalization scheme for a MU MIMO downlink channel with multi-antenna users.

We define the following singular value decomposition (SVD) [67]

$$\left[\boldsymbol{H}_1^T \ \cdots \ \boldsymbol{H}_{k-1}^T \ \boldsymbol{H}_{k+1}^T \ \cdots \ \boldsymbol{H}_K^T\right]^T = \bar{\boldsymbol{U}}_k \left[\bar{\boldsymbol{\Lambda}}_k \ \boldsymbol{0}\right] \left[\bar{\boldsymbol{V}}_k^{(1)} \ \bar{\boldsymbol{V}}_k^{(0)}\right]^H. \tag{2.13}$$

Note that $\left[\boldsymbol{H}_1^T \ \cdots \ \boldsymbol{H}_{k-1}^T \ \boldsymbol{H}_{k+1}^T \ \cdots \ \boldsymbol{H}_K^T\right]^T \bar{\boldsymbol{V}}_k^{(0)} = \boldsymbol{0}$. The columns of $\bar{\boldsymbol{V}}_k^{(0)}$ thus are the candidates to form $\boldsymbol{A}_k$. We have

$$\boldsymbol{H}_{\text{eff}} = \boldsymbol{H}\left[\bar{\boldsymbol{V}}_1^{(0)}, \bar{\boldsymbol{V}}_2^{(0)}, \ldots, \bar{\boldsymbol{V}}_K^{(0)}\right] = \begin{bmatrix} \boldsymbol{H}_1\bar{\boldsymbol{V}}_1^{(0)} & \boldsymbol{0} & \ldots & \boldsymbol{0} \\ \boldsymbol{0} & \boldsymbol{H}_2\bar{\boldsymbol{V}}_2^{(0)} & \ldots & \boldsymbol{0} \\ \vdots & \vdots & \ddots & \vdots \\ \boldsymbol{0} & \boldsymbol{0} & \ldots & \boldsymbol{H}_K\bar{\boldsymbol{V}}_K^{(0)} \end{bmatrix} \tag{2.14}$$

Suppose that the objective is to maximize the throughput. We define the following SVD [67]

$$\boldsymbol{H}_k \bar{\boldsymbol{V}}_k^{(0)} = \left[\boldsymbol{U}_k^{(1)}\ \boldsymbol{U}_k^{(0)}\right] \begin{bmatrix} \boldsymbol{\Lambda}_k & \boldsymbol{0} \\ \boldsymbol{0} & \boldsymbol{0} \end{bmatrix} \left[\boldsymbol{V}_k^{(1)}\ \boldsymbol{V}_k^{(0)}\right]^H. \tag{2.15}$$

The receive and transmit precoding matrix can be chosen as

$$\boldsymbol{B}_k = \boldsymbol{U}_k^{(1)}, \tag{2.16}$$

$$\boldsymbol{A}_S = \left[\bar{\boldsymbol{V}}_1^{(0)}\boldsymbol{V}_1^{(1)}, \bar{\boldsymbol{V}}_2^{(0)}\boldsymbol{V}_2^{(1)}, \cdots, \bar{\boldsymbol{V}}_K^{(0)}\boldsymbol{V}_K^{(1)}\right] \times \boldsymbol{P}^{1/2}. \tag{2.17}$$

Here, $\boldsymbol{P}^{1/2}$ is the power allocation matrix, $Tr(\boldsymbol{P}) = P_T$. We can further decompose $\boldsymbol{P}^{1/2}$ into $\boldsymbol{P}^{1/2} = diag\big(\boldsymbol{P}_1^{1/2}, \boldsymbol{P}_2^{1/2}, \cdots, \boldsymbol{P}_K^{1/2}\big)$ in which the matrix $\boldsymbol{P}_k^{1/2}$ allocates the power to the eigenvalues of $\boldsymbol{\Lambda}_k$. The received signal of user k, $\boldsymbol{r}_k$, can be expressed in the following form

$$\boldsymbol{r}_k = \boldsymbol{\Lambda}_k \boldsymbol{P}_k^{1/2} \boldsymbol{s}_k + \tilde{\boldsymbol{n}}_k, \tag{2.18}$$

where the elements of $\tilde{\boldsymbol{n}}_k$'s $(= \boldsymbol{U}_k^{(1)}\ \boldsymbol{n}_k)$ are i.i.d. $\mathcal{CN}(0,1)$, $k = 1, \ldots, K$.

The sum-rate thus can be expressed as

$$R_{BD} = \sum_{k=1}^{K} \log_2 \det\left[\boldsymbol{\Lambda}_k^2 \boldsymbol{P}_k + \boldsymbol{I}\right] = \sum_{k=1}^{K}\sum_{i=1}^{L_k} \log_2\left(p_{k,i}\lambda_{k,i}^2 + 1\right), \tag{2.19}$$

in which $\sqrt{p_{k,i}}$ and $\lambda_{k,i}$ are the elements of $\boldsymbol{P}_k^{1/2}$ and $\boldsymbol{\Lambda}_k$, respectively. The transmit power constraint is $\sum_{k=1}^{K}\sum_{i=1}^{L_k} p_{k,i} = P_T$. Note that a joint power allocation is implemented for all of the eigenvalues of K users. To maximize the sum-rate, standard water-filling power allocation is applied. That means $p_{k,i}$ can be chosen as:

$$p_{k,i} = (\rho - 1/\lambda_{k,i}^2)^+, \tag{2.20}$$

where,

$$\rho = \frac{P_T + \sum_{k=1}^{K} \sum_{i=1}^{\bar{L}_k} \lambda_{k,i}^{-2}}{\bar{N}_T}, \tag{2.21}$$

and $\bar{L}_k$ denotes the number of non-zero elements in $\boldsymbol{P}_k$, i.e., $p_{k,i} > 0, i \in \{1, 2, \cdots, \bar{L}_k\}$ and $p_{k,i} = 0$ otherwise. The total number of supported beams is $\bar{N} = \sum_{k=1}^{K} \bar{L}_k$. We obtain the following sum-rate expression for the BD scheme:

$$R_{BD} = \sum_{k=1}^{K} \sum_{i=1}^{L_k} \Big(\log(\rho \lambda_{k,i}^2) \Big)^+. \tag{2.22}$$

2.1.3.3 Asymptotic Scaling Laws

A relevant investigation is to compare the rate performance of any sub-optimal scheme to the (optimal) DPC scheme. However, such exact study is difficult and often leads to no significant insight. A widely-accepted alternative method is to consider asymptotic analyses instead. There are two major approaches: high-SNR and large-number-of-user analyses. In the following results, we assume that the channels are i.i.d. Rayleigh fading, i.e., the components of $\boldsymbol{H}_k$ in (2.1) are i.i.d. CSCG random variable and each distributed as $\mathcal{CN}(0, 1)$.

Theorem 2.1.1 ([42]) *As the transmit power is asymptotically large, the ergodic sum capacity and rate obtained by DPC and BD, respectively, converge to the same scaling law*

$$E[C_{sum}], E[R_{BD}] \overset{P_T \to \infty}{\to} \min \left(N_T, \sum_{k=1}^{K} N_{R,k} \right) \log_2 (1 + P_T). \tag{2.23}$$

Furthermore, assume that $N_T \geq \sum_{k=0}^{K} N_{R,k}$. *The expected loss due to BD is given by*

$$E[C_{sum}] - E[R_{BD}] \overset{P_T \to \infty}{\to} \log_2(e) \sum_{k=0}^{K-1} \sum_{n=0}^{N-1} \sum_{i=kN+1}^{K(N-1)} \frac{1}{M-n-i}. \tag{2.24}$$

Consider a MIMO point-to-point link with an $\left(\sum_{k=1}^{K} N_{R,k}\right)$-antenna receiver and an N_T-antenna transmitter, it is well-known that the ergodic capacity of this channel scales as $\min\left(N_T, \sum_{k=1}^{K} N_{R,k}\right) \log_2(1+P_T)$ as $P_T \to \infty$ [70]. We thus see that the DoF for this point-to-point MIMO link and the MU MIMO downlink employing DPC or BD are all equal to $\min\left(N_T, \sum_{k=1}^{K} N_{R,k}\right)$. This result is intuitive. Note that the DPC pre-subtracts the interference, while the BD scheme cancels the inter-user interference, creating K separate point-to-point links with $N_{R,k}$ DoF each. Finally, Theorem 2.1.1 effectively states the optimality of the BD scheme as the transmit power approaches infinity.

In Fig. 2.3, we compare the numerical sum-rates of the DPC and BD schemes and the scaling law $N_T \log_2(1+P_T)$ as the transmit power $P_T \to \infty$. The parameters for the two systems are: (a) $K = 100$, $N_T = 6$, and each user in the system employing the DPC or BD has $N_{R,k} = L_k = 2$; (b) $K = 50$, $N_T = 4$, and each user in the system employing the DPC or BD has $N_{R,k} = L_k = 2$. The DPC scheme successively encodes the transmit beams for all K users, while $\sum_{k=1}^{K} N_{R,k}/N_T$ groups of users are pre-defined for the BD and an exhausted search is performed within these groups to find the assignment with the maximum sum-rate. It is observed that the scaling law matches well with the numerical results.

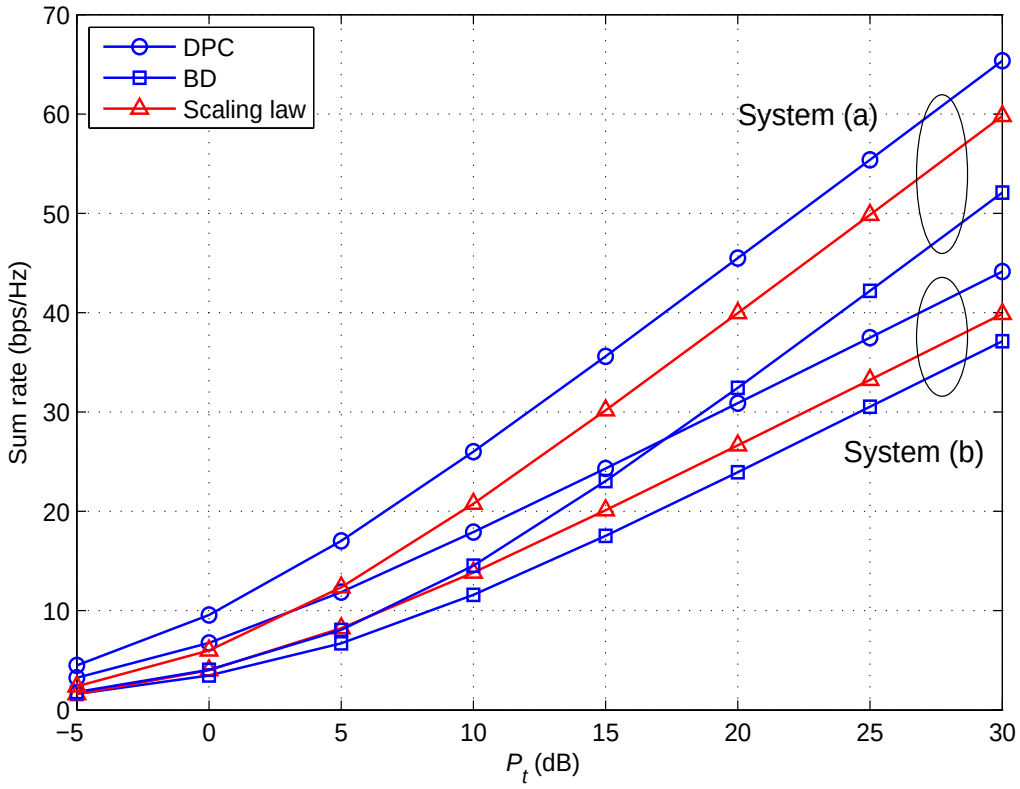

Figure 2.3: Comparisons of the numerical sum-rates of the DPC and BD schemes and the scaling law $N_T \log_2(1 + P_T)$ as functions of the transmit power P_T.

Theorem 2.1.2 ([65], [80]) [1] *As the number of users is asymptotically large, the ergodic sum capacity and rate obtained by DPC and BD (with semi-orthogonal user selection*[2]*), respectively, converge to the same scaling law*

[1]The result in [80] only states for the CI scheme. However, we can easily extend it to BD using simple bounds.

[2]The semi-orthogonal user selection iteratively selects the user based on the interference it causes to the existing users. The user with the least interference is added to the list. Please refer to [80] for more information.

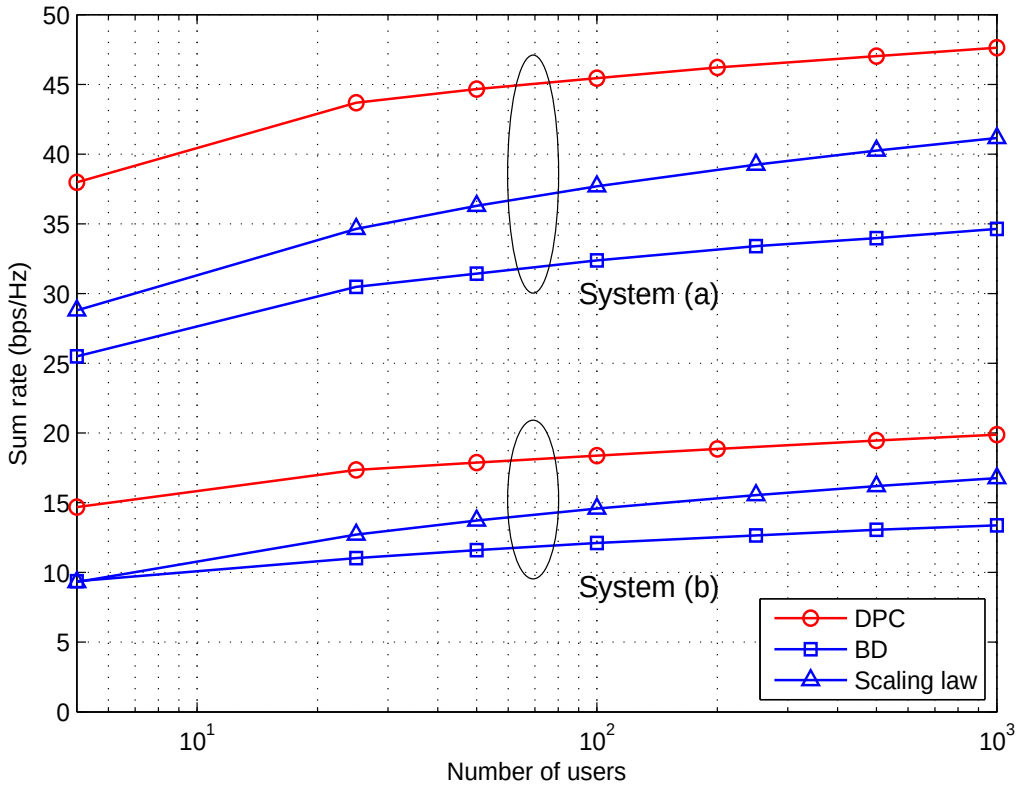

Figure 2.4: Comparisons of the numerical sum-rates of the DPC and BD schemes, and the scaling law $N_T \log_2\left(1+\frac{P_T}{N_T}\log\left(\sum_{k=1}^{K} N_{R,k}\right)\right)$ as functions of the number of users K.

$$E[C_{sum}], E[R_{BD}] \overset{P_T\to\infty}{\to} N_T \log_2\left(1+\frac{P_T}{N_T}\log\left(\sum_{k=1}^{K} N_{R,k}\right)\right). \tag{2.25}$$

Essentially, Theorem 2.1.2 confirms the optimality of the BD scheme as the number of users grows large. More information on this asymptotic analysis can be found in the following Chapter 3.

In Fig. 2.4, we compare the numerical sum-rates of the DPC and BD schemes and the scaling law as the number of users $K \to \infty$. The DPC successively encodes

the transmit beams for all K users, while $\sum_{k=1}^{K} N_{R,k}/N_T$ groups of users are pre-defined for the BD and an exhausted search is performed within these groups to find the group with the maximum sum-rate. The parameters for the two systems are: (a) SNR = 20 dB, $N_T = 6$, and each user in the system employing the DPC or BD has $N_{R,k} = L_k = 2$; (b) SNR = 10 dB, $N_T = 4$, and each user in the system employing the DPC or BD has $N_{R,k} = L_k = 2$. It is quite clear that the optimal multiuser diversity $N_T \log_2 \left(1 + \frac{P_T}{N_T} \log \left(\sum_{k=1}^{K} N_{R,k}\right)\right)$ is achievable for the BD with exhaustive group-searching. We note that the rate performance does not improve significantly as $K \to \infty$. As an example, consider system (a). The rate improvement as K grows from 100 to 1000 is roughly 2.5 bps/Hz, i.e., merely 0.06 %. It is not surprising, since the rate scaling law states that the rate only grows double-logarithmically with respect to K as K is asymptotically large.

2.2 Multi-Cell/Interference Channel: Interference Alignment

In the previous section, we have introduced the DPC scheme which can achieve the capacity region and the sum capacity of single-cell MIMO BCs. A natural extension is to find a scheme which is optimal for multi-cell MIMO BC with additional ICI. Note that the multi-cell downlink system in general can be modelled as a Gaussian IC. A complete characterization of the capacity region of the Gaussian IC, even for the two-user case, is still open. The largest achievable rate region known to date is

the so-called Han-Kobayashi region [22].

Although the exact capacity region and/or sum capacity are still unknown, there have been considerable developments which reveal useful insights on IC systems. An important recent advance is the IA technique. With the aid of IA, the maximum achievable DoF has been obtained for various IC models which provides useful insights on designing optimal transmission schemes. In a sense, we can consider IA as the asymptotically optimal, sum-capacity achieving scheme under high-SNR regime for certain ICs.

In this section, we describe the mathematical model of the K-user IC. We then review the (asymptotic) IA scheme with symbol extensions, i.e., the signal is encoded over multiple dimensions such as varying channel realizations. The asymptotic IA scheme is primarily of theoretical interest because of its strongly asymptotic nature which limits its practical applications. Therefore, we also introduce three IA-based schemes, which do not consider symbol extensions and thus are practical and applicable even when the channel is static.

2.2.1 Channel Model

Consider a flat-fading K-user MIMO IC with K transmitters each with N_T antennas and K receivers each with N_R antennas. The received signal at the k-th receiver over the t-th time slot is given by

$$\boldsymbol{y}_k(t) = \boldsymbol{H}_{k,k}(t)\boldsymbol{V}_k(t)\boldsymbol{s}_k(t) + \sum_{l=1,\ l\neq k}^{K} \boldsymbol{H}_{k,l}(t)\boldsymbol{V}_l(t)\boldsymbol{s}_l(t) + \boldsymbol{w}_k(t), \tag{2.26}$$

where t is the time-slot, frequency-slot, or time-frequency tuple index; $\boldsymbol{H}_{k,l}(t) \in \mathbb{C}^{N_R \times N_T}$ is the channel between receiver k and transmitter l; $\boldsymbol{V}_k(t) \in \mathbb{C}^{N_T \times N_T}$ and $\boldsymbol{s}_k(t) \in \mathbb{C}^{N_T \times 1}$ are the linear precoder and the signal symbol from the k-th transmitter, respectively; $\boldsymbol{w}_k(t) \in \mathbb{C}^{N_T \times 1}$ is the AWGN at the k-th receiver with i.i.d. components each distributed as $\mathcal{CN}(0, \sigma_k^2)$. The transmit power constraint is P_T, i.e., $\boldsymbol{Tr}\left(\mathbb{E}_t[\boldsymbol{s}_k(t)\boldsymbol{s}_k^H(t)]\right) \leq P_T$. Each receiver then linearly processes the received signal with a decoder $\boldsymbol{U}_k^H$ and obtain

$$\boldsymbol{r}_k(t) = \boldsymbol{U}_k^H(t)\boldsymbol{H}_{k,k}(t)\boldsymbol{V}_k(t)\boldsymbol{s}_k(t) + \sum_{l=1,\ l\neq k}^{K} \boldsymbol{U}_k^H(t)\boldsymbol{H}_{k,l}(t)\boldsymbol{V}_l(t)\boldsymbol{s}_l(t) + \boldsymbol{U}_k^H(t)\boldsymbol{w}_k(t). \tag{2.27}$$

As usual, the objective is to design $\boldsymbol{U}_k^H(t)$ and $\boldsymbol{V}_k(t)$ such that a high throughput, or a low bit-error-rate, or a mixture of these two criteria, is achieved at each user. Most of the IA-based schemes focus on maximizing the user throughput. The fundamental idea is to design the precoding matrices $\boldsymbol{V}_k(t)$ such that the space spanned by the interference signals is consolidated within a number of dimensions, which does not overlap with the desired signals' space. Therefore, a simple zero-forcing decoder $\boldsymbol{U}_k^H(t)$ can be employed to recover the desired, free-of-interference signals at each receiver.

2.2.2 Asymptotic Interference Alignment with Symbol Extensions

Asymptotic IA plays an important role in the development of IA-based schemes and the investigation of ICs. First and foremost, it is the first IA-based scheme proposed

in [8], in which the idea of IA is formally established. More importantly, it shows that by coding over multiple symbols, the maximum number of interference-free symbols can be simultaneously transmitted over the IC, i.e., the maximum sum of DoF is attainable. Achieving the IC's maximum sum of DoF implies that the asymptotic IA can approach the IC sum capacity at high SNR regime.

To illustrate the asymptotic IA scheme, we consider the K-user SISO IC. In this case, (2.26) becomes

$$y_k(t) = H_{k,k}(t)V_k(t)s_k(t) + \sum_{l=1,\ l\neq k}^{K} H_{k,l}(t)V_l(t)s_l(t) + w_k(t). \tag{2.28}$$

The following assumption is essential [8]

Assumption 2.2.1 *The channel coefficient values are drawn i.i.d. from a continuous distribution and the absolute value of all the channel coefficient is bounded between a non-zero minimum value and a finite maximum value, i.e.,* $0 < H_{min} < \left|H_{k,k}(t)\right| < H_{max} < \infty$.

Suppose that there are d_k symbols transmitted over d_k time or frequency slots as a super-symbol. The super-symbol can be expressed as

$$\bar{\boldsymbol{s}}_k(t) = \begin{bmatrix} s_k(d_k(t-1)+1) \\ s_k(d_k(t-1)+2) \\ \vdots \\ s_k(d_k t) \end{bmatrix}. \tag{2.29}$$

Furthermore, assume that the signal is encoded over $M > d_k$ symbols. The symbol extensions of the precoder and noise are denoted as $\bar{\boldsymbol{V}}_k(t)$ and $\bar{\boldsymbol{w}}_k(t)$, respec-

tively, where $\bar{\boldsymbol{V}}_k(t) \in \mathbb{C}^{M \times d_k}$ and where $\bar{\boldsymbol{w}}_k(t) \in \mathbb{C}^{M \times 1}$. The symbol extension of the channel is a diagonal $M \times M$ matrix, which is given as

$$\bar{\boldsymbol{H}}_{k,l}(t) = \begin{bmatrix} \boldsymbol{H}_{k,l}(M(t-1)+1) & 0 & \dots & 0 \\ 0 & \boldsymbol{H}_{k,l}(M(t-1)+2) & \dots & 0 \\ \vdots & \dots & \vdots & \vdots \\ 0 & 0 & \dots & \boldsymbol{H}_{k,l}(Mt) \end{bmatrix}. \quad (2.30)$$

We thus have

$$\bar{\boldsymbol{y}}_k(t) = \bar{\boldsymbol{H}}_{k,k}(t)\bar{\boldsymbol{V}}_k(t)\bar{\boldsymbol{s}}_k(t) + \sum_{l=1,\ l\neq k}^{K} \bar{\boldsymbol{H}}_{k,l}(t)\bar{\boldsymbol{V}}_l(t)\bar{\boldsymbol{s}}_l(t) + \bar{\boldsymbol{w}}_k(t). \quad (2.31)$$

From this point onwards, we consider the channel model (2.31). The index t is dropped for brevity. In [8], it was proved that the maximum sum of DoF achievable for the K-user SISO IC is $\frac{K}{2}$. The asymptotic IA scheme is then introduced and shown that it can achieve $\frac{K}{2}$ DoF, thus establishing the optimality of the asymptotic IA under high-SNR regime with symbol extensions. We describe the scheme in the following sections.

2.2.2.1 Interference Alignment Objectives

At user 1, we want to ensure that the interference space spans no more than $M - d_1$ dimensions. One way is to align the interference from the other users

$$\bar{\boldsymbol{H}}_{1,2}\bar{\boldsymbol{V}}_2 = \bar{\boldsymbol{H}}_{1,3}\bar{\boldsymbol{V}}_3 = \cdots = \bar{\boldsymbol{H}}_{1,K}\bar{\boldsymbol{V}}_K. \quad (2.32)$$

To recover d_k interference-free dimensions for user k, we can choose $\bar{\boldsymbol{V}}_k$, $k \neq 1$

so that

$$\text{span}\big(\bar{\boldsymbol{H}}_{k,j}\bar{\boldsymbol{V}}_j\big) \in \text{span}\big(\bar{\boldsymbol{H}}_{k,1}\bar{\boldsymbol{V}}_1\big); j \neq 1, k, \tag{2.33}$$

where span($\boldsymbol{A}$) denotes the space spanned by the column vectors of the matrix $\boldsymbol{A}$.

Under condition (2.32) and (2.33), all the interference are aligned at each user. We have to verify that the desired signal subspace does not overlap with the interference subspace, i.e., the columns of the $M \times M$ matrix $\big[\bar{\boldsymbol{H}}_{k,k}\bar{\boldsymbol{V}}_k \;\; \bar{\boldsymbol{H}}_{k,j}\bar{\boldsymbol{V}}_j\big]$ are linearly independent for a given $j \neq k$. This can be proved using Assumption 2.2.1 [8].

2.2.2.2 Asymptotic Interference Alignment Scheme

Denote $N = (K-1)(K-2)-1$, $M = (n+1)^N + n^N$, $d_1 = (n+1)^N$ and $d_k = n^N$, $k = 2, 3, \ldots, K$, where n is an arbitrary number. We further define

$$\boldsymbol{B} = \big(\bar{\boldsymbol{H}}_{2,1}\big)^{-1}\bar{\boldsymbol{H}}_{2,3}\bar{\boldsymbol{V}}_3; \tag{2.34}$$

$$\boldsymbol{S}_k = \big(\bar{\boldsymbol{H}}_{1,k}\big)^{-1}\bar{\boldsymbol{H}}_{1,3}\big(\bar{\boldsymbol{H}}_{2,3}\big)^{-1}\bar{\boldsymbol{H}}_{2,1}; k = 2, 3, \ldots, K; \tag{2.35}$$

$$\boldsymbol{T}_k^{(i)} = \big(\bar{\boldsymbol{H}}_{i,1}\big)^{-1}\bar{\boldsymbol{H}}_{i,k}\boldsymbol{S}_k; i, k = 2, 3, \ldots, K, i \neq k. \tag{2.36}$$

Note that due to Assumption 2.2.1, $\bar{\boldsymbol{H}}_{i,k}$ is full rank and thus invertible; and $\boldsymbol{T}_k^{(i)} \neq \boldsymbol{T}_m^{(l)}$ with $i \neq l$ or $k \neq m$. Condition (2.32) and (2.33) can be expressed as

$$\text{At user } 1 : \bar{\boldsymbol{V}}_k = \boldsymbol{S}_k\boldsymbol{B}; k = 2, 3, \ldots, K; \tag{2.37}$$

$$\text{At user 2}: \begin{cases} \text{span}\big(\boldsymbol{T}_3^{(2)}\boldsymbol{B}\big) = \text{span}\big(\boldsymbol{B}\big) \in \text{span}\big(\bar{\boldsymbol{V}}_1\big), \\ \text{span}\big(\boldsymbol{T}_3^{(2)}\boldsymbol{B}\big) \in \text{span}\big(\bar{\boldsymbol{V}}_1\big), \\ \quad \vdots \\ \text{span}\big(\boldsymbol{T}_K^{(2)}\boldsymbol{B}\big) \in \text{span}\big(\bar{\boldsymbol{V}}_1\big), \end{cases} \tag{2.38}$$

$$\text{At user k, k=3,4,...,K}: \begin{cases} \text{span}\big(\boldsymbol{T}_2^{(k)}\boldsymbol{B}\big) \in \text{span}\big(\bar{\boldsymbol{V}}_1\big), \\ \quad \vdots \\ \text{span}\big(\boldsymbol{T}_{k-1}^{(k)}\boldsymbol{B}\big) \in \text{span}\big(\bar{\boldsymbol{V}}_1\big), \\ \text{span}\big(\boldsymbol{T}_{k+1}^{(k)}\boldsymbol{B}\big) \in \text{span}\big(\bar{\boldsymbol{V}}_1\big), \\ \quad \vdots \\ \text{span}\big(\boldsymbol{T}_K^{(k)}\boldsymbol{B}\big) \in \text{span}\big(\bar{\boldsymbol{V}}_1\big). \end{cases} \tag{2.39}$$

The goal is to determine $\bar{\boldsymbol{V}}_1$ and $\boldsymbol{B}$ so that they satisfy the relations in (2.38) and (2.39). Then $\bar{\boldsymbol{V}}_k$, $k = 2, 3, \ldots, K$ can be found using (2.37). We let $\boldsymbol{w}$ be the $M \times 1$ column vector $\boldsymbol{w} = [1, 1, \ldots, 1]^T$. The sets of column vectors $\boldsymbol{B}$ and $\bar{\boldsymbol{V}}_1$ can be chosen to be equal to the following sets

$$\mathcal{B} = \left\{ \left(\prod_{m,k \in \{2,3,\ldots,K\}, m \neq l, (m,k) \neq (2,3)} \big(\boldsymbol{T}_k^{(m)}\big)^{\alpha_{m,k}} \right) \boldsymbol{w} : \quad \alpha_{m,k} \in \{0, 1, 2, \ldots, n-1\} \right\}, \tag{2.40}$$

$$\mathcal{V}_1 = \left\{ \left(\prod_{m,k \in \{2,3,\ldots,K\}, m \neq l, (m,k) \neq (2,3)} \big(\boldsymbol{T}_k^{(m)}\big)^{\alpha_{m,k}} \right) \boldsymbol{w} : \quad \alpha_{m,k} \in \{0, 1, 2, \ldots, n\} \right\}. \tag{2.41}$$

It can be shown that the above construction satisfies the IA conditions (2.37)-(2.39) [8].

2.2.2.3 Optimality of IA for the K-user SISO IC

In the previous sections, we have described the asymptotic IA for the K-user SISO IC. The reason why the asymptotic IA scheme is important is that it can achieve the maximum sum of DoF of a K-user SISO IC. We first state the following theorem

Theorem 2.2.1 *[8, Theorem 1] The number of degrees of freedom for the K-user SISO IC is upper-bounded by $\frac{K}{2}$*

$$d_1 + d_2 + \cdots + d_K \leq \frac{K}{2}. \tag{2.42}$$

With the construction given in the previous section, it has been shown that the following DoF tuple is attainable [8]

$$(d_1(n), d_2(n), \ldots, d_K(n)) = \left(\frac{(n+1)^N}{(n+1)^N + n^N}, \frac{n^N}{(n+1)^N + n^N}, \ldots, \frac{n^N}{(n+1)^N + n^N} \right). \tag{2.43}$$

Now by letting $n \to \infty$, we see that each user can achieve $\frac{1}{2}$ DoF, and $d_1 + d_2 + \cdots + d_K = \frac{K}{2}$. We thus observe that the asymptotic IA scheme is asymptotically optimal under high-SNR regime with symbol extensions.

The first drawback of the asymptotic IA scheme is that it requires a very large number of symbol extensions to achieve the perfect IA. When the time domain is used for IA, a *non-causal* knowledge of the CSI is required, which is practically difficult to obtain. On the other hand, when the frequency domain is used for IA, this results in an unreasonable number of sub-carriers and a correspondingly large bandwidth. The second drawback is due to the CSI estimation and feedback, since asymptotic

IA scheme requires the acquisition of accurate CSI to perform the calculation. The back-haul communication thus is expected to be large. Finally, the synchronization and cooperation between the nodes also prove to be costly and excruciating.

2.2.3 Interference Alignment without Symbol Extensions

In the previous section, we have introduced the asymptotic IA scheme assuming that symbol extensions are available. In this section, we briefly discuss the IA-based schemes without symbol extensions. This case arises when the channels are static flat-fading or asymptotic IA is not realizable due to the constraints in estimation, complexity, etc.

Assume the MIMO IC channel model as stated in (2.27) and suppose that the number of information streams communicated by the k-th user is d_k. Since only one channel realization is considered, the time index t can be dropped and the channel is given as

$$\begin{aligned}\boldsymbol{r}_k &= \boldsymbol{U}_k^H \boldsymbol{r}_k \\ &= \boldsymbol{U}_k^H \boldsymbol{H}_{k,k} \boldsymbol{V}_k \boldsymbol{s}_k + \sum_{l=1,\ l\neq k}^{K} \boldsymbol{U}_k^H \boldsymbol{H}_{k,l} \boldsymbol{V}_l \boldsymbol{s}_l + \boldsymbol{U}_k^H \boldsymbol{w}_k, \end{aligned} \tag{2.44}$$

where now $\boldsymbol{U}_k \in \mathbb{C}^{N_R \times d_k}$ and $\boldsymbol{V}_k \in \mathbb{C}^{N_T \times d_k}$. The perfect IA requirements are [18]

$$\boldsymbol{U}_k^H \boldsymbol{H}_{k,l} \boldsymbol{V}_l = \boldsymbol{0}_{d_k \times d_l}, \forall l \neq k \tag{2.45}$$

$$\text{rank}\left(\boldsymbol{U}_k^H \boldsymbol{H}_{k,k} \boldsymbol{V}_k\right) = d_k. \tag{2.46}$$

Finding the precoding and decoding matrices $\boldsymbol{U}_k^H$ and $\boldsymbol{V}_k$ satisfying (2.45) and (2.46) is computationally intractable. Particularly, even the problem of checking the

achievability of (2.45) and (2.46) with a certain DoF tuple $(d_1, d_2, \ldots, d_K)$ is NP-hard when N_T, $N_R > 2$ [59]. In the following, we describe three existing (heuristic) IA-based schemes which aim to solve (2.45) and (2.46) given $(d_1, d_2, \ldots, d_K)$.

2.2.3.1 Minimizing the Interference Leakage

The first approach to solve (2.45) and (2.46) is to minimize the interference leakage. Here, the quality metric is the power of the leakage interference at each receiver, i.e. the interference power remaining in the received signal after the receive interference suppression filter is applied. The goal is to achieve the IA conditions (2.45) and (2.46) by progressively reducing the leakage interference. The motivation for this scheme is that when IA is realizable, the total interference leakage at each user will be zero and we obtain perfect IA.

The interference leakage algorithm is given as follows

Algorithm 2 The first IA-based scheme - Minimizing the interference leakage [18] [56]

Input: Arbitrary precoding matrices $\boldsymbol{V}_k \in \mathbb{C}^{N_T \times d_k}$, $\boldsymbol{V}_k \boldsymbol{V}_k^H = \boldsymbol{I}_{d_k \times d_k}$.

1. Compute interference covariance matrix at the receivers:

$$\boldsymbol{Q}_k = \sum_{j=1, j \neq k}^{K} \frac{P_T}{d_j} \boldsymbol{H}_{k,j} \boldsymbol{V}_j \boldsymbol{V}_j^H \boldsymbol{H}_{k,j}^H. \tag{2.47}$$

2. Compute the interference suppression matrix at each receiver. The d-th column of $\boldsymbol{U}_k$ is given by:

$$\boldsymbol{u}_{k,d} = \nu_d \left(\boldsymbol{Q}_k \right), \ d = 1, \ldots, d_k, \tag{2.48}$$

where $\nu_d \left(\boldsymbol{A} \right)$ is the eigenvector corresponding to the d-th smallest eigenvalue of $\boldsymbol{A}$.

3. Set the auxiliary reciprocal matrices $\bar{\boldsymbol{V}}_k = \boldsymbol{U}_k$.

4. Compute the new interference covariance matrix

$$\bar{\boldsymbol{Q}}_j = \sum_{k=1, k \neq j}^{K} \frac{P_T}{d_k} \bar{\boldsymbol{H}}_{j,k} \bar{\boldsymbol{V}}_j \bar{\boldsymbol{V}}_j^H \bar{\boldsymbol{H}}_{j,k}^H, \tag{2.49}$$

where $\bar{\boldsymbol{H}}_{j,k} = \boldsymbol{H}_{k,j}^H$ is the reciprocal channel matrix.

5. Compute the interference suppression matrix at each receiver. The d-th column of $\bar{\boldsymbol{U}}_k$ is given by:

$$\bar{\boldsymbol{u}}_{j,d} = \nu_d \left(\bar{\boldsymbol{Q}}_j \right), \ d = 1, \ldots, d_j, \tag{2.50}$$

6. Reverse the communication direction and set $\boldsymbol{V}_k = \bar{\boldsymbol{U}}_k$.

7. Repeat Step 1-6 until convergence or after a number of predefined iterations.

2.2.3.2 Maximizing the SINR

Note that the algorithm in Section 2.2.3.1 only suppresses the interference at each user, while ignoring the desired signal. The algorithm might perform well at high-SNR regime, however, it is not optimal in general at intermediate SNR values. In this section, we present an algorithm to maximize the SINRs at each user [18]. The quality metric is the SINR for each stream of each user

$$\text{SINR}_{k,l} = \frac{\boldsymbol{u}_{k,l}^H \boldsymbol{H}_{k,k} \boldsymbol{v}_{k,l} \boldsymbol{v}_{k,l}^H \boldsymbol{H}_{k,k}^H \boldsymbol{u}_{k,l}}{\boldsymbol{u}_{k,l}^H \boldsymbol{B}_{k,l} \boldsymbol{u}_{k,l}} \frac{P_T}{d_k}, \tag{2.51}$$

where

$$\boldsymbol{B}_{k,l} = \sum_{j=1}^{K} \frac{P_T}{d_j} \sum_{d=1}^{d_j} \boldsymbol{H}_{k,j} \boldsymbol{v}_{k,d} \boldsymbol{v}_{k,d}^H \boldsymbol{H}_{k,j}^H - \frac{P_T}{d_k} \boldsymbol{H}_{k,k} \boldsymbol{v}_{k,l} \boldsymbol{v}_{k,l}^H \boldsymbol{H}_{k,k}^H + \boldsymbol{I}_{N_R \times N_R}, \tag{2.52}$$

and the unit vector that maximizes $\text{SINR}_{k,l}$ is given by

$$\boldsymbol{u}_{k,l} = \frac{\boldsymbol{B}_{k,l}^{-1} \boldsymbol{H}_{k,k} \boldsymbol{v}_{k,l}}{||\boldsymbol{B}_{k,l}^{-1} \boldsymbol{H}_{k,k} \boldsymbol{v}_{k,l}||}. \tag{2.53}$$

The max-SINR algorithm is given as follows [18]

Algorithm 3 The second IA-based scheme - Maximizing the SINR [18]

Input: Arbitrary precoding matrices $\boldsymbol{V}_k \in \mathbb{C}^{N_T \times d_k}$ where columns of $\boldsymbol{V}_k$ are linearly independent unit vectors.

1. Compute the interference plus noise covariance matrix $\boldsymbol{B}_{k,l}$ for stream l at user k as in (2.52), $\forall\ k \in \{1, \ldots, K\}$, $l \in \{1, \ldots, d_k\}$.

2. Compute the l-th column of the decoder $\boldsymbol{u}_{k,l}$ at user k as in (2.53), $\forall\ k \in \{1, \ldots, K\}$, $l \in \{1, \ldots, d_k\}$.

3. Reverse the communication direction and use the decoder as precoder: $\bar{\boldsymbol{V}}_k = \boldsymbol{U}_k$.

4. In the reciprocal channel, compute the interference plus noise covariance matrix $\bar{\boldsymbol{B}}_{k,l}$ for stream l at user k as in (2.52), $\forall\ k \in \{1, \ldots, K\}$, $l \in \{1, \ldots, d_k\}$.

5. In the reciprocal channel, compute the l-th column of the decoder $\bar{\boldsymbol{u}}_{k,l}$ at user k as in (2.53), $\forall\ k \in \{1, \ldots, K\}$, $l \in \{1, \ldots, d_k\}$.

6. Reverse the communication direction and set $\boldsymbol{V}_k = \bar{\boldsymbol{U}}_k$.

7. Repeat Step 1-6 until convergence or after a number of predefined iterations.

2.2.3.3 Maximizing the Sum of DoF

Although the interference leakage and SINR are meaningful metrics to optimize for the IC, they are not directly related to the DoF of each user. Another approach is hence to maximize the available spatial DoF [52]. It was shown in [52] that the conditions (2.45) and (2.46) naturally lead to a rank constrained rank minimization (RCRM), where the rank constraints ensure that the desired signal spans all available dimensions, while the rank minimization ensures that the interference spans as few dimensions as possible.

Define the signal and interference matrices as

$$\boldsymbol{S}_k = \boldsymbol{U}_k^H \boldsymbol{H}_{k,k} \boldsymbol{V}_k \in \mathbb{C}^{d \times d}, \tag{2.54}$$

$$\boldsymbol{J}_k = \boldsymbol{U}_k^H \left[\boldsymbol{H}_{k,l} \boldsymbol{V}_l {}_{l=1,l\neq k}^{K} \right] \in \mathbb{C}^{d \times (K-1)d}, \tag{2.55}$$

where each useful signal space spans d dimensions. Here we assume that $d_1 = \ldots = d_K = d$.

Solving (2.45) and (2.46) is equivalent to solving the following set of K parallel RCRM problem

$$\begin{aligned} (\text{P1(k)}): \quad & \underset{\boldsymbol{U}_k, \{\boldsymbol{V}_l\}_{l=1,l\neq k}^{K}}{\texttt{min.}} && \text{rank}(\boldsymbol{J}_k) \\ & \texttt{s.t.} && \text{rank}(\boldsymbol{S}_k) = d. \end{aligned} \tag{2.56}$$

Since it is not possible to solve in parallel the K optimization problem (P1(k)), $k = 1, \ldots, K$, the following RCRM is solved instead to maximize the sum of interference-

free dimensions

$$(\text{P2}): \quad \underset{\{\boldsymbol{U}_l\}_{l=1}^K, \{\boldsymbol{V}_l\}_{l=1}^K}{\texttt{min.}} \quad \sum_{k=1}^{K} \text{rank}(\boldsymbol{J}_k)$$

$$\texttt{s.t.} \quad \text{rank}(\boldsymbol{S}_k) = d, \forall k. \tag{2.57}$$

The problem (P2) is nonconvex and intractable. In [52], a heuristic solution is proposed by approximating (P2) using the nuclear norm and relaxing the rank constraints. The algorithm is given as follows

Algorithm 4 The third IA-based scheme - Maximizing the sum of DoF [52]

Input: Arbitrary precoding matrices $\boldsymbol{U}_k$.

1. Given $\boldsymbol{U}_k$'s, solve the following convex optimization problem

$$\begin{aligned} (\text{P3}): \quad \underset{\{\boldsymbol{V}_l\}_{l=1}^K}{\texttt{min.}} \quad & \sum_{k=1}^{K} ||\boldsymbol{J}_k)||_* \\ \texttt{s.t.} \quad & \boldsymbol{S}_k \succeq \boldsymbol{0}_{d\times d}; \\ & \lambda_{\min}(\boldsymbol{S}_k) \geq \epsilon, \forall k, \end{aligned}$$

where $||\boldsymbol{A}||_* = \boldsymbol{Tr}\left(\sqrt{\boldsymbol{A}^H\boldsymbol{A}}\right)$ is the nuclear norm of matrix $\boldsymbol{A}$.

2. Given $\boldsymbol{V}_k$'s, solve the following convex optimization problem

$$\begin{aligned} (\text{P4}): \quad \underset{\{\boldsymbol{U}_l\}_{l=1}^K}{\texttt{min.}} \quad & \sum_{k=1}^{K} ||\boldsymbol{J}_k)||_* \\ \texttt{s.t.} \quad & \boldsymbol{S}_k \succeq \boldsymbol{0}_{d\times d}; \\ & \lambda_{\min}(\boldsymbol{S}_k) \geq \epsilon, \forall k. \end{aligned}$$

3. Orthogonalize $\{\boldsymbol{U}_l\}_{l=1}^K$ and $\{\boldsymbol{V}_l\}_{l=1}^K$.

4. Repeat Step 1-3 for a predefined number of iterations.

2.2.3.4 Numerical Results and Discussions

In this sub-section, we compare the rate performance of the three IA-based algorithms introduced in Section 2.2.3.1, 2.2.3.2, and 2.2.3.3. The channel matrices are drawn i.i.d. from a real Gaussian distribution with zero mean and unit variance.

In Fig. 2.5, we consider a 3-user interference channel with 2 antennas at each node. The requested DoF for each user is $d = 1$. We also plot the upper-bound scaling law, which can be obtained with asymptotic IA and symbol extensions [8]. Under this setup, we observe that the max-SINR algorithm outperforms the other schemes when the power is small. However, as the power becomes larger, the interference leakage algorithm achieves a better sum-rate. Also note that the upper-bound scaling law is not achievable in this case, since the request DoF can only be an integer.

In Fig. 2.6, we consider a 2-user interference channel with 4 antennas at each node. Here we set the requested DoF for each user as either $d = 1$ or $d = 2$. For $d = 1$, it is observed that the max-SINR and sum of DoF algorithm perform equivalently well and provide a large rate benefit over the interference leakage scheme. For $d = 2$, the same conclusion holds for high-SNR regime. However, the leakage minimization algorithm achieves a higher sum-rate than the other (equivalent) two schemes at low-SNR regime. Note that the upper-bound scaling law is achievable in this setup, even without symbol extensions.

Finally we consider a 3-user interference channel with 6 antennas at each node. The request DoF is set at $d = 3$. In this case, the interference leakage offers a huge rate

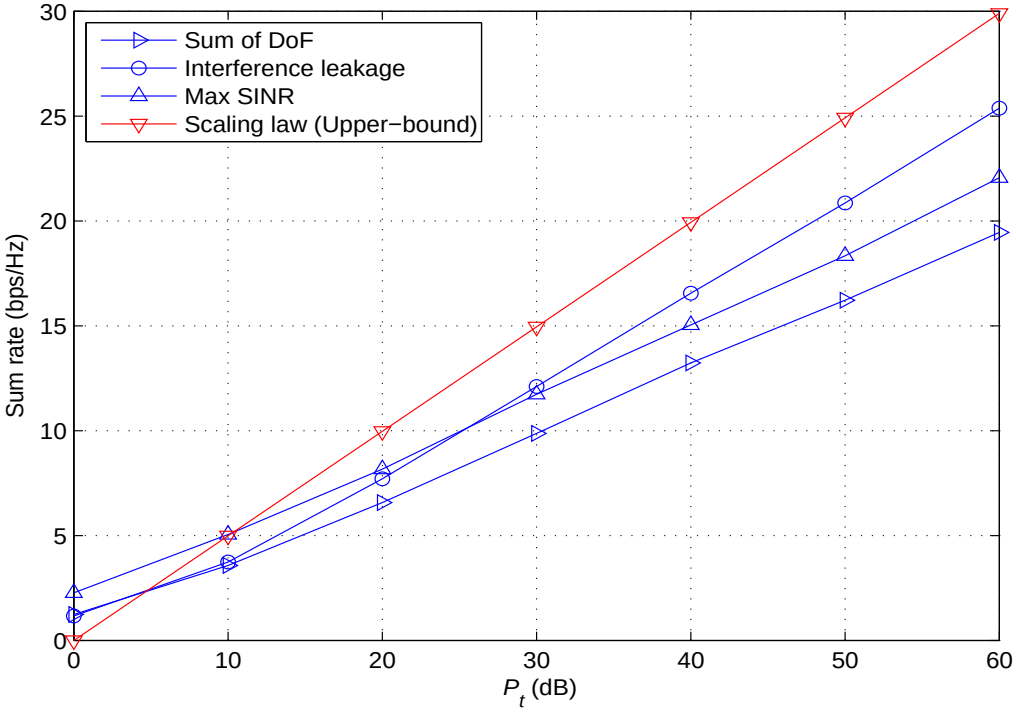

Figure 2.5: Comparisons of the three IA algorithms and the upper-bound scaling law $\frac{3}{2}\log_2(P_T)$.

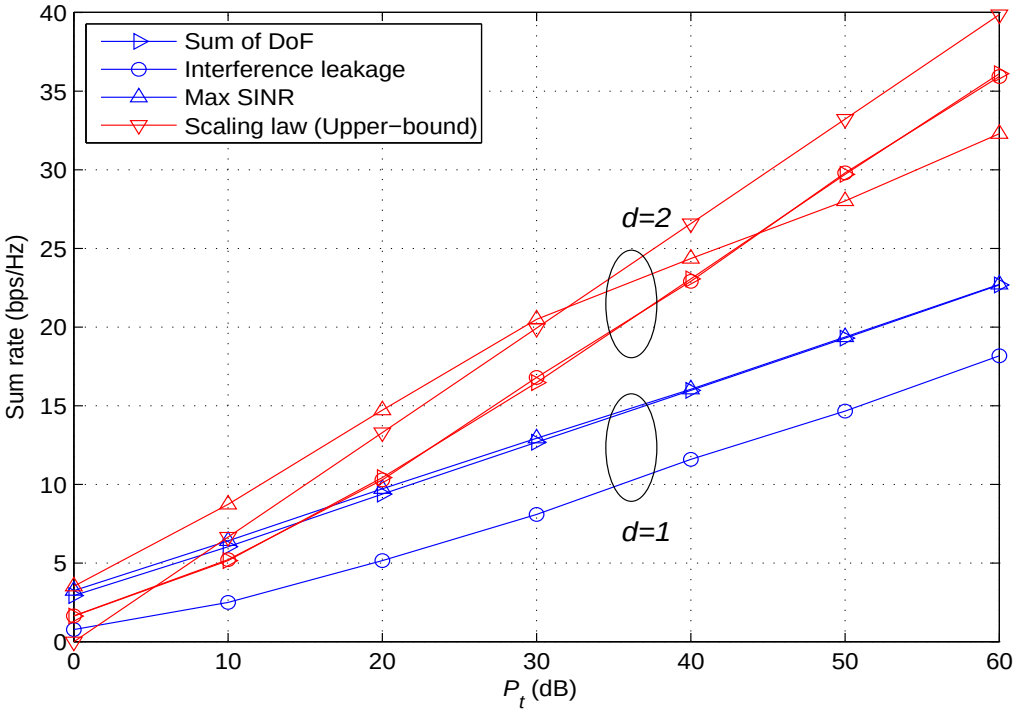

Figure 2.6: Comparisons of the three IA algorithms with $d = 1$ and $d = 2$ and the upper-bound scaling law $2\log_2(P_T)$.

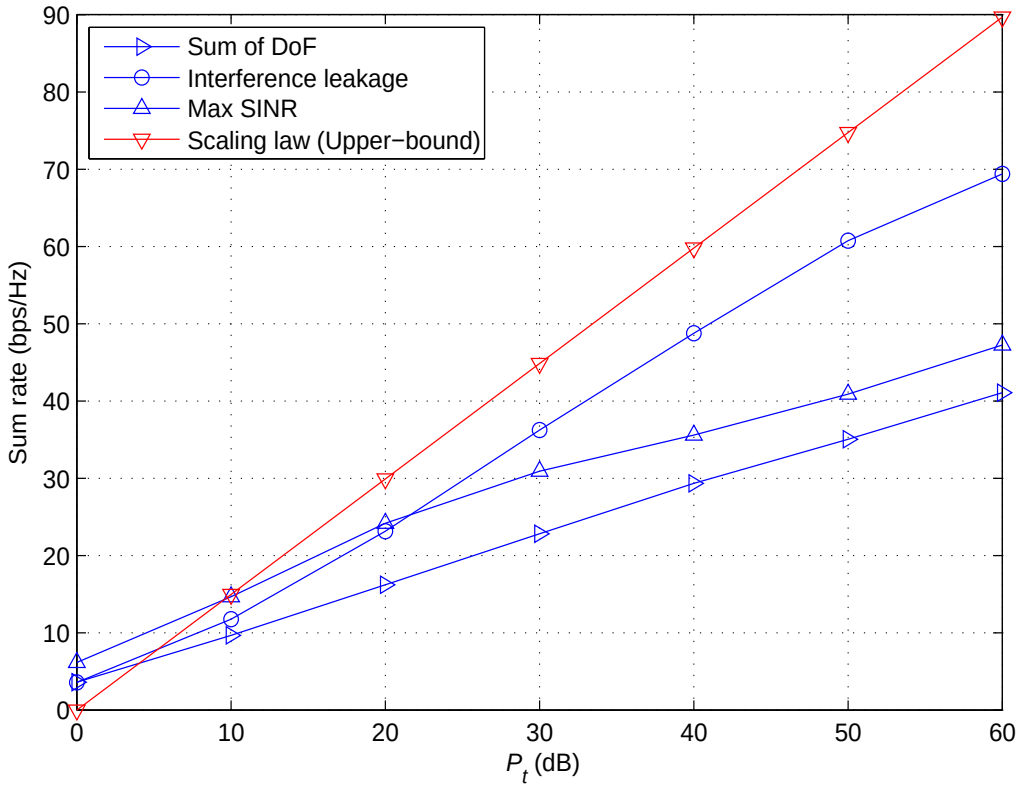

Figure 2.7: Comparisons of the three IA algorithms and the upper-bound scaling law $\frac{9}{2}\log_2(P_T)$.

gain when compared with the max-SINR and sum of DoF schemes, especially under high-SNR regime. It is observed that the three schemes also cannot appropriately match with the upper-bound scaling law.

In summary, it is not possible to conclude which is the best IA-based algorithms among the three algorithms. Under certain setups, one scheme can be better than the others and vice versa. Furthermore, perfect IA is achievable with the IA-based schemes in some cases, even without symbol extensions. This shows the usefulness of the introduced algorithms, albeit they are heuristic and does not directly solve the

IA conditions (2.45) and (2.46).

Chapter 3

Single-Cell MISO RBF

The transmission schemes briefly described in Chapter 2 have a common requirement of perfect and instantaneous CSI for all of the direct and cross-link channels at each transmitter. As a consequence, these schemes are susceptible to CSI delay and estimation error. Furthermore, the backhaul communication to transfer all CSI data to all transmitting nodes is expected to be large. OBF and RBF schemes, introduced in [72] and [64], respectively, have attracted a great deal of attention since they require only *partial* CSI fedback to the BS. The fundamental idea in these schemes is to achieve nearly interference-free downlink transmissions by exploiting the multi-user channel diversity with *opportunistic* user scheduling. For single-cell case, it has been shown that the achievable sum-rates with the RBF and optimal DPC both scale identically as the number of users in the cell approaches infinity, for any given SNR [64], [65] (see Theorem 3.3.1 and 3.3.2).

This optimistic result shows the optimality of RBF in the regime of large

number of users and has motivated extensive subsequent studies on, e.g., sum-rate characterization [36], [53], quantized channel feedback [51] [60] [78], and precoder design with opportunistic scheduling [44], [80]. Opportunistic communication thus has developed to a broad area with various constituent topics. In this chapter, we review the key developments of OBF/RBF, summarizing some of the most important results contributed to the field. Since virtually all the works in the literature consider the single-cell case, we restrict this overview to the single-cell OBF/RBF. The extensions of OBF/RBF to the multi-cell and/or MIMO case, which are the major contributions of this thesis, will be discussed in Chapter 4 and 5.

3.1 System Model

Consider a multiple-antenna Gaussian BC with a BS having N_T antennas and K single-antenna mobile stations (MSs), $K \geq 1$. We assume the channels to be flat-fading and constant over each transmission period of interest. The BS transmits $M \leq N_T$ orthonormal beams and selects M from K users for transmission at each time. The received signal of user k is given by

$$y_k = \boldsymbol{h}_k^H \sum_{m=1}^{M} \boldsymbol{\phi}_m s_m + n_k, \tag{3.1}$$

where $\boldsymbol{h}_k \in \mathbb{C}^{M\times 1}$ is the channel vector between BS and the k-th user, and it is assumed that all elements of $\boldsymbol{h}_k$ are i.i.d. $\mathcal{CN}(0,1)$; $\boldsymbol{\phi}_m \in \mathbb{C}^{M\times 1}$ and s_m are the m-th randomly generated unit-norm beamforming vector and transmitted data symbol, respectively. It is assumed that the total sum power is P_T, i.e., $\boldsymbol{Tr}\left(\mathbb{E}[\boldsymbol{s}\boldsymbol{s}^H]\right) \leq P_T$,

where $\boldsymbol{s} = [s_1, \cdots, s_M]^T$. It is also assumed that the background noise n_k is AWGN, $n_k \sim \mathcal{CN}(0, \sigma^2)$, $\forall k$.

The RBF scheme, introduced in [64], is as follows. In the training phase, the BS generates M orthonormal beams, $\boldsymbol{\phi}_1$, $\cdots$,$\boldsymbol{\phi}_M$ and uses them to broadcast the training signals to all K users. The total power of each BS is assumed to be distributed equally over M beams. Each user measures the SINR values for all M beams, which are shown in (3.2) below [64]

$$\text{SINR}_{k,m} = \frac{\frac{P_T}{M}\left|\boldsymbol{h}_k^H \boldsymbol{\phi}_m\right|^2}{\sigma^2 + \frac{P_T}{M}\sum_{i=1, i\neq m}^{M}\left|\boldsymbol{h}_k^H \boldsymbol{\phi}_i\right|^2}. \tag{3.2}$$

where $m = 1, \cdots, M$. Each user then

(F1) feeds *all* SINR values and the corresponding beam indexes back to the corresponding BS; or

(F2) feeds the largest SINR value, i.e., $\text{SINR}_{k,\text{FB}} = \max_{m=1,\cdots,K} \text{SINR}_{k,m}$, and the corresponding beam index FB_k back to the corresponding BS.

When the number of users K is large, it is obvious that there might not enough beams to be assigned to all users. Therefore, it is necessary to incorporate a certain user-scheduling scheme to OBF/RBF. The following user scheduling scheme is widely accepted due to its simpleness which leads to an easy implementation and investigation. Please refer to Section 3.6 for more discussion.

The BS schedules transmission at each time by assigning its m-th beam to the

user with the highest SINR, i.e.,

$$k_m = \arg \max_{k=1,\cdots,K} \text{SINR}_{k,m}. \tag{3.3}$$

For the feedback scheme (F2), there is a small probability that one user may be the strongest user for more than one beam. Therefore, a modified user scheduling scheme is necessary. Here we introduce the scheme proposed in [34] and [79]. Specifically, the BS ranks all K feed-backed beam SINRs. If $\text{SINR}_{k,m}$ is the largest one among all K SINRs, then the BS selects the k-th user for the m-th beam. After that, the BS will rank the feed-backed SINRs for the remaining beams. If now $\text{SINR}_{l,n}$ is the largest one, where $l \neq k$ and $n \neq m$, then the BS assigns the n-th beam to the l-th user. This process continues until either all beams have been assigned to selected users or there are some unrequested beams remaining. In the later case, the BS will randomly select users for the remaining beams. The algorithm is given as follows.

Algorithm 5 User-scheduling procedure for the feedback scheme (F2) [34] [79]

Input: The set of SINR values $\mathcal{S}_S = \{\text{SINR}_{1,\text{FB}}, \ldots, \text{SINR}_{K,\text{FB}}\}$ and the set of corresponding beam indexes $\mathcal{S}_F = \{\text{FB}_1, \ldots, \text{FB}_K\}$.

1. Initialize the chosen beam and user index set $\mathcal{S}_{CB} = \{\ \emptyset\ \}$, $\mathcal{S}_{CU} = \{\ \emptyset\ \}$.

2. Select (different) users who feedback different strongest beam indexes.

for $m = 1$ to M **do**

Select $\mathcal{S}_m \subseteq \mathcal{S}_S$ such that the beam indexes correspond to the SINRs in $\mathcal{S}_m$ are the same $\text{FB}_j = m$ and the user index $j \notin \mathcal{S}_{CU}$

if $(\mathcal{S}_m \neq \{\ \emptyset\ \})$ **then**

Select the largest SINR value in $\mathcal{S}_m$.

Add m into $\mathcal{S}_{CB}$.

Add the corresponding user index j_m into $\mathcal{S}_{CU}$.

end if

end for

3. Randomly select the remaining beams with the remaining users.

for $m = 1$ to M **do**

if $(m \notin \mathcal{S}_{CB})$ **then**

Randomly select an index k_m from $\{1, \ldots, K\ \} \setminus \mathcal{S}_{CU}$

Add m into $\mathcal{S}_{CB}$

Add k_m into $\mathcal{S}_{CU}$

end if

end for

Then, the achievable sum rate in bits per complex dimension is given by

(F1) (with (F1) feedback scheme)

$$R_{\mathrm{RBF,F1}} = \mathbb{E}\left[\sum_{m=1}^{M} \log_2\left(1+\mathrm{SINR}_{k_m,m}\right)\right] = M\mathbb{E}\left[\log_2\left(1+\mathrm{SINR}_{k_1,1}\right)\right], \quad (3.4)$$

(F2) (with (F2) feedback scheme)

$$R_{\mathrm{RBF,F2}} \overset{(a)}{\approx} \mathbb{E}\left[\sum_{m=1}^{M} \log_2\left(1+\mathrm{SINR}_{k_m,m}\right)\right] = M\mathbb{E}\left[\log_2\left(1+\mathrm{SINR}_{k_1,1}\right)\right] = R_{\mathrm{RBF,F1}}, \quad (3.5)$$

where (a) holds due to the negligibly small probability of assigning multiple beams to one user, since an user k might be the strongest user for more than one beam; and "=" due to the homogeneous distribution of the SINR.

The PDF and cumulative density function (CDF) of $S := \mathrm{SINR}_{k,m}, \forall k, m$ can be expressed as [64]

$$f_S(s) = \frac{e^{-s/\eta}}{(s+1)^M}\left(M-1+\frac{s+1}{\eta}\right). \quad (3.6)$$

$$F_S(s) = 1 - \frac{e^{-s/\eta}}{(s+1)^{M-1}}. \quad (3.7)$$

where $\eta = P_T/(M\sigma^2)$ is the SNR per beam.

Remark 3.1.1 *The OBF scheme is a special case of RBF. It corresponds to the case of $M = 1$, i.e., the BS sends exactly one beam to communicate with the MSs.*

Remark 3.1.2 *The objective for introducing the feedback scheme (F2) is to get a fair comparison with OBF, since each user in the OBF scheme also feeds back only two scalar values to the BS. Note that $R_{sum,F2} \leq R_{sum,F1}$ and as $K \to \infty$, $R_{sum,F2} \to R_{sum,F1}$.*

3.2 Achievable Rate

3.2.1 Rate Expression for (F1) Scheme

Closed-form expressions for the sum-rate in RBF systems have been investigated in many studies, where most of them concentrate on the rate with (F1) feedback scheme (see (3.1)). It is expected, since the rate in this case is fairly simple (see (3.4)). Loose approximations for (3.4) are presented in [36] and [53] using Gaussian hypergeometric functions. The results thus are quite complicated. However, the sum-rate approximations in [36] and [53] can directly lead to some asymptotic results, e.g., the sum-rate scaling law $M \log_2 \log K$ as $K \to \infty$.

Recently, two accurate results for the rate expression have been reported in the literature [50] [26]. Our contribution will be presented later in Chapter 4. The following result is due to [26].

Lemma 3.2.1 *([26, Theorem 1]) The average sum rate of a single-cell RBF system is given by*

$$R_{RBF,F1} = \frac{M}{\log 2} \sum_{l=0}^{K-1} \binom{K-1}{l} \frac{(-1)^l}{l+1} \mathcal{I}\left(\frac{M(l+1)}{P_T}, (M-1)(l+1)+1\right), \qquad (3.8)$$

where $\mathcal{I}(a,b)$ is defined as

$$\mathcal{I}(a,b) = \begin{cases} \dfrac{(-1)^{b-1} a^{b-1} e^a E_1(a)}{(b-1)!} + \displaystyle\sum_{i=1}^{b-1} \frac{(i-1)!}{(b-1)!} (-1)^{b-i-1} a^{b-i-1}, & b \geq 2 \text{ (3.9a)} \\ e^a E_1(a), & b = 1 \text{ (3.9b)} \end{cases}$$

and $E_1(x) = \int_x^\infty \frac{e^{-t}}{t} dt$ is the exponential integral function.

Assuming the feedback scheme (F1), (3.8) becomes a close rate approximation for the scheme (F2), especially when the number of users K is large.

3.2.2 Rate Expression for (F2) Scheme

The exact expression of the sum rate with (F2) feedback scheme is derived in [79], which involves a numerical integral with the SINR CDF of the first beam:

Lemma 3.2.2 *([79]) Assuming the feedback scheme (F2), the average sum rate of the single-cell RBF is given by*

$$R_{RBF,F2} = M \int_0^\infty \log_2(1+x) \hat{f}_{SINR_{k_1,1}}(x) dx, \tag{3.10}$$

in which

$$\hat{f}_{SINR_{k_1,1}}(x) = \sum_{k=1}^{K} \frac{1}{M} \left(1 - \frac{1}{M}\right)^{k-1} \frac{K!}{(K-k)!(k-1)!} \left(F_1(x)\right)^{K-k} \left[1 - F_1(x)\right]^{k-1} f_1(x) + \left(1 - \frac{1}{M}\right)^{K} \frac{1}{M-1} \sum_{m=2}^{M} f_{2,m}(x), \tag{3.11}$$

$$F_1(x) = \int_0^x f_1(t) dt, \tag{3.12}$$

$$f_1(x) = \sum_{m=0}^{M-1} \frac{(-1)^m M!}{(M-m-1)!m!} \exp\left(-\frac{(1+m)x}{\eta(mx-1)}\right) \times \times \frac{(M + 1/\eta - 1 + (1/\eta - mM + m)x)(1-mx)^{M-3}}{(1+x)^M}, \tag{3.13}$$

$$f_{2,m}(x) = \int_0^\infty \int_0^{\frac{(M-m)w}{m-1}} \left(\frac{1}{\eta} + z + w\right) f_{w_m,\beta_{m:M},z_m}\left(w, x\left(\frac{1}{\rho} + z + w\right), z\right) dz dw. \tag{3.14}$$

Finally, the function $f_{w_m,\beta_{m:M},z_m}(w,\beta,z)$ is given in [37, (28)]

$$f_{w_m,\beta_{m:M},z_m}(w,\beta,z) = \frac{M![w-(m-1)\beta]^{m-1}}{(L-1)!(l-1)!\bar{\beta}^M}\frac{\exp\left(-\frac{w+\beta+z}{\beta}\right)}{(m-2)!(M-m-1)!}\mathcal{U}(1-(m-1)\beta)\times$$
$$\times\sum_{i=0}^{M-m}\binom{M-m}{i}(-1)^i(z-i\beta)^{M-m-1}\mathcal{U}(z-i\beta),$$

$$\beta>0, w>(m-1)\beta, z<(M-1)\beta, \tag{3.15}$$

where $\rho = P_T/M$, $\mathcal{U}(x)$ is the unit step function, and $\bar{\beta}=1$ due to the Rayleigh fading channel model.

In a recent study [34], Kim *et. al.* also shows that the CDF of the largest beam SINR of a user $F_1(x)$ can be expressed as

$$F_1(x) = 1-\frac{1}{M(1+x)^{M-1}}\sum_{r=0}^{\min\left(M-1,\lceil\frac{1}{x}\rceil-1\right)}(-1)^r\binom{M}{r+1}(1-rx)^{M-1}e^{-\frac{(r+1)Mx}{\rho(1-rx)}}. \tag{3.16}$$

In Fig. 3.1, we show the sum rate performance of the feedback scheme (F1) and (F2) with respect to different numbers of beam M and users K. The transmit power is $P_T = 20$ dB. Note that the simulation results and the analytical expressions are in full agreement. We observe that the rate performance of (F1) and (F2) feedback schemes are quite equivalent, even with a small number of users. Particularly, only for the case of $M = 4$ and $K = 5$ that there is a noticeable difference between the two schemes. The reason is due to the fact that K is approximately equal to M. Thus, there is a high chance that the user assigned to a beam is chosen based on the random selection step. We also observe that the sum-rates for the cases $M = 2$ are

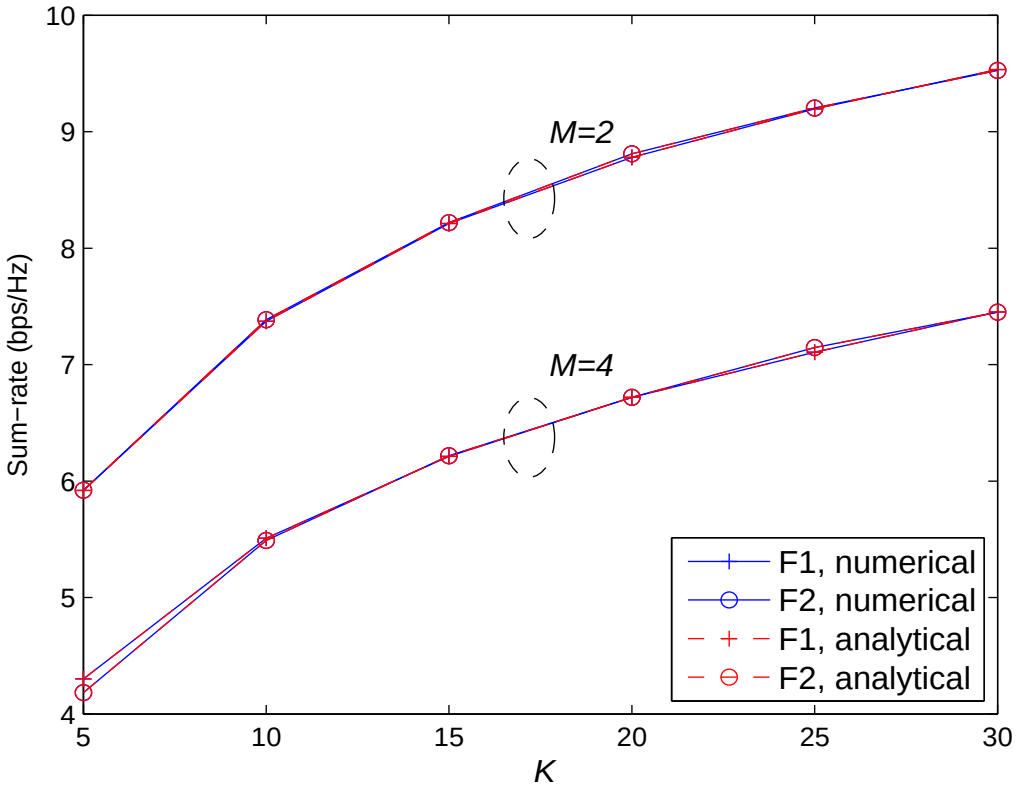

Figure 3.1: Comparison of numerical and analytical sum-rates with respect to the number of users for $P_T = 20$ dB and $M = 2, 4$.

larger than those of the case $M = 4$. In fact, this observation can be explained based on our newly obtained results presented in Chapter 4.

In Fig. 3.2, we depict the sum rate performance of the feedback scheme (F1) and (F2) with respect to different numbers of beam M and transmit power P_T. The number of users is fixed at $K = 25$. Again, the simulation results and the analytical expressions are closely matched. At low-SNR regime, we notice that the setting $M = 4$ gives better rate performance. However, at high-SNR regime, the setting $M = 2$ outperforms $M = 4$. As we will see later, the DoF results, discussed in

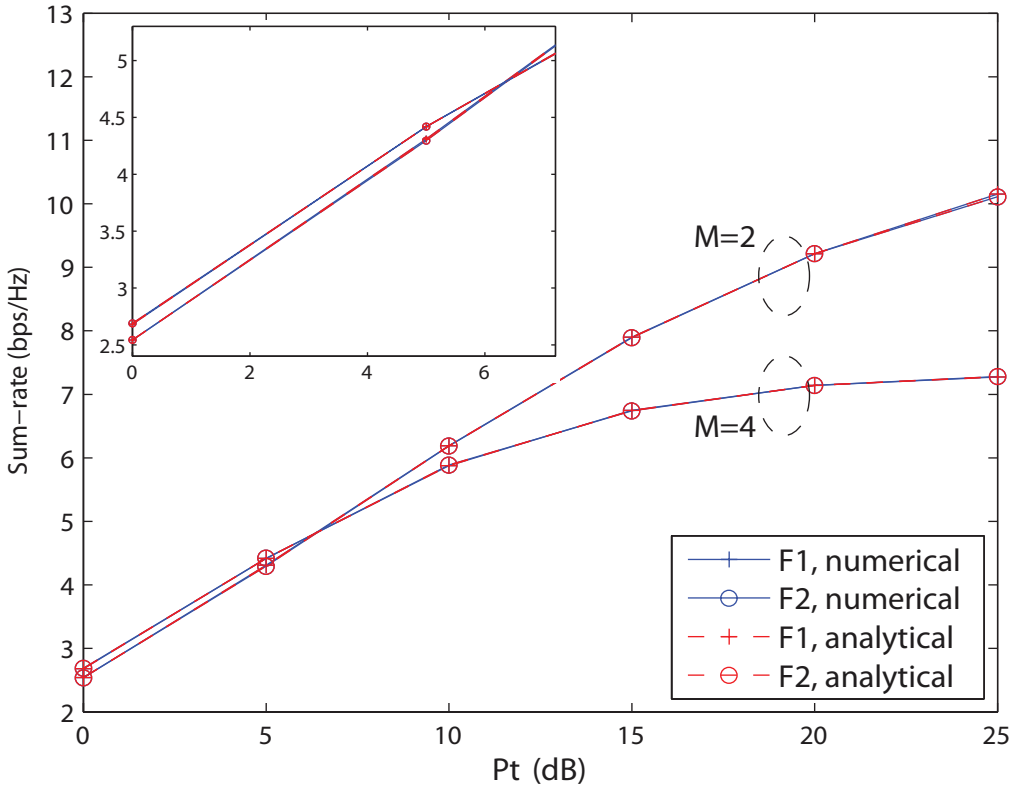

Figure 3.2: Comparison of numerical and analytical sum-rates with respect to the transmit power for $K = 25$ and $M = 2, 4$.

Chapter 4, can provide a theoretical explanation for such an observation.

3.3 Asymptotic Analysis

Accurate expressions for the achievable sum rate, albeit important, are often too complicated. To reveal more insights on the performance of single-cell RBF, asymptotic analyses have been considered in other studies. There are two main approaches, namely, large-number-of-users and large-system analyses.

3.3.1 Large Number of Users

The conventional asymptotic investigation of OBF/RBF is to consider the number of users approaches infinity for a given finite SNR. Based on *extreme value theory* [13], one of the most important results in opportunistic communication is proved in [64]. Strictly speaking, Theorem 3.3.1 only states for the single-cell RBF with the feedback scheme (F2) in [64]. However, it is easy to see that the same result applies when the scheme (F1) in Section 3.1 is considered.

Theorem 3.3.1 *([64, Theorem 1]) For fixed $M \leq N_T$ and P_T, the single-cell RBF sum rate grows double-logarithmically with respect to the number of users, i.e.,*

$$\lim_{K\to\infty} \frac{R_{RBF}}{M \log_2(1 + \frac{P_T}{M} \log K)} = 1. \tag{3.17}$$

Furthermore, in [65], Sharif *et. al.* showed that $N_T \log_2(1 + \frac{P_T}{N_T} \log K)$ is also the rate scaling law of the optimal DPC scheme assuming perfect CSI as the number of users goes to infinity, for any given user's SNR. The result is stated below

Theorem 3.3.2 *([65, Lemma 3]) For fixed number of transmit antennas N_T and transmit power P_T, the (single-cell) DPC sum-rate grows double-logarithmically with respect to the number of users, i.e.,*

$$\lim_{K\to\infty} \frac{R_{DPC}}{N_T \log_2(1 + \frac{P_T}{N_T} \log K)} = 1. \tag{3.18}$$

Essentially, the result implies that the intra-cell interference in a single-cell RBF system can be completely eliminated when the number of users is sufficiently

large, and an "interference-free" MU broadcast system is attainable. This important result therefore establishes the optimality of single-cell RBF and motivates further studies on opportunistic communication. Various MIMO-BC transmission schemes with different assumptions on the fading model, feedback scheme, user scheduling, etc., can be shown achieving $M \log_2(1 + \frac{P_T}{N_T} \log K)$ as $K \to \infty$, suggesting that it is a very universal rate scaling law. For more information, please refer to, e.g., [24] [25] [53] [68] [71] [80].

Finally, it is worth noting that the RBF sum rate grows only *logarithmically* with K when the background noise is ignored [24] [71], i.e., as $n_k = 0$, we have

$$\lim_{K \to \infty} \frac{R_{RBF}}{\frac{M}{M-1} \log_2 K} = 1. \tag{3.19}$$

This suggests that a judicious approach is required when investigating RBF under interference-limited channels such as multi-cell systems. Under such situation, the background noise is of limited importance compared with the more dominant intra-/inter-cell interference.

As an example, we compare the sum rates with the DPC and RBF schemes employed at the BS with respect to the number of users K. The parameters are $N_T = 3$, $P_T = 10$ dB. For RBF system, we assume that the feedback scheme (F1) is used. We also depict the scaling laws $N_T \log_2(1 + \frac{P_T}{N_T} \log K)$ and $\frac{N_T}{N_T - 1} \log_2 K$ as comparisons. The single-logarithmically scaling law fails to match the rate performance of the RBF scheme. However, it is observed that the double-logarithmically scaling law can capture the deceleration of the rate improvement as $K \to \infty$. More discussions on

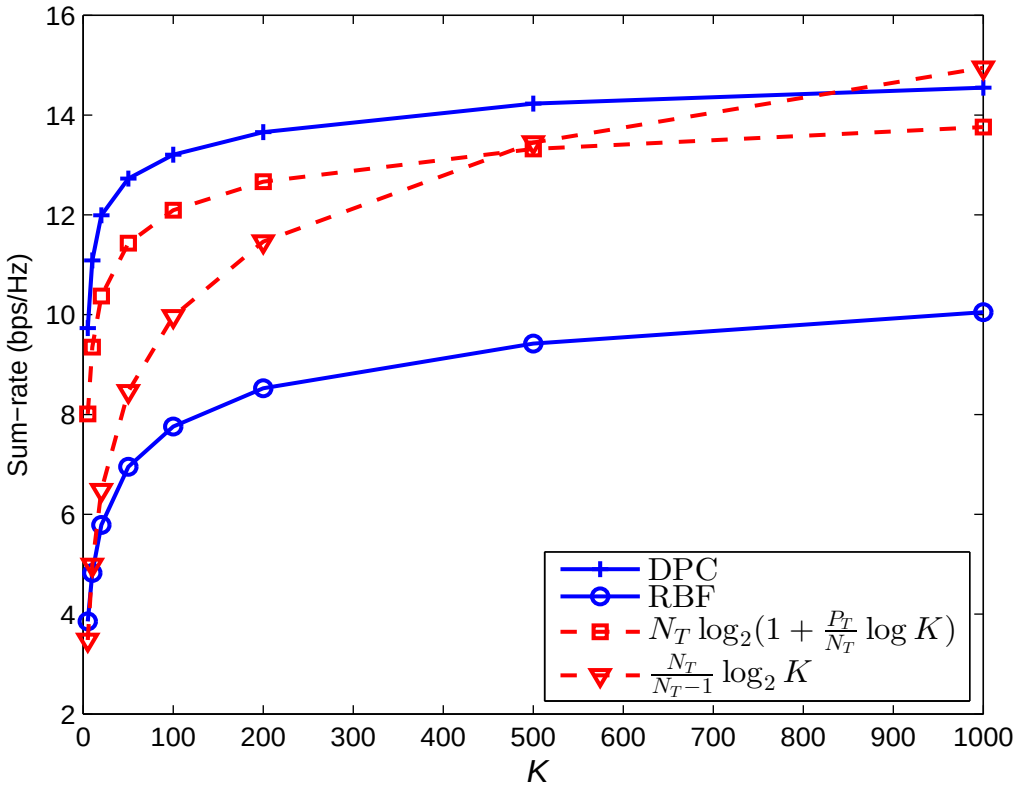

Figure 3.3: Comparison of the numerical sum-rates with DPC and RBF employed at the BS and two rate scaling laws with respect to the number of users K for $P_T = 10$ dB and $M = 3$.

the large-number-of-users analysis will be given in Chapter 4 and 5.

3.3.2 Large System

The large-system analysis, which is based on *random matrix theory* (RMT), is a well-known and widely-accepted method to investigate the performance of communication systems. A recent development of RMT is the *deterministic equivalent* approach, which overcomes some limitations of traditional RMT.

An application of the deterministic equivalent approach to single-cell RBF is introduced in [11], in which a general MIMO-BC setup with MMSE receiver and different fading models is considered. Assuming the numbers of transmit/receive antennas and data beams to approach infinity at the same time with fixed ratios for any given finite SNR, Couillet *et. al.* obtained "almost closed-form" numerical solutions which provide deterministic approximations for various performance criteria. Although these results are derived under the large-system assumption, Monte-Carlo simulations demonstrate that they can be applied to study small-dimensional systems with modest errors. Note that [11] is a major contribution to RMT and its applications do not limit to the RBF investigation only. However, [11] does not consider opportunistic scheduling, which is one of the main features of RBF.

3.4 Reduced and Quantized Feedback in OBF/RBF

In practical systems, only a limited number of bits representing the quantized channel gain/SINR can be sent from each user to the corresponding BS. Note that the feedback schemes (F1) and (F2) in Section 3.1 require the transmission of $2MK$ and $2K$ scalar values from K users, respectively, i.e., a linear increase with respect to the number of users. It is thus of great interest to develop schemes which can reduce the numbers of users and/or bits to be fed back. The idea of using only one-bit feedback is introduced in several works, e.g., [51] [60] [78]. In this scheme, the user sends "1" when the SINR value is above a pre-determined threshold, and "0" vice-versa. Since the performance

of OBF/RBF (with user scheduling) only depends on the favourable channels, one bit of feedback per user can capture almost all gain available due to the multi-user diversity. Optimal quantization strategy for OBF systems with more than one bit feedback is proposed in [51]. It is also worth noting the group random access-based feedback scheme in [66] and the multi-user diversity/throughput tradeoff analysis in [58]. The main tool to study the performance of OBF/RBF under reduced feedback schemes is the large-number-of-users analysis.

3.5 Non-Orthogonal RBF and Grassmanian Line Packing Problem

Denote the space of unit-norm transmit beamforming vectors in $\mathbb{C}^{N_T \times 1}$ as $\mathbb{O}(N_T, 1)$. A distance function of $\boldsymbol{v}_1$, $\boldsymbol{v}_2 \in \mathbb{O}(N_T, 1)$ can be defined to be the sine of the angle between them [4]

$$d(\boldsymbol{v}_1, \boldsymbol{v}_2) = sin(\boldsymbol{v}_1, \boldsymbol{v}_2) = \sqrt{1 - |\boldsymbol{v}_1^H \boldsymbol{v}_2|^2}, \tag{3.20}$$

which is known as the chordal distance. The problem of finding the packing of M unit-norm vectors in $\mathbb{C}^{N_T \times 1}$ that has the maximum minimum distance between any pair of them is called the *Grassmannian line packing problem* (GLPP). The GLPP appears in the problem of designing beamforming codebook for space-time codes (see, e.g., [23] [45] and the reference therein).

Given that the number of transmit beams is less than or equal to the number

of transmit antennas, i.e., $M \leq N_T$, any orthonormal set $\{\boldsymbol{\phi}_m\}_{m=1}^{M}$ is a solution of the GLPP. However, assuming that the BS sends $M > N_T$ beams to serve more users simultaneously and improve the fairness of the system, finding $\{\boldsymbol{\phi}_m\}_{m=1}^{M}$ is a nontrivial GLPP. The idea of using more than N_T beams in RBF is first proposed in [85] with $M = N_T + 1$, and further studied in [77]. The conclusions, however, are in distinctly sharp contrast. Particularly, Zorba *et. al.* argues that the scaling law $M \log_2 \log K$ is still true for $M = N_T + 1$ case [85], while the results in [77] imply that non-orthogonal beamforming matrix induces an interference-limited effect on the sum rate, and the multi-user diversity vanishes. Since both studies are based on approximated derivations, more rigorous investigations are necessary before any conclusion is drawn.

3.6 User Scheduling Schemes

The user-scheduling scheme described in Section 3.1 is widely used in the literature since it is simple and easy to be investigated. Consider a fading and homogeneous channel, i.e., the users' average channel gains are nearly the same while the instantaneous gains are varied after some communication time slots. The above user-scheduling scheme then ensures that each user is selected fairly in the long term.

The difficulty arises when the channel is heterogeneous and/or relatively stationary, i.e., unchanged for many time slots. To ensure the fairness, [72] proposed the "proportional fair scheduling (PFS)" scheme. The idea of the PFS is to use a

metric, which is proportional to the available data rate, and inversely proportional to the past average throughput. In each time slot, the user with the highest metric value is selected. That means:

- The selected user is the one with a high instantaneous data rate.
- The selected user is the one with a low past average throughput, i.e., he was not selected frequently in the previous time slots.

The PFS provides some sense of fairness in that users frequently in the bad channel status have low throughput which in turn tends to increase their probability of being scheduled.

The advantages and disadvantages of the PFS are:

- Advantage(s): PFS can retain the multi-user diversity gain, while still ensures a fairness to the system. This makes it superior to the traditional ones such as round-robin (RR) and opportunistic schedulers as in 3.1.
- Disadvantage(s): A small problem is that PFS requires memory to keep track of the past average throughput of each user.

It is not surprising that most of the subsequent works approach PFS from a network layer's perspective. In [2], PFS was shown to be unstable for finite queues in one case. That is, if the data for each user arrives at the BS according to a data arrival process, then all data is not transmitted in a bounded amount of time. The reason is due to the asymmetry of the network (data) flows. However, the convergence of PFS

algorithm for many-user cases under general conditions is proved in [39]. It implies that PFS is stable under many situations, and the case considered in [2] is one of few exceptions. Also, through the employment of weights, different quality of service (QoS) can be provided for different users [3]. In [75], Westphal *et al.* introduced a monitoring-based feedback algorithm to correct the unfairness of the PFS under heterogeneous systems. Finally, Zhou *et. al* introduced and investigated a global PFS for multi-cell systems [84]

3.7 Other Studies

Beam selection and beam power control algorithms for single-cell RBF are proposed in [38] [40] [71] [73]. The objective is to improve the rate performance especially when the number of users is not so large.

Single-cell RBF systems with heterogeneous users and diverse large-scale fading channel effects are first investigated in [64]. Sharif *et. al.* observes that the system becomes interference-limited when the number of transmit beams M is large enough, i.e., scaling with respect to the number of users. Under this setup, the probability of scheduling any user is asymptotically equiprobable. The problem is further studied in [27] under the case of finite M, where an alternate scheduling policy is proposed which ensures fairness while exploits multiuser diversity simultaneously.

The idea of employing a codebook of predetermined orthonormal beamforming matrices is introduced in [24] [25] [36]. While [24] [25] investigated RBF when quan-

tized, normalized channel vectors are fed back to the BS, [35] studied the codebook design problem and the rate performance assuming that opportunistic selection is also performed on the codebook. These problems are related to Section 3.4 and the GLPP in Section 3.5.

Chapter 4

Multi-Cell MISO RBF

In the previous chapter, we have summarized the most important results for single-cell MISO RBF systems. It is obvious that RBF has become an important and active research field since its introduction in [72]. However, it is surprising that there is virtually no study investigating *multi-cell* RBF systems. A notable work is [47], in which the sum-rate scaling law for the multi-cell system with RBF has been shown to be similar to the single-cell result in [64], [65] as the number of per-cell users goes to infinity, regardless of the ICI.

This chapter presents our contributions on multi-cell MISO RBF. The main results of this chapter are summarized as follows.

- **Finite-SNR Case**: We first consider the single-cell setup and show a new closed-form expression for the achievable sum-rate with RBF, based on the known distribution of the per-beam SINR given in [64]. We then study the

multi-cell RBF and derive the SINR distribution in presence of the ICI, which is a non-trivial extension of the single-cell result in [64].

Based upon this new SINR distribution, we obtain a closed-form expression of the sum-rate in the multi-cell case, and characterize the asymptotic sum-rate scaling law as the number of users per cell goes to infinity, which is shown to be identical to that for the single-cell case [64] without the ICI. Notice that the same scaling law for the multi-cell RBF has been obtained in [47] based on an approximation of the SINR distribution, while in this chapter we provide a more rigorous proof of this result using the exact SINR distribution.

- **High-SNR Case**: Although the achievable rates for the multi-cell RBF have been obtained for any given SNR with arbitrary number of users, such results do not provide any insight to the effects of the interference on the system throughput. This motivates us to investigate the multi-cell RBF for the asymptotic high-SNR regime, under the assumption that the number of users per cell scales in a given order with the per-cell SNR (a larger order indicates a higher user density in one particular cell). Under this setup, we first consider the single-cell case and derive the maximum DoF for the achievable sum-rate with RBF, which is shown to be dependent on the user density and the number of transmit antennas, and attainable with an optimal number of random beams (data streams) employed at the transmitter. The DoF analysis thus provides a succinct description of the interplay between the multiuser diversity and spatial

multiplexing gains achievable by RBF.

We then seek to obtain a general characterization of the DoF region for the multi-cell RBF, which consists of all the achievable DoF tuples for all the cells subject to their mutual ICI. Different from the existing DoF region characterization based on IA [28] for the case of finite number of users, in this chapter we address the case with an asymptotically large number of users that scales with SNR. Our results reveal that coordination among the BSs in assigning their respective number of data beams based on different per-cell user densities is essential to achieve the optimal throughput tradeoffs among different cells. Moreover, we show that the DoF region by employing the multi-cell RBF coincides with the "interference-free" DoF region upper bound and thus is the exact DoF region of a multi-cell downlink system, when the user densities in different cells are sufficiently large. This result is in sharp contrast with existing studies on the achievable DoF region with the full transmitter CSI obtained by schemes such as IA [28].

The rest of the chapter is organized as follows. Section 4.1 describes the multi-cell downlink system model and the multi-cell RBF scheme. Section 4.2 studies the sum-rate for both single- and multi-cell RBF systems with finite SNR. Section 4.3 characterizes the achievable DoF for single-cell RBF as well as the DoF region for multi-cell RBF at the high-SNR regime. We conclude the chapter with some final remarks in Section 4.4.

4.1 System Model

We consider a multi-cell downlink system consisting of C cells, each of which has a BS with N_T antennas to coordinate the transmission with K_c single-antenna mobile stations (MSs), $K_c \geq 1$ and $c = 1, \cdots, C$. In the c-th cell, the c-th BS transmits $M_c \leq N_T$ orthonormal beams and selects M_c from K_c users for transmission at each time. We assume the channels to be flat-fading and constant over each transmission period of interest. For the ease of analysis, we also assume a "homogeneous" channel setup, i.e., the average signal attenuation from a BS to any user of the same cell have the same values, in which the received baseband signal of user k in the c-th cell is given by

$$y_k^{(c)} = \boldsymbol{h}_k^{(c,c)} \sum_{m=1}^{M_c} \boldsymbol{\phi}_m^{(c)} s_m^{(c)} + \sum_{l=1,\ l\neq c}^{C} \sqrt{\gamma_{l,c}} \boldsymbol{h}_k^{(l,c)} \sum_{m=1}^{M_l} \boldsymbol{\phi}_m^{(l)} s_m^{(l)} + n_k^{(c)}, \tag{4.1}$$

where $\boldsymbol{h}_k^{(l,c)} \in \mathbb{C}^{1\times M_l}$ is the channel vector from the l-th BS to the k-th user of the c-th cell; it is assumed that all the elements of $\boldsymbol{h}_k^{(l,c)}$ are i.i.d. $\mathcal{CN}(0,1)$; $0 \leq \gamma_{l,c} < 1$ stands for the distance-dependent signal attenuation from the l-th BS to any user in the c-th cell, $l \neq c$, which is less than the assumed unit direct channel gain from the c-th BS[1]; $\boldsymbol{\phi}_m^{(c)} \in \mathbb{C}^{M_c\times 1}$ and $s_m^{(c)}$ are the m-th randomly generated beamforming

[1]This homogeneous channel setup is required to obtain the closed-form expressions for the achievable sum-rates at finite SNRs, as will be detailed in Section 4.2. However, the DoF region analysis for the asymptotically high-SNR regime as will be given in Section 4.3 of the chapter can be shown to hold even without the homogeneous channel assumption, i.e., the average signal attenuation from any BS to any user of any cell can take different values. Also note that Lemma 4.2.2 can be extended to the case of arbitrary signal attenuation as well.

vector of unit norm and transmitted data symbol from the c-th BS, respectively; it is assumed that each BS has the total sum power, P_T, i.e., $\boldsymbol{Tr}\left(\mathbb{E}[\boldsymbol{s}_c\boldsymbol{s}_c^H]\right) \leq P_T$, where $\boldsymbol{s}_c = [s_1^{(c)}, \cdots, s_{M_c}^{(c)}]^T$; it is also assumed that the background noise is AWGN, $n_k^{(c)} \sim \mathcal{CN}(0, \sigma^2)$, $\forall k, c$. In the c-th cell, the total SNR, the SNR per beam, and the interference-to-noise ratio (INR) per beam from the l-th cell, $l \neq c$, are denoted as $\rho = P_T/\sigma^2$, $\eta_c = P_T/(M_c\sigma^2)$, and $\mu_{l,c} = \gamma_{l,c}P_T/(M_l\sigma^2)$, respectively.

In this chapter, we consider a multi-cell RBF scheme, in which all BSs in different cells are assumed to be able to implement the conventional single-cell RBF similarly to that given in [64] at the same time, which is described as follows:

- In the training phase, the c-th BS generates M_c orthonormal beams, $\boldsymbol{\phi}_1^{(c)}$, $\cdots$,$\boldsymbol{\phi}_{M_c}^{(c)}$, and uses them to broadcast the training signals to all users in the c-th cell. The total power of each BS is assumed to be distributed equally over M_c beams.

- Each user in the c-th cell measures the SINR value for each of M_c beams (shown in (4.2) below), and feeds it back to the corresponding BS.

$$\begin{aligned}\mathrm{SINR}_{k,m}^{(c)} &= \frac{\frac{P_T}{M_c}\left|\boldsymbol{h}_k^{(c,c)}\boldsymbol{\phi}_m^{(c)}\right|^2}{\sigma^2 + \frac{P_T}{M_c}\sum\limits_{i=1,i\neq m}^{M_c}\left|\boldsymbol{h}_k^{(c,c)}\boldsymbol{\phi}_i^{(c)}\right|^2 + \sum\limits_{l=1,l\neq c}^{C}\gamma_{l,c}\frac{P_T}{M_l}\sum\limits_{i=1}^{M_l}\left|\boldsymbol{h}_k^{(l,c)}\boldsymbol{\phi}_i^{(l)}\right|^2} \\ &= \frac{\eta_c\left|\boldsymbol{h}_k^{(c,c)}\boldsymbol{\phi}_m^{(c)}\right|^2}{1 + \eta_c\sum\limits_{i=1,i\neq m}^{M_c}\left|\boldsymbol{h}_k^{(c,c)}\boldsymbol{\phi}_i^{(c)}\right|^2 + \sum\limits_{l=1,l\neq c}^{C}\mu_{l,c}\sum\limits_{i=1}^{M_l}\left|\boldsymbol{h}_k^{(l,c)}\boldsymbol{\phi}_i^{(l)}\right|^2},\end{aligned} \tag{4.2}$$

where $m = 1, \cdots, M_c$. Essentially, this is the multi-cell extension of the feedback scheme (F1) described in Section 3.1, which is for the single-cell case.

- The c-th BS schedules transmission to a set of M_c users at each time by assigning its m-th beam to the user with the highest SINR, i.e.,

$$k_m^{(c)} = \arg \max_{k \in \{1, \cdots, K_c\}} \text{SINR}_{k,m}^{(c)}. \tag{4.3}$$

Thus, the achievable average sum-rate in bits-per-second-per-Hz (bps/Hz) of the c-th cell is given by

$$R_{\text{RBF}}^{(c)} = \mathbb{E}\left[\sum_{m=1}^{M_c} \log_2\left(1 + \text{SINR}_{k_m^{(c)},m}^{(c)}\right)\right] = M_c \mathbb{E}\left[\log_2\left(1 + \text{SINR}_{k_1^{(c)},1}^{(c)}\right)\right]. \tag{4.4}$$

4.2 Achievable Rate of Multi-Cell Random Beamforming: Finite-SNR Analysis

In this section, we study the achievable sum-rate of a C-cell RBF system with finite SNR. We first derive a closed-form expression of the sum-rate for the single-cell case, then extend the result to the multi-cell case subject to ICI, and finally investigate the asymptotic sum-rate scaling law as the number of users per cell goes to infinity.

4.2.1 Single-Cell RBF

We first consider the single-cell case, and drop the cell index c for brevity. Thus, (4.2) and (4.4) reduce to

$$\text{SINR}_{k,m} = \frac{\frac{P_T}{M} \left|\boldsymbol{h}_k \boldsymbol{\phi}_m\right|^2}{\sigma^2 + \frac{P_T}{M} \sum_{i=1, i \neq m}^{M} \left|\boldsymbol{h}_k \boldsymbol{\phi}_i\right|^2}, \tag{4.5}$$

$$R_{\text{RBF}} = M\mathbb{E}\left\{\log_2\left(1+\max_{k\in\{1,\cdots,K\}}\text{SINR}_{k,1}\right)\right\}. \tag{4.6}$$

The PDF and CDF of $S := \text{SINR}_{k,m}, \forall k, m$ can be expressed as [64]

$$f_S(s) = \frac{e^{-s/\eta}}{(s+1)^M}\left(M-1+\frac{s+1}{\eta}\right), \tag{4.7}$$

$$F_S(s) = 1 - \frac{e^{-s/\eta}}{(s+1)^{M-1}}, \tag{4.8}$$

where $\eta = P_T/(M\sigma^2)$ is the SNR per beam. A closed-form expression for the sum-rate R_{RBF} is then given in the following lemma.

Lemma 4.2.1 *The average sum-rate of the single-cell RBF is given by*

$$R_{RBF} = \frac{M}{\log 2}\sum_{n=1}^{K}(-1)^n\binom{K}{n}\left[\left(-\frac{n}{\eta}\right)^{n(M-1)}\frac{e^{n/\eta}Ei(-n/\eta)}{(n(M-1))!} - \sum_{m=1}^{n(M-1)}\left(-\frac{n}{\eta}\right)^{m-1}\frac{(n(M-1)-m)!}{(n(M-1))!}\right], \tag{4.9}$$

where $Ei(x) = \int_{-\infty}^{x}\frac{e^t}{t}dt$ is the exponential integral function.

Proof 1 *Please refer to Appendix B.1.*

4.2.2 Multi-Cell RBF

For the single-cell RBF case, the SINR distributions given in (4.7) and (4.8) were obtained in prior work [64]. Now consider the multi-cell RBF case. If $\mu_{l,c} = \eta_c$, $\forall l \in \{1,\cdots,C\}\setminus\{c\}$, it is easy to see that the SINR distributions take the same forms as (4.7) and (4.8). However, if $\exists l \in \{1,\cdots,C\}\setminus\{c\}$ such that $\mu_{l,c} \neq \eta_c$, then the derivation of the SINR distributions in the multi-cell case becomes a new task due

to the unevenly distributed ICI. Note that no closed-form expressions for the PDF and CDF of the SINR in this general case are available in the literature, while only approximated ones have been obtained (see, e.g., [47]). Therefore, in this subsection we first show a lemma on the exact SINR distributions for the multi-cell RBF, and then use them to investigate the achievable rate of this scheme.

Lemma 4.2.2 *In the multi-cell RBF, the PDF and CDF of the SINR* $S := SINR_{k,m}^{(c)}$, $\forall k, m$, *are given by*[2]

$$f_S^{(c)}(s) = \frac{e^{-s/\eta_c}}{(s+1)^{M_c-1}\prod_{l=1,l\neq c}^{C}\left(\frac{\mu_{l,c}}{\eta_c}s+1\right)^{M_l}}\left[\frac{1}{\eta_c}+\frac{M_c-1}{s+1}+\sum_{l=1,l\neq c}^{C}\frac{M_l}{s+\frac{\eta_c}{\mu_{l,c}}}\right], \quad (4.10)$$

$$F_S^{(c)}(s) = 1-\frac{e^{-s/\eta_c}}{(s+1)^{M_c-1}\prod_{l=1,l\neq c}^{C}\left(\frac{\mu_{l,c}}{\eta_c}s+1\right)^{M_l}}. \quad (4.11)$$

Proof 2 *Please refer to Appendix B.2.*

It is worth noting that Lemma 4.2.2 nicely extends the single-cell results in (4.7) and (4.8), and clearly demonstrates the effect of ICI on the resulting SINR distributions. In Fig. 4.1, we compare the analytical and numerical SINR CDFs to confirm the validity of Lemma 4.2.2. We consider the SINR CDF of the first cell for two RBF systems with the following parameters: (1) $\eta_1 = 30$dB, $M_1 = 4$, $[\mu_{2,1}, \mu_{3,1}] = [-3, 3]$dB, $[M_2, M_3] = [2, 4]$; and (2) $\eta_1 = 20$dB, $M_1 = 6$, $[\mu_{2,1}, \mu_{3,1}, \mu_{4,1}] = [-3, 2, 3]$dB,

[2]Although Lemma 4.2.2 can be considered as a consequence of Corollary 5.2.1, some steps in its derivation are required to obtain Theorem 5.2.2. Furthermore, the direct proof of Lemma 4.2.2, as shown in Appendix B.2, is more concise and elementary than that of Corollary 5.2.1.

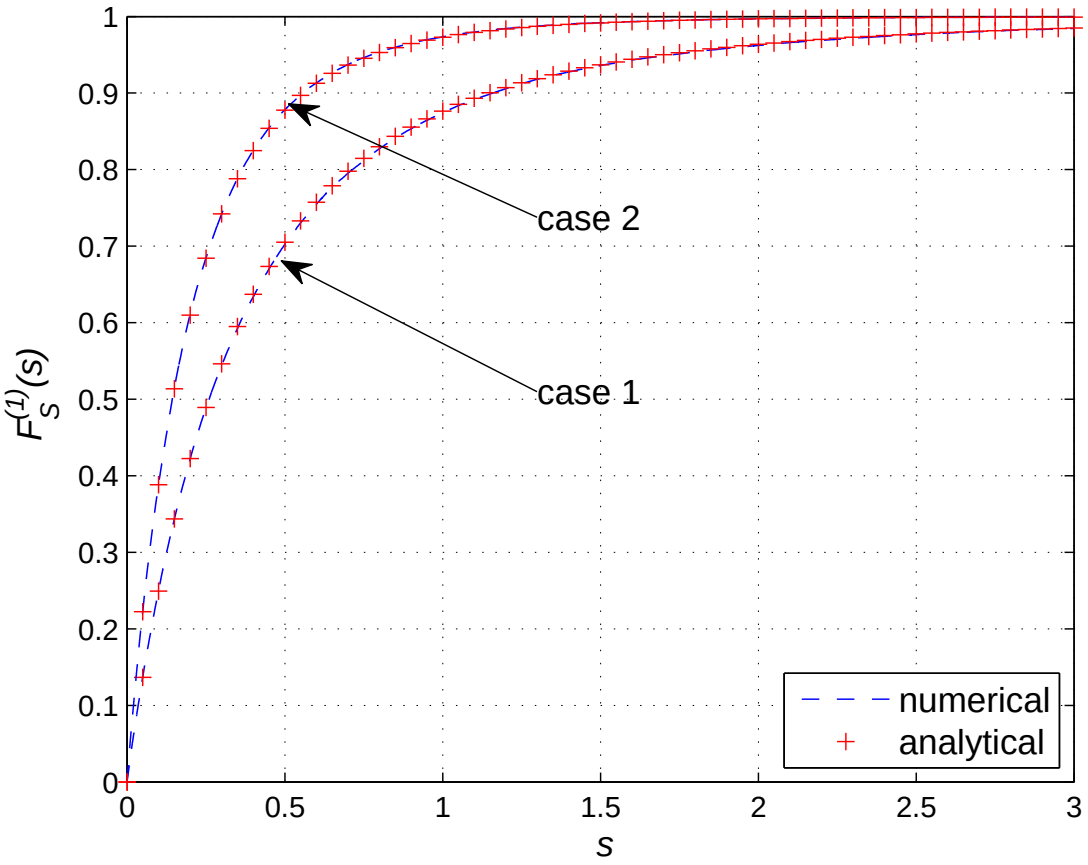

Figure 4.1: Comparison of the analytical and numerical CDFs of the per-cell SINR.

$[M_2, M_3, M_4] = [2, 3, 4]$. It is observed that both analytical and numerical results match closely, thus justifying our derivation.

With Lemma 4.2.2, Lemma 4.2.1 is readily generalized to the multi-cell case in the following theorem.

Theorem 4.2.1 *Denote the total sum-rate of a C-cell RBF system as $\sum_{c=1}^{C} R_{RBF}^{(c)}$, where the individual sum-rate of the c-th cell, $R_{RBF}^{(c)}$, is given by*

$$R_{RBF}^{(c)} = \frac{M_c}{\log 2}\sum_{n=1}^{K_c}(-1)^n\binom{K_c}{n}\prod_{l=1,l\neq c}^{C}\left(\frac{\eta_c}{\mu_{l,c}}\right)^{nM_l}\times$$
$$\left\{\sum_{p=1}^{n(M_c-1)+1}\frac{A_{n,c,p}}{(p-1)!}\left[e^{\frac{n}{\eta_c}}\left(-\frac{n}{\eta_c}\right)^{p-1}Ei\left(-\frac{n}{\eta_c}\right)-\sum_{m=1}^{p-1}\left(-\frac{n}{\eta_c}\right)^{m-1}(p-1-m)!\right]\right.$$
$$+\sum_{l=1,l\neq c}^{C}\sum_{q=1}^{nM_l}\frac{A_{n,l,q}}{(q-1)!}\left[e^{\frac{n}{\mu_{l,c}}}\left(-\frac{n}{\eta_c}\right)^{q-1}Ei\left(-\frac{n}{\mu_{l,c}}\right)\right.$$
$$\left.\left.-\sum_{m=1}^{q-1}\left(-\frac{n}{\eta_c}\right)^{m-1}\left(\frac{\mu_{l,c}}{\eta_c}\right)^{q-m}(q-1-m)!\right]\right\}, \quad (4.12)$$

where $A_{n,c,p}$'s and $A_{n,l,q}$'s are the coefficients from the following partial fractional decomposition:

$$\frac{1}{(x+1)^{n(M_c-1)+1}\prod_{l\neq c}^{C}\left(x+\frac{\eta_c}{\mu_{l,c}}\right)^{nM_l}} = \sum_{p=1}^{n(M_c-1)+1}\frac{A_{n,c,p}}{(x+1)^p}+\sum_{l=1,l\neq c}^{C}\sum_{q=1}^{nM_l}\frac{A_{n,l,q}}{\left(x+\frac{\eta_c}{\mu_{l,c}}\right)^q}, \quad (4.13)$$

and given by [20, 2.102]:

$$A_{n,c,p} = \frac{1}{(n(M_c-1)-p+1)!}\frac{d^{n(M_c-1)-p+1}}{dx^{n(M_c-1)-p+1}}\left[\frac{1}{\prod_{l\neq c}^{C}\left(x+\frac{\eta}{\mu_l}\right)^{nM_l}}\right]\Bigg|_{x=-1}, \quad (4.14)$$

$$A_{n,l,q} = \frac{1}{(nM_l-q)!}\frac{d^{nM_l-q}}{dx^{nM_l-q}}\left[\frac{1}{(x+1)^{n(M_c-1)+1}\prod_{t\neq l,c}^{C}\left(x+\frac{\eta}{\mu_t}\right)^{nM_t}}\right]\Bigg|_{x=-\eta_c/\mu_{l,c}}. \quad (4.15)$$

Proof 3 *Please refer to Appendix B.3.*

In Fig. 4.2, we show the analytical and numerical results on the RBF sum-rate as a function of the number of users for both single-cell and two-cell systems.We also compare the approximation obtained in [36], which is only applicable to the

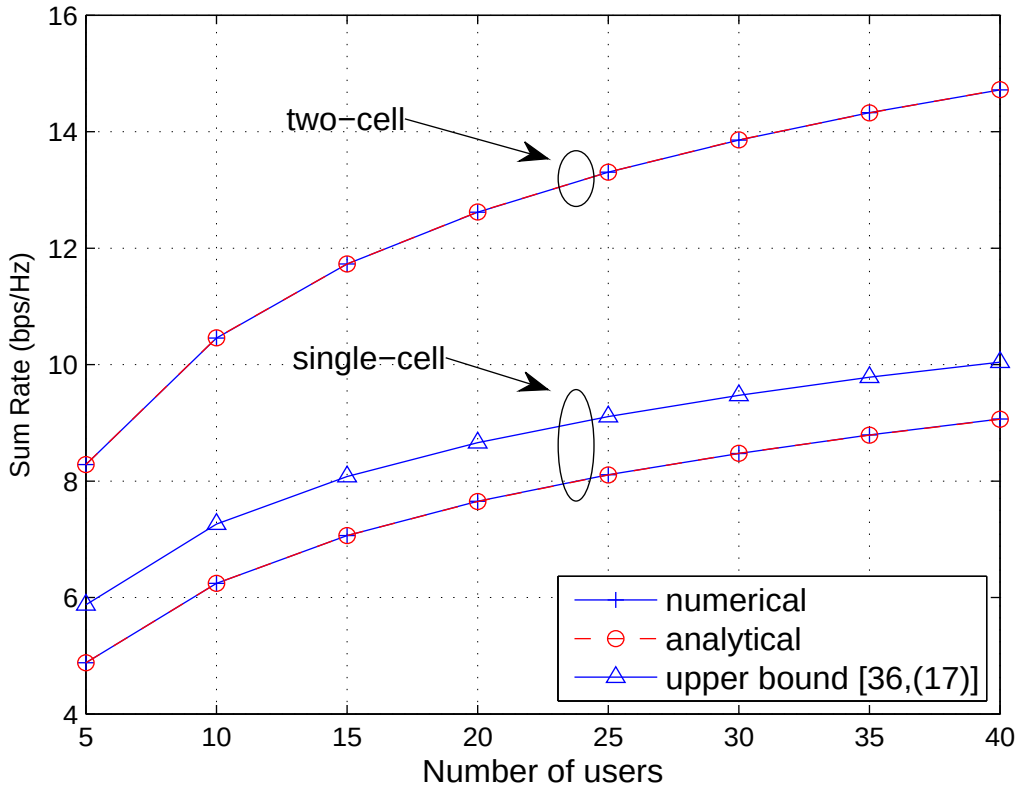

Figure 4.2: Comparison of the analytical and numerical results on the RBF sum-rate.

single-cell system. In the single-cell case, $M = N_T = 3$, $\eta = 20$ dB, while in the two-cell case, $K_1 = K_2$, $M_1 = M_2 = N_T = 3$, $\eta_1 = \eta_2 = 20$ dB, $\mu_{2,1} = 6$ dB, and $\mu_{1,2} = 10$ dB. It is observed that the approximation [36, (17)] is only an upper bound of the achievable sum-rate. In contrast, the sum-rate expressions in (4.9) and (4.12) are exact. Thus, it is feasible to use Theorem 4.2.1 to characterize all the sum-rate tradeoffs among different cells in a multi-cell RBF system, which leads to the achievable rate region. However, such a characterization requires intensive computations, and does not provide any useful insight. In Section 4.3, we adopt an

alternative approach based on the DoF region to provide a more efficient as well as insightful tradeoff analysis for the multi-cell RBF.

4.2.3 Asymptotic Sum Rate as $K_c \to \infty$

It is worth noting that a conventional asymptotic investigation of RBF is to consider the case when the number of users per cell approaches infinity for a given finite SNR. Consider the single-cell RBF case with $M \leq N_T$ transmit beams and K single-antenna users. The scaling law of the sum-rate is shown to be $M \log_2 \log K$ as $K \to \infty$ with any fixed SNR, ρ, in [64], [65] (see Section 3.3). An attempt to extend this result to the multi-cell RBF case has been made in [47] based on an approximation of the SINR's PDF (which is applicable if the SNR and INRs are all roughly equal), by showing that the same asymptotic sum-rate $M_c \log_2 \log K_c$ for each individual cell holds as the single-cell case. However, we note that with the exact SINR distributions in Lemma 4.2.2, a more rigorous proof can be obtained, as given in the following proposition.

Proposition 4.2.1 *For fixed M_c's and P_T, $c = 1, \cdots, C$, we have*

$$\lim_{K_c \to \infty} \frac{R_{RBF}^{(c)}}{M_c \log_2(\eta_c \log K_c)} = 1. \tag{4.16}$$

Proof 4 *Please refer to Appendix B.4.*

In Fig. 4.3, we depict both the numerical and theoretical asymptotic sum-rates for a single-cell RBF system, and the cells of a two-cell RBF system. In the single-cell case, $\eta = 5$ dB, and $M = N_T = 3$, while in the two-cell case, $M_1 = M_2 = N_T = 3$,

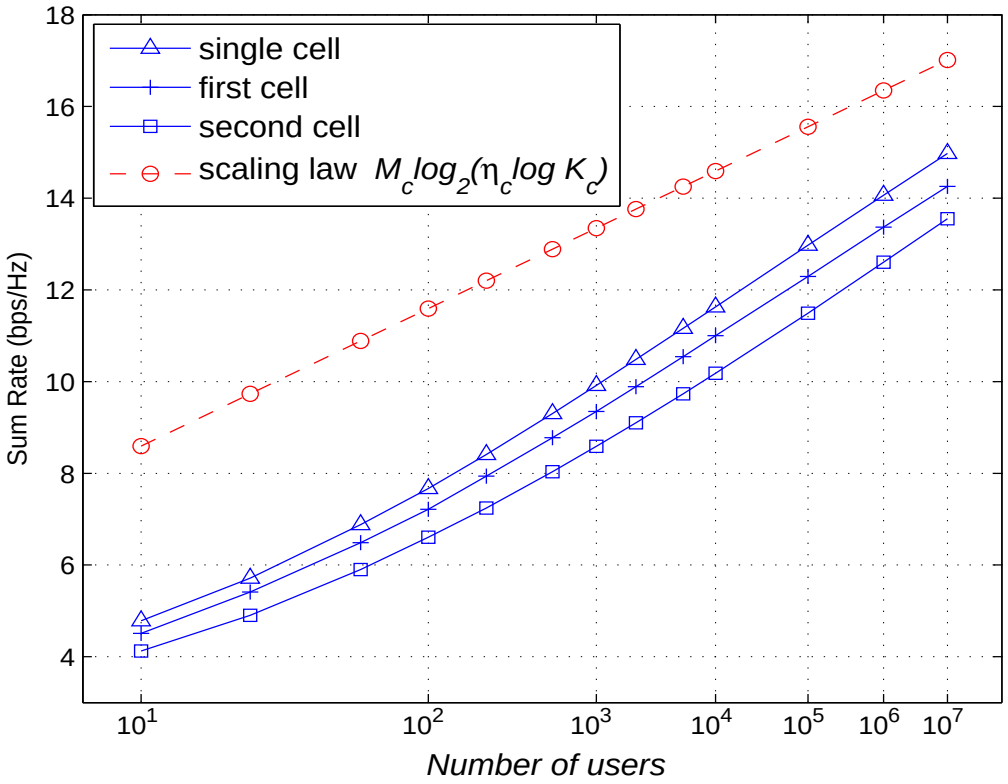

Figure 4.3: Comparison of the numerical sum-rate and the sum-rate scaling law for RBF.

$\eta_1 = \eta_2 = 5$ dB, and $\left[\mu_{2,1}, \mu_{1,2}\right] = [-10, -5]$ dB. We observe that the convergence to the sum-rate scaling law $M_c \log_2(\eta_c \log K_c)$ is rather slow in both cases. For example, even with K or K_c to be 10^4, the convergence is still not clearly shown. Furthermore, Proposition 4.2.1 implies that the sum-rate scaling law $M_c \log_2(\eta_c \log K_c)$ holds for any cell regardless of the ICI as $K_c \to \infty$. As a consequence, this result implies that each BS should apply the maximum number of transmit beams, i.e., $M_c = N_T, \forall c$, to maximize the per-cell throughput. Such a conclusion may be misleading in a practical multi-cell system with non-negligible ICI. The above two main drawbacks, namely,

slow convergence and misleading interpretation, have limited the usefulness of the conventional sum-rate scaling law $M_c \log_2(\eta_c \log K_c)$ for the multi-cell RBF. As will be shown in the next section, the DoF region approach is able to more precisely characterize the ICI effect on the throughput of the multi-cell RBF.

4.3 Degrees of Freedom Region in Multi-Cell Random Beamforming: High-SNR Analysis

In this section, we investigate the performance of the multi-cell RBF in the high-SNR regime, i.e., when the per-cell SNR $\rho \to \infty$. In particular, we consider the approach of the DoF region, which has been defined in Section 1.2.1.

If the multi-cell RBF is deployed, the achievable DoF region defined in (1.6) is reduced to

Definition 4.3.1 *(DoF region with RBF) The DoF region of a C-cell RBF system is given by*

$$\mathcal{D}_{RBF} = \Bigg\{ (d_1, d_2, \cdots, d_C) \in \mathbb{R}_+^C : \forall (\omega_1, \omega_2, \cdots, \omega_C) \in \mathbb{R}_+^C; \sum_{c=1}^{C} \omega_c d_c \leq \lim_{\rho \to \infty} \max_{M_1, \ldots, M_C \in \{0, \cdots, N_T\}} \sum_{c=1}^{C} \omega_c \frac{R_{RBF}^{(c)}}{\log_2 \rho} \Bigg\}. \quad (4.17)$$

Certainly, $\mathcal{D}_{RBF} \subseteq \mathcal{D}$. Note that the DoF region is, in general, applicable for any number of users per cell, K_c. However, if it is assumed that all K_c's are constant with $\rho \to \infty$, it can be shown that the DoF region for the multi-cell RBF given in (4.17) will collapse to the null point, i.e., a zero DoF for all the cells, due to

the intra-/inter-cell interference[3]. It means that for RBF systems, a large number of users is more preferable than a large SNR value. It thus follows that for analytical tractability, the DoF region characterization for the multi-cell RBF should have K_c increase in a certain order with the SNR, ρ. We thus make the following assumption for the rest of this chapter:

Assumption 4.3.1 *The number of users in each cell scales with ρ in the order of ρ^{α_c}, with $\alpha_c \geq 0$, denoted by $K_c = \Theta(\rho^{\alpha_c}), c = 1, \ldots, C$, i.e., $K_c/\rho^{\alpha_c} \to a_c$ as $\rho \to \infty$, with a_c being a positive constant independent of α_c.*

Considering the number of per-cell users to scale polynomially with the SNR is general as well as convenient. The linear scaling law, i.e., $K_c = \beta_c \rho$, with constant $\beta_c > 0$, is only a special case of $K_c = \Theta(\rho^{\alpha_c})$ with $\alpha_c = 1$; if K_c is a constant, then the corresponding α_c is zero. We can thus consider α_c as a measure of the user density in the c-th cell given the same coverage area for all the cells, where a larger α_c indicates a higher number of users, K_c. As will be shown later in this section, Assumption 4.3.1 enables us to obtain an efficient as well as insightful characterization of the DoF region for the multi-cell RBF. Note that the DoF region under Assumption 4.3.1 can be considered as a generalization of the conventional DoF region analysis based on IA [28] for the case of finite number of users, to the case of asymptotically large number of users that scales with the SNR. For the notational convenience, we use

[3]A rigorous proof of this claim can be deduced from Lemma 4.3.2 and Theorem 4.3.2 later for the special case of $\alpha_c = 0$, $\forall c$, i.e., all cells having a constant number of users.

$\mathcal{D}(\boldsymbol{\alpha})$ and $\mathcal{D}_{RBF}(\boldsymbol{\alpha})$ to denote the achievable DoF regions $\mathcal{D}$ and $\mathcal{D}_{RBF}$, respectively, corresponding to $K_c = \Theta(\rho^{\alpha_c})$, $c = 1,\cdots,C$, and $\boldsymbol{\alpha} = [\alpha_1, \cdots, \alpha_C]^T$.

4.3.1 Single-Cell Case

First, we investigate the DoF for the achievable sum-rate in the single-cell RBF case without the ICI. We drop the cell index c for brevity. In the single-cell case, the DoF region collapses to a line, bounded by 0 and $d^*_{RBF}(\alpha)$, where $d^*_{RBF}(\alpha) \geq 0$ denotes the maximum DoF achievable for the RBF sum-rate.

We define the achievable DoF for single-cell RBF with a given pair of α and M as

$$d_{RBF}(\alpha, M) = \lim_{\rho\to\infty} \frac{R_{\text{RBF}}}{\log_2 \rho} = \lim_{\eta\to\infty} \frac{R_{\text{RBF}}}{\log_2 \eta} \tag{4.18}$$

since $\eta = \rho/M$. Thus, we have $d^*_{RBF}(\alpha) = \max\limits_{M\in\{1,\cdots,N_T\}} d_{RBF}(\alpha, M)$ for a given $\alpha \geq 0$. We first characterize $d_{RBF}(\alpha, M)$ in the following lemma.

Lemma 4.3.1 *Assuming $K = \Theta(\rho^{\alpha})$, the DoF of single-cell RBF with $M \leq N_T$ orthogonal transmit beams is given by*

$$d_{RBF}(\alpha, M) = \begin{cases} \dfrac{\alpha M}{M-1}, & 0 \leq \alpha \leq M-1, \quad (4.19a) \\ M, & \alpha > M-1. \quad (4.19b) \end{cases}$$

Proof 5 *Please refer to Appendix B.5.*

Remark 4.3.1 *With RBF and under the assumption $K = \Theta(\rho^{\alpha})$, it is interesting to observe from Lemma 4.3.1 that the achievable DoF can be a non-negative real number (as compared to the conventional integer DoF in the literature with finite K).*

Moreover, it is observed that for any given $0 < \alpha < N_T - 1$*, assigning more transmit beams by increasing* M *initially improves the sum-rate DoF if* $M \leq \alpha + 1$*; however, as* $M > \alpha + 1$*, the DoF may not necessarily increase with* M *due to the more dominant inter-beam/intra-cell interference. Note that the term* $M - 1$ *in the denominator of (4.19a) is exactly the number of interfering beams to one particular data beam. Thus, Lemma 4.3.1 provides a succinct description of the interplay between the available multiuser diversity (specified by* α *with a larger* α *denoting a higher user density or the number of users in a cell), the level of the intra-cell interference (specified by* $M - 1$*), and the achievable spatial multiplexing gain or DoF,* $d_{RBF}(\alpha, M)$*.*

Next, we obtain the maximum achievable DoF for a given α by searching over all possible values of M. We note that for any $M < \lfloor \alpha \rfloor + 1$, $d_{RBF}(\alpha, M) < d_{RBF}(\alpha, \lfloor \alpha \rfloor + 1)$, while for any $M > \lfloor \alpha \rfloor + 2$, $d_{RBF}(\alpha, M) < d_{RBF}(\alpha, \lfloor \alpha \rfloor + 2)$. Thus we only need to compare $d_{RBF}(\alpha, \lfloor \alpha \rfloor + 1)$ and $d_{RBF}(\alpha, \lfloor \alpha \rfloor + 2)$ in searching for the optimal M. A detailed proof is omitted for brevity. The result is shown in the following theorem.

Theorem 4.3.1 *For the single-cell RBF with* N_T *transmit antennas and user density coefficient* α*, the maximum achievable DoF and the corresponding optimal number of transmit beams are*[4]

[4]The notations $\lfloor \alpha \rfloor$ and $\{\alpha\}$ denote the integer and fractional parts of a real number α, respectively.

$$d^*_{RBF}(\alpha) = \begin{cases} \lfloor \alpha \rfloor + 1, & \alpha \leq N_T - 1, 1 \geq \{\alpha\}(\lfloor \alpha \rfloor + 2), \\ \frac{\alpha(\lfloor \alpha \rfloor + 2)}{\lfloor \alpha \rfloor + 1}, & \alpha \leq N_T - 1, \{\alpha\}(\lfloor \alpha \rfloor + 2) > 1, \\ N_T, & \alpha > N_T - 1. \end{cases} \tag{4.20}$$

$$M^*_{RBF}(\alpha) = \begin{cases} \lfloor \alpha \rfloor + 1, & \alpha \leq N_T - 1, 1 \geq \{\alpha\}(\lfloor \alpha \rfloor + 2), \\ \lfloor \alpha \rfloor + 2, & \alpha \leq N_T - 1, \{\alpha\}(\lfloor \alpha \rfloor + 2) > 1, \\ N_T, & \alpha > N_T - 1. \end{cases} \tag{4.21}$$

In Fig. 4.4, we use simulations to confirm Lemma 4.3.1. It is observed that the newly obtained sum-rate scaling law, $R_{\text{RBF}} = d_{RBF}(\alpha, M) \log_2 \rho$, in the single-cell RBF case is very accurate, even for small values of SNR ρ and number of users $K = \lfloor \rho^{\alpha} \rfloor$. Compared with Fig. 4.3 for the conventional scaling law $R_{\text{RBF}} = M \log_2(\eta \log K)$, a much quicker convergence is observed here. The DoF approach thus provides a more efficient way of characterizing the achievable sum-rate for single-cell RBF. Also observe that the sum-rate for $M = 2$ is higher than that for $M = 4$. This is because with $N_T = 4$ and $\alpha = 1$ in this example, the optimal number of beams to achieve $d^*_{RBF}(1) = 2$ is $M^*_{RBF}(1) = 2$ from (4.21). Since many previous studies have observed that adjusting the number of beams according to the number of users in single-cell RBF can improve the achievable sum-rate (see, e.g., [38]) [71] [73], our result here can be considered as a theoretical explanation for such an observation.

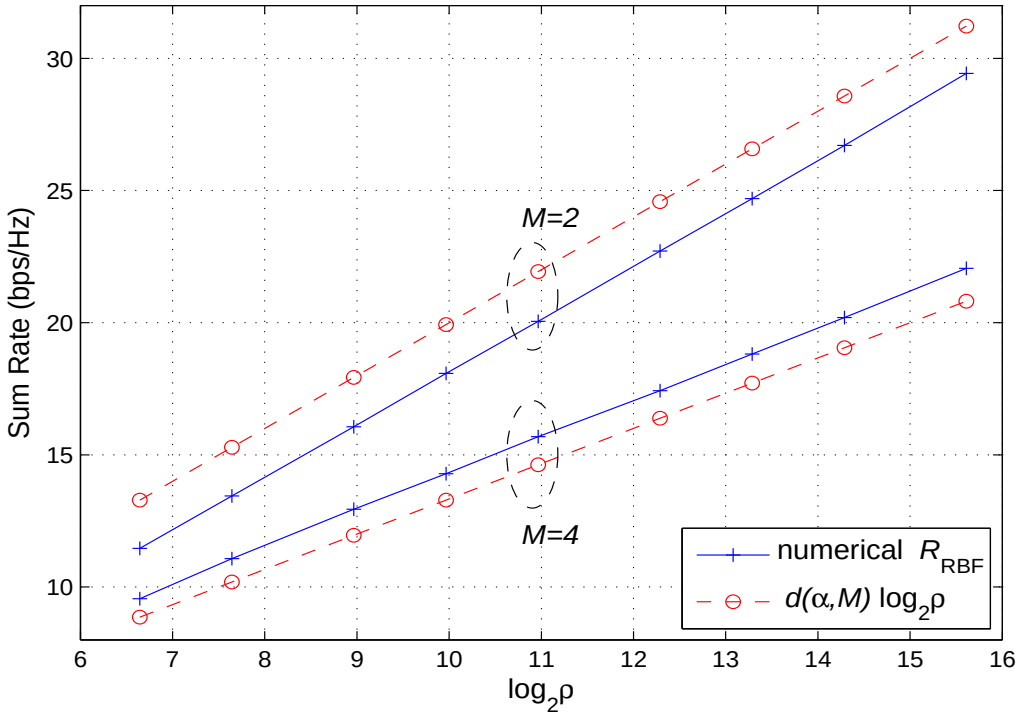

Figure 4.4: Comparison of the numerical sum-rate and the scaling law $d_{RBF}(\alpha, M)\log_2\rho$, with $N_T = 4$, $\alpha = 1$, and $K = \lfloor \rho^{\alpha} \rfloor$.

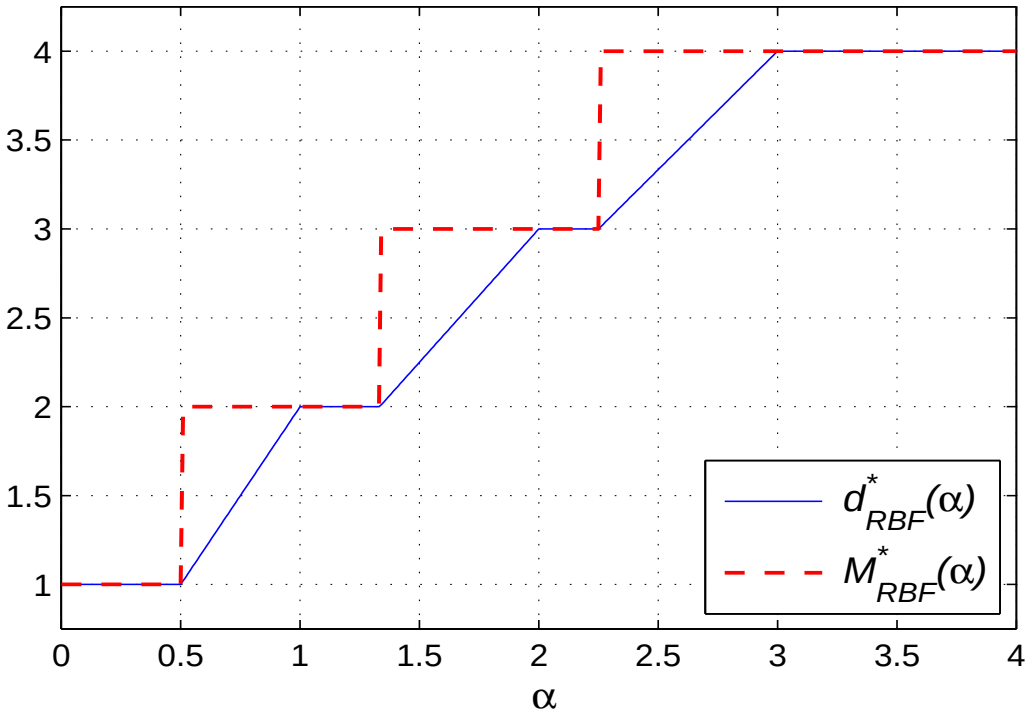

Figure 4.5: The maximum DoF $d^*_{RBF}(\alpha)$ and optimal number of beams $M^*_{RBF}(\alpha)$ with $N_T = 4$.

In Fig. 4.5, we show the maximum DoF and the corresponding optimal number of transmit beams versus the user density coefficient α with $N_T = 4$ for single-cell RBF, according to Theorem 4.3.1. It is observed that to maximize the achievable sum-rate, we should only transmit more data beams when the number of users increases beyond a certain threshold. It is also observed that the maximum DoF $d^*_{RBF}(\alpha) = 4$ with $M = N_T = 4$ is attained when $\alpha \geq 3$ since $M^*_{RBF}(3) = 4$.

4.3.2 Multi-Cell Case

In this subsection, we extend the DoF analysis for the single-cell RBF to the more general multi-cell RBF subject to the ICI. For convenience, we denote the achievable sum-rate DoF of the c-th cell as $d_{RBF,c}(\alpha_c, \boldsymbol{m}) = \lim_{\rho\to\infty} \frac{R^{(c)}_{\text{RBF}}}{\log_2 \rho}$, where $\boldsymbol{m} = [M_1,\cdots,M_C]^T$ is a given set of numbers of transmit beams at different BSs. We then state the following lemma on the achieve DoF of the c-th cell.

Lemma 4.3.2 *In the multi-cell RBF, assuming $K_c = \Theta(\rho^{\alpha_c})$, the achievable DoF of the c-th cell $d_{RBF,c}(\alpha_c, \boldsymbol{m})$, $c \in \{1,\ldots,C\}$, for a given $\boldsymbol{m}$ is*

$$d_{RBF,c}(\alpha_c, \boldsymbol{m}) = \begin{cases} \dfrac{\alpha_c M_c}{\sum_{l=1}^{C} M_l - 1}, & 0 \leq \alpha_c \leq \sum_{l=1}^{C} M_l - 1, \quad (4.22a) \\ M_c, & \alpha_c > \sum_{l=1}^{C} M_l - 1. \quad (4.22b) \end{cases}$$

Proof 6 *The proof uses Lemma 4.2.2 and similar arguments in the proof of Lemma 4.3.1, and is thus omitted for brevity.*

Remark 4.3.2 *Similar to Lemma 4.3.1 for the single-cell case, Lemma 4.3.2 reveals the relationship among the multi-user diversity, the level of the interference, and the*

achievable DoF for multi-cell RBF. However, as compared to the single-cell case, there are not only $M_c - 1$ intra-cell interfering beams, but also $\sum_{l=1,l\neq c}^{C} M_l$ inter-cell interfering beams for any data beam of the c-th cell in the multi-cell case, as observed from the denominator in (4.22a), which results in a decrease of the achievable DoF per cell.

Next, we obtain characterization of the DoF region defined in (4.17) for the multi-cell RBF with any given set of per-cell user density coefficients, denoted by $\boldsymbol{\alpha} = [\alpha_1, \cdots, \alpha_C]^T$ in the following theorem; for convenience, we denote $\boldsymbol{d}_{RBF}(\boldsymbol{\alpha}, \boldsymbol{m}) = \left[d_{RBF,1}(\alpha_1, \boldsymbol{m}) \ ,\cdots, d_{RBF,C}(\alpha_C, \boldsymbol{m})\right]^T$, with $d_{RBF,c}(\alpha_c, \boldsymbol{m})$ given in Lemma 4.3.2.

Theorem 4.3.2 *Assuming $K_c = \Theta\left(\rho^{\alpha_c}\right), c = 1, \ldots, C$, the achievable DoF region of a C-cell RBF system is given by*

$$\mathcal{D}_{RBF}(\boldsymbol{\alpha}) = \boldsymbol{conv}\Big\{ \boldsymbol{d}_{RBF}(\boldsymbol{\alpha}, \boldsymbol{m}), M_c \in \{0, \cdots, N_T\},\ c = 1, \cdots, C \Big\}, \tag{4.23}$$

*where **conv** denotes the convex hull operation.*

Theorem 4.3.2 is obtained directly using Lemma 4.3.2 and the definition of the DoF region, for which the proof is omitted for brevity. This theorem implies that we can obtain the DoF region of multi-cell RBF $\mathcal{D}_{RBF}(\boldsymbol{\alpha})$ by taking the convex hull over all achievable DoF points $\boldsymbol{d}_{RBF}(\boldsymbol{\alpha}, \boldsymbol{m})$ with all different values of $\boldsymbol{m}$, i.e., different BS beam number assignments.

In Fig. 4.6, we depict the DoF region of a two-cell RBF system with $N_T = 4$, and for different user density coefficients α_1 and α_2. The vertices of these regions can

be obtained by setting appropriate numbers of beams $0 \leq M_1 \leq 4$ and $0 \leq M_2 \leq 4$, while time-sharing between these vertices yields the entire boundary. To achieve the maximum sum-DoF of both cells, it is observed that a rule of thumb is to transmit more beams in the cell with a higher user density, and when α_1 and α_2 are both small, even turn off the BS of the cell with the smaller user density. Since the maximum sum-DoF does not consider the throughput fairness, the DoF region clearly shows all the achievable sum-rate tradeoffs among different cells, by observing its (Pareto) boundary as shown in Fig. 4.6. It is also observed that switching the two BSs to be on/off alternately achieves the optimal DoF boundary when the numbers of users in both cells are small, but is strictly suboptimal when the user number becomes large (see the dashed line in Fig. 4.6).

Furthermore, consider the case without any cooperation between these two BSs in assigning their numbers of transmit beams, i.e., both cells act selfishly by transmitting $M_c = N_T$ beams to aim to maximize their own DoF.The resulting DoF pairs, denoted by $\boldsymbol{d}_{RBF}([\alpha_1, \alpha_2], [4, 4])$, for three sets of $\boldsymbol{\alpha}$ are shown in Fig. 4.6 as P_1, P_2, and P_3, respectively. It is observed that the smaller the user densities are, the further the above non-cooperative multi-cell RBF scheme deviates from the Pareto boundary. In general, the optimal DoF tradeoffs or the boundary DoF pairs are achieved when both cells cooperatively assign their numbers of transmit beams based on their respective user densities, especially when the numbers of users in both cells are not sufficiently large. Since the information needed to determine the optimal operating DoF point is only the individual cell user density coefficients, the DoF

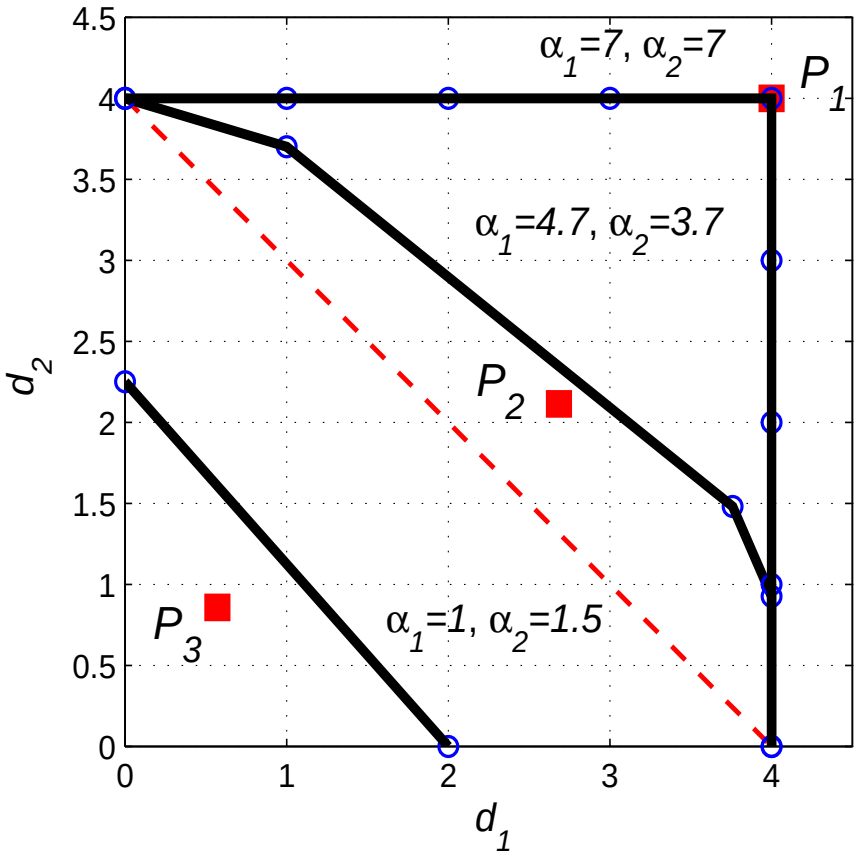

Figure 4.6: DoF region of two-cell RBF system with $N_T = 4$.

region provides a very useful method to globally optimize the coordinated multi-cell RBF scheme in practical systems.

4.3.3 Optimality of Multi-Cell RBF

So far, we have characterized the achievable DoF region for the multi-cell RBF scheme that requires only partial CSI at the transmitter. One important question that remains unaddressed yet is how the multi-cell RBF performs as compared to the optimal transmission scheme (e.g., IA) for the multi-cell downlink system with the full transmitter CSI, in terms of achievable DoF region. In this subsection, we attempt to

partially answer this question by focusing on the regime given in Assumption 4.3.1, i.e., the number of users per cell scales with a polynomial order with the SNR as the SNR goes to infinity.

4.3.3.1 Single-Cell Case

First, we consider the single-cell case to draw some useful insights. It is well known that the maximum sum-rate DoF for a single-cell MISO-BC with N_T transmit antennas and $K \geq N_T$ single-antenna users with independent channels is N_T [9], which is achievable by the DPC scheme or even simple linear precoding schemes. However, it is not immediately clear whether such a result still holds for the case of $K = \Theta(\rho^\alpha) \gg N_T$ with $\alpha > 0$, since in this case N_T may be only a lower bound on the maximum DoF. We thus have the following proposition.

Proposition 4.3.1 *Assuming $K = \Theta(\rho^\alpha)$ with $\alpha > 0$, the maximum sum-rate DoF of a single-cell MISO-BC with N_T transmit antennas is $d^*(\alpha) = N_T$.*

Proof 7 *Please refer to Appendix B.6.*

Proposition 4.3.1 confirms that the maximum DoF of the MISO-BC is still N_T, even with the asymptotically large number of users that scales with SNR, i.e., multiuser diversity does not yield any increment of DoF. Also, from Theorem 4.3.1, we have for $\alpha \geq N_T - 1$, $d^*_{RBF}(\alpha) = N_T$. We thus have the following proposition.

Proposition 4.3.2 *Assuming $K = \Theta(\rho^\alpha)$, the single-cell RBF scheme is DoF-optimal if $\alpha \geq N_T - 1$.*

From the above proposition, it follows that the single-cell RBF achieves the maximum DoF with $M = N_T$ if the number of users is sufficiently large, thanks to the multiuser diversity effect that completely eliminates the intra-cell interference given a sufficiently large number of users.

4.3.3.2 Multi-Cell Case

For the convenience of analysis, we use $\mathcal{D}_{\text{UB}}(\boldsymbol{\alpha})$ to denote an upper bound on the DoF region defined in (1.6), for a given $\boldsymbol{\alpha}$ in the multi-cell case. Clearly, under Assumption 4.3.1, it follows that $\mathcal{D}_{RBF}(\boldsymbol{\alpha}) \subseteq \mathcal{D}_{\text{MISO}}(\boldsymbol{\alpha}) \subseteq \mathcal{D}_{\text{UB}}(\boldsymbol{\alpha})$. Here $\mathcal{D}_{\text{MISO}}(\boldsymbol{\alpha})$ is the DoF region of the C-cell MISO downlink system as described in Definition 1.2.1.

The following proposition establishes a DoF region upper bound $\mathcal{D}_{\text{UB}}(\boldsymbol{\alpha})$.

Proposition 4.3.3 *Given $K_c = \Theta(\rho^{\alpha_c})$, $c = 1, \cdots, C$, a DoF region upper bound for a C-cell MISO downlink system is given by*

$$\mathcal{D}_{\text{UB}}(\boldsymbol{\alpha}) = \left\{(d_1, d_2, \cdots d_C) \in \mathbb{R}_+^C : d_c \leq N_T, c = 1, \cdots, C\right\}. \tag{4.24}$$

The above proposition can be easily shown by noting that $d_c \leq N_T$ is a direct consequence of Proposition 4.3.1 for the single-cell case, which should also hold for the multi-cell case by ignoring the ICI in each of the cells, i.e., an ICI-free multi-cell downlink system is considered. Supposing $\alpha_c \geq CN_T - 1$, $c = 1, \cdots, C$, from Lemma 4.3.2 and Theorem 4.3.2, it easily follows that the achievable DoF region of multi-cell RBF in this case is $\mathcal{D}_{RBF}(\boldsymbol{\alpha}) = \mathcal{D}_{\text{UB}}(\boldsymbol{\alpha})$. This leads to $\mathcal{D}_{RBF}(\boldsymbol{\alpha}) \subseteq \mathcal{D}_{\text{MISO}}(\boldsymbol{\alpha}) \subseteq \mathcal{D}_{\text{UB}}(\boldsymbol{\alpha}) = \mathcal{D}_{RBF}(\boldsymbol{\alpha})$, and thus $\mathcal{D}_{RBF}(\boldsymbol{\alpha}) = \mathcal{D}_{\text{MISO}}(\boldsymbol{\alpha})$, i.e., the multi-cell RBF

achieves the exact DoF region in this regime. We thus have the following proposition.

Proposition 4.3.4 *Given $K_c = \Theta(\rho^{\alpha_c})$, $c = 1, \cdots, C$, the multi-cell RBF scheme achieves the DoF region of a C-cell MISO downlink system, i.e., $\mathcal{D}_{RBF}(\boldsymbol{\alpha}) = \mathcal{D}_{MISO}(\boldsymbol{\alpha})$, if $\alpha_c \geq CN_T - 1$, $\forall c \in \{1, \cdots, C\}$.*

Remark 4.3.3 *The above proposition implies that the multi-cell RBF is indeed DoF-optimal when the numbers of users in all cells are sufficiently large. Due to the overwhelming multiuser diversity gain, RBF compensates the lack of full CSI at transmitters without any compromise of DoF degradation. However, it is important to point out that such a result should not undermine the benefits of having the more complete CSI at transmitters in practical multi-cell systems, where more sophisticated precoding schemes than RBF such as IA-based ones [28] can be applied to achieve substantial throughput gains, especially when the numbers of per-cell users are not so large. Due to the space limitation, we do not make a detailed comparison of the achievable rates between IA and RBF for the case of finite number of users in this chapter, and will leave this interesting study in our further work.*

4.4 Conclusions

In this chapter, the achievable rates of the RBF scheme in a multi-cell setup subject to the ICI are thoroughly investigated. Both finite-SNR and high-SNR regimes are considered. For the finite-SNR case, we provide closed-form expressions of the achievable average sum-rates for both single- and multi-cell RBF with a finite number of

users per cell. We also derive the sum-rate scaling law in the conventional asymptotic regime, i.e., when the number of users goes to infinity with a fixed SNR. Since the finite-SNR analysis has major limitations, we furthermore consider the high-SNR regime by adopting the DoF-region approach to characterize the optimal throughput tradeoffs among different cells in multi-cell RBF, assuming that the number of users per cell scales in a polynomial order with the SNR as the SNR goes to infinity. We show the closed-form expressions of the achievable DoF and the corresponding optimal number of transmit beams, both as functions of the user number scaling order or the user density, for the single-cell case. From this result, we obtain a complete characterization of the DoF region for the multi-cell RBF, in which the optimal boundary DoF point is achieved by BSs' cooperative assignment of their numbers of transmit beams according to individual cell's user densities. Finally, if the numbers of users in all cells are sufficiently large, we show that the multi-cell RBF, albeit requiring only partial CSI at transmitters, achieve the optimal DoF region even without the full transmitter CSI. The results presented in this chapter are useful for the optimal design of multi-cell MISO RBF in practical cellular systems with limited channel feedback.

Chapter 5

Multi-Cell MIMO RBF

Receive spatial diversity is another topic which is not fully understood even in a single-cell RBF setup. As shown in [65], RBF with and without receive diversity schemes still achieve the same sum-rate scaling law, assuming that the number of users pre cell goes to infinity for any given user's SNR. Based on the conventional asymptotic analysis, it is thus concluded that receive diversity only provides *marginal* gain to the rate performance.

This chapter presents our contributions on multi-cell MIMO RBF. The main results of this chapter are summarized as follows.

- **Multi-cell MIMO RBF**: We propose three MIMO RBF schemes for multi-cell downlink systems. In these schemes, RBF is applied at each BS and either the MMSE, MF, or AS based spatial receiver is employed at each mobile terminal (denoted as RBF-MMSE, RBF-MF, and RBF-AS schemes, respectively). These schemes preserve the same low-feedback requirement as that for the special case

of single-cell OBF/RBF [64] [72], but bring in the new benefits of receive spatial diversity with different performance-complexity trade-offs.

- **SINR Distribution**: By applying the tools from *multivariate analysis* (MVA), we derive the exact distribution of the SINR at each multi-antenna receiver in a multi-cell MIMO RBF system subject to both the intra- and inter-cell interferences, assuming either the MMSE, MF, or AS based spatial diversity technique. Note that these results are non-trivial extensions of Lemma 4.2.2 for the MISO RBF case with only single-antenna receivers.

- **DoF Region Characterization**: We further investigate the multi-cell MIMO RBF system with MMSE, MF, or AS based spatial receivers under the asymptotically high-SNR regime, by assuming that the number of users per cell scales in a certain order with the SNR (a larger scaling order indicates a higher user density in one particular cell). We first derive the achievable sum-rate DoF under a single-cell setup without the ICI to gain useful insights and then obtain a general characterization of the DoF region for the multi-cell case, which constitutes all the achievable DoF tuples for the individual sum-rate of all the cells subject to the additional ICI.

  Our analysis reveals that significant sum-rate DoF gains can be achieved by employing the MMSE-based spatial receiver as compared to the cases with single-antenna receivers or with the suboptimal spatial receivers such as MF and AS. This is in sharp contrast to the existing result (e.g., [64], [65]) that

spatial diversity receivers only yield marginal rate gains in RBF, which is based on the conventional asymptotic analysis in the regime of large number of users but with fixed SNR per cell. With MMSE receivers, our result shows that a significantly less number of users in each cell is required to achieve a given sum-rate DoF target as compared to the cases without receiver spatial diversity or with MF/AS receivers. Our new high-SNR DoF analysis thus provides a more realistic characterization of the rate trade-offs in multi-cell MIMO RBF systems.

The remainder of this chapter is organized as follows. Section 5.1 describes the multi-cell MIMO downlink system model and the MIMO RBF scheme with MMSE, MF, or AS based spatial receivers. Section 5.2 investigates the SINR distribution in each receiver case based on MVA. Section 5.3 characterizes the achievable sum-rate DoF for single-cell MIMO RBF, and then extends the result to the DoF region characterization for multi-cell MIMO RBF. Finally, we conclude the paper in Section 5.4.

5.1 System Model

Consider a cellular system consisting of C cells and K_c MSs in the c-th cell, $c = 1, \cdots, C$. In this chapter, we focus on the downlink transmission assuming universal frequency reuse, i.e., all cells are assigned the same bandwidth for transmission. For the ease of analysis, we also assume that all BSs/MSs have the same number of

transmit/receive antennas, denoted as N_T and N_R, respectively. Extensions to the case of different number of transmit/receive antennas are straightforward. Consider time-slotted transmissions, at each time slot, the c-th BS transmits M_c orthonormal beams and selects M_c users in the c-th cell for transmission, with $M_c \leq N_T$ and $M_c \leq K_c$, $\forall c$. The received baseband signal of user k in the c-th cell is given by

$$\boldsymbol{y}_k^{(c)} = \boldsymbol{H}_k^{(c,c)} \sum_{m=1}^{M_c} \boldsymbol{\phi}_m^{(c)} s_m^{(c)} + \sum_{l=1,\ l\neq c}^{C} \sqrt{\gamma_{l,c}} \boldsymbol{H}_k^{(l,c)} \sum_{m=1}^{M_l} \boldsymbol{\phi}_m^{(l)} s_m^{(l)} + \boldsymbol{z}_k^{(c)}, \tag{5.1}$$

where $\boldsymbol{H}_k^{(l,c)} \in \mathbb{C}^{N_R \times M_l}$ denotes the MIMO channel matrix from the l-th BS to the k-th user of the c-th cell, which is assumed to be i.i.d. Rayleigh fading, i.e., all elements are i.i.d. and have the same distribution $\mathcal{CN}(0,1)$; $\boldsymbol{\phi}_m^{(c)} \in \mathbb{C}^{M_c \times 1}$ and $s_m^{(c)}$ are the m-th randomly generated beamforming vector of unit norm and the corresponding transmitted data symbol from the c-th BS, respectively; it is assumed that each BS has an average sum power constraint, P_T, i.e., $\boldsymbol{Tr}\left(\mathbb{E}[\boldsymbol{s}_c \boldsymbol{s}_c^H]\right) \leq P_T$, where $\boldsymbol{s}_c = [s_1^{(c)}, \cdots, s_{M_c}^{(c)}]^T$; $\gamma_{l,c} < 1$ stands for the (more severe) signal attenuation from the l-th BS to any user in the c-th cell, $l \neq c$; and $\boldsymbol{z}_k^{(c)} \in \mathbb{C}^{N_R \times 1}$ is the receiver AWGN vector, which consists of i.i.d. random variables each distributed as $\mathcal{CN}(0, \sigma^2)$, $\forall k, c$. In the c-th cell, the total SNR, the SNR per beam, and the INR per beam from the l-th cell, $l \neq c$, are denoted as $\rho = P_T/\sigma^2$, $\eta_c = P_T/(M_c\sigma^2)$, and $\mu_{l,c} = \gamma_{l,c}P_T/(M_l\sigma^2)$, respectively.

5.1.1 Multi-Cell RBF

With multiple receive antennas, each MS can apply spatial diversity techniques to enhance the performance. In this chapter, we propose the optimal MMSE -based spatial

receiver and two suboptimal spatial receivers based on MF and AS, respectively. We describe the multi-cell RBF scheme with MMSE, MF, and AS receivers as follows.

1. Training phase:

   a) The c-th BS generates M_c orthonormal beams, $\boldsymbol{\phi}_1^{(c)}, \cdots, \boldsymbol{\phi}_{M_c}^{(c)}$, and uses them to broadcast the training signals to all users in the c-th cell. The total power of the c-th BS is assumed to be distributed equally over M_c beams.

   b1) RBF-MMSE: For each of the M_c beams, user k in the c-th cell does the following:

      i. Estimate the effective channel with training from the c-th BS: $\tilde{\boldsymbol{h}}_{k,m}^{(c,c)} = \boldsymbol{H}_k^{(c,c)} \boldsymbol{\phi}_m^{(c)}$, $1 \leq m \leq M_c$.

      ii. Use the training signal from the BSs to estimate the interference-plus-noise covariance matrix due to the other $M_c - 1$ beams from the c-th BS and all beams from the other $C - 1$ BSs:

$$\boldsymbol{W}_k^{(c)} = \frac{P_T}{M_c} \tilde{\boldsymbol{H}}_{k,-m}^{(c,c)} \left(\tilde{\boldsymbol{H}}_{k,-m}^{(c,c)} \right)^H + \sum_{l=1, l \neq c}^{C} \frac{P_T \gamma_{l,c}}{M_l} \tilde{\boldsymbol{H}}_k^{(l,c)} \left(\tilde{\boldsymbol{H}}_k^{(l,c)} \right)^H + \sigma^2 \boldsymbol{I}, \tag{5.2}$$

      where $\tilde{\boldsymbol{H}}_{k,-m}^{(c,c)} = \boldsymbol{H}_k^{(c,c)} [\boldsymbol{\phi}_1^{(c)}, \cdots, \boldsymbol{\phi}_{m-1}^{(c)}, \boldsymbol{\phi}_{m+1}^{(c)}, \cdots, \boldsymbol{\phi}_{M_c}^{(c)}]$, and $\tilde{\boldsymbol{H}}_k^{(l,c)} = \boldsymbol{H}_k^{(c,c)} [\boldsymbol{\phi}_1^{(l)}, \cdots, \boldsymbol{\phi}_{M_l}^{(l)}]$.

      iii. Apply the MMSE spatial receiver, i.e., $\boldsymbol{t}_{k,m}^{(c)} = \sqrt{\frac{P_T}{M_c}} \left(\boldsymbol{W}_k^{(c)} \right)^{-1} \tilde{\boldsymbol{h}}_{k,m}^{(c,c)}$, $1 \leq m \leq M_c$, and compute the SINR corresponding to the m-th beam

$\boldsymbol{\phi}_m^{(c)}$, i.e.,

$$\mathrm{SINR}_{k,m}^{(\mathrm{MMSE},c)} = \frac{P_T}{M_c}\left(\tilde{\boldsymbol{h}}_{k,m}^{(c,c)}\right)^H \left(\boldsymbol{W}_k^{(c)}\right)^{-1} \tilde{\boldsymbol{h}}_{k,m}^{(c,c)}. \tag{5.3}$$

iv. Send back $\mathrm{SINR}_{k,m}^{(\mathrm{MMSE},c)}$, $1 \le m \le M_c$, to the c-th BS.

b2) RBF-MF: For each of the M_c beams, user k in the c-th cell does the following:

i. Estimate the effective channel with training from the c-th BS: $\tilde{\boldsymbol{h}}_{k,m}^{(c,c)} = \boldsymbol{H}_k^{(c,c)}\boldsymbol{\phi}_m^{(c)}$, $1 \le m \le M_c$.

ii. Apply the MF spatial receiver, i.e., $\boldsymbol{t}_{k,m}^{(c)} = \tilde{\boldsymbol{h}}_{k,m}^{(c,c)} \;/\; ||\tilde{\boldsymbol{h}}_{k,m}^{(c,c)}||$. The rationale is to maximize the power received from the m-th beam. The receiver output is given by

$$r_{k,m}^{(c)} = \sqrt{\frac{P_T}{M_c}}\left(\boldsymbol{t}_{k,m}^{(c)}\right)^H \tilde{\boldsymbol{h}}_{k,m}^{(c,c)} s_m^{(c)} + \sqrt{\frac{P_T}{M_c}}\left(\boldsymbol{t}_{k,m}^{(c)}\right)^H \tilde{\boldsymbol{H}}_{k,-m}^{(c,c)} \boldsymbol{s}_{-m}^{(c)} + \sum_{l=1,l\neq c} \sqrt{\frac{P_T\gamma_{l,c}}{M_l}}\left(\boldsymbol{t}_{k,m}^{(c)}\right)^H \tilde{\boldsymbol{H}}_k^{(l,c)} \boldsymbol{s}_l + \left(\boldsymbol{t}_{k,m}^{(c)}\right)^H \boldsymbol{z}_k^{(c)}, \tag{5.4}$$

where $\boldsymbol{s}_{-m}^{(c)} = [s_1^{(c)}, \cdots, s_{m-1}^{(c)}, s_{m+1}^{(c)}, \cdots, s_{M_c}^{(c)}]^T$ and $\boldsymbol{s}_l = [s_1^{(l)}, \cdots, s_{M_l}^{(c)}]^T$.

iii. Estimate the total power of the interference given in (5.4), which can be equivalently expressed as $\left(\tilde{\boldsymbol{h}}_{k,m}^{(c,c)}\right)^H \boldsymbol{W}_k^{(c)} \tilde{\boldsymbol{h}}_{k,m}^{(c,c)}$, in which $\boldsymbol{W}_k^{(c)}$ is defined in (5.2); and compute the SINR corresponding to the m-th beam $\boldsymbol{\phi}_m^{(c)}$, which is expressed as

$$\mathrm{SINR}_{k,m}^{(\mathrm{MF},c)} = \frac{\frac{P_T}{M_c}||\tilde{\boldsymbol{h}}_{k,m}^{(c,c)}||^4}{\left(\tilde{\boldsymbol{h}}_{k,m}^{(c,c)}\right)^H \boldsymbol{W}_k^{(c)} \tilde{\boldsymbol{h}}_{k,m}^{(c,c)}}. \tag{5.5}$$

iv. Send back $\text{SINR}_{k,m}^{(\text{MF},c)}$, $1 \le m \le M_c$, to the c-th BS.

b3) RBF-AS: The received signal at the n-th receive antenna of user k in the c-th cell is given by

$$y_{k,n}^{(c)} = \boldsymbol{h}_{k,n}^{(c,c)} \sum_{m=1}^{M_c} \boldsymbol{\phi}_m^{(c)} s_m^{(c)} + \sum_{l=1,\ l\neq c}^{C} \sqrt{\gamma_{l,c}} \boldsymbol{h}_{k,n}^{(l,c)} \sum_{m=1}^{M_l} \boldsymbol{\phi}_m^{(l)} s_m^{(l)} + z_{k,n}^{(c)}, \quad 1 \le n \le N_R, \tag{5.6}$$

where $y_{k,n}^{(c)}$ and $z_{k,n}^{(c)}$ are the n-th element of $\boldsymbol{y}_k^{(c)}$ and $\boldsymbol{z}_k^{(c)}$, respectively; $\boldsymbol{h}_{k,n}^{(l,c)}$ $\in \mathbb{C}^{1\times M_l}$ is the n-th row of $\boldsymbol{H}_k^{(l,c)}$, $n \in \{1,\ldots,N_R\}$, $l,c \in \{1,\ldots,C\}$. For each of the M_c beams, user k does the following:

i. Estimate the SINR corresponding to the m-th beam $\boldsymbol{\phi}_m^{(c)}$ at the n-th antenna:

$$\text{SINR}_{k,n,m} = \frac{\frac{P_T}{M_c}\left|\boldsymbol{h}_{k,n}^{(c,c)}\boldsymbol{\phi}_m^{(c)}\right|^2}{\frac{P_T}{M_c}\sum_{i=1,i\neq m}^{M_c}\left|\boldsymbol{h}_{k,n}^{(c,c)}\boldsymbol{\phi}_i^{(c)}\right|^2 + \sum_{l=1,l\neq c}^{C}\gamma_{l,c}\frac{P_T}{M_l}\sum_{i=1}^{M_l}\left|\boldsymbol{h}_{k,n}^{(l,c)}\boldsymbol{\phi}_i^{(l)}\right|^2 + \sigma^2}. \tag{5.7}$$

ii. Select the antenna that has the largest SINR among all N_R receive antennas for the m-th beam, and obtain the SINR as

$$\text{SINR}_{k,m}^{(\text{AS},c)} := \max_{n\in\{1,\cdots,N_R\}} \text{SINR}_{k,n,m}. \tag{5.8}$$

iii. Send back $\text{SINR}_{k,m}^{(\text{AS},c)}$, $1 \le m \le M_c$, to the c-th BS.

2. Transmission phase: After receiving the SINR feedback from all K_c users, the c-th BS assigns the m-th beam to the user with the highest SINR for transmission,

i.e.,

$$k_m^{(\mathrm{Rx},c)} = \arg \max_{k \in \{1,\cdots,K_c\}} \mathrm{SINR}_{k,m}^{(\mathrm{Rx},c)}, \tag{5.9}$$

where "Rx" denotes MMSE, MF, or AS.

The achievable sum-rate in bits per second per Hz (bps/Hz) of the c-th cell by the above RBF scheme with different spatial receivers is then expressed as

$$R_{\text{RBF-Rx}}^{(c)} = \mathbb{E}\left[\sum_{m=1}^{M_c} \log_2\left(1 + \mathrm{SINR}_{k_m^{(\mathrm{Rx},c)},m}^{(\mathrm{Rx},c)}\right)\right] \overset{(a)}{=} M_c \mathbb{E}\left[\log_2\left(1 + \mathrm{SINR}_{k_1^{(\mathrm{Rx},c)},1}^{(\mathrm{Rx},c)}\right)\right], \tag{5.10}$$

where (a) is due to the fact that all the beams in each cell have the same SINR distribution with a given spatial receiver scheme.

5.1.2 DoF Region

In this chapter, we apply the high-SNR analysis to draw insightful comparisons on the achievable rates of multi-cell MIMO RBF with different spatial diversity receivers. Similar to Section 4.3, we adopt the DoF region, which is defined in Section 1.2.1, as one key performance metric in our analysis.

With MIMO RBF schemes, the achievable DoF region in (1.6) is more specifically given as follows.

Definition 5.1.1 *(DoF region with RBF) The DoF region of a C-cell MIMO down-*

link system with RBF is given by

$$\mathcal{D}_{RBF\text{-}Rx} = \Bigg\{ (d_1, \cdots, d_C) \in \mathbb{R}_+^C : \forall (\omega_1, \omega_2, \cdots, \omega_C) \in \mathbb{R}_+^C; \sum_{c=1}^{C} \omega_c d_c \leq \lim_{\rho \to \infty} \left[\max_{M_1, \ldots, M_C \in \{0, \cdots, N_T\}} \sum_{c=1}^{C} \omega_c \frac{R_{RBF\text{-}Rx}^{(c)}}{\log_2 \rho} \right] \Bigg\}. \quad (5.11)$$

where "Rx" denotes MMSE, MF or AS.

Certainly, $\mathcal{D}_{\text{RBF-Rx}} \subseteq \mathcal{D}_{\text{MIMO}}$ regardless of MMSE, MF or AS spatial receivers used. Here $\mathcal{D}_{\text{MIMO}}$ is the DoF region of the C-cell MIMO downlink system as described in Definition 1.2.1.

Furthermore, we assume a certain growth rate for the number of users in each cell K_c with respect to the SNR, ρ, as ρ goes to infinity. Similar to Section 4.3, we make the Assumption 4.3.1.

As will be seen later in this chapter, the DoF region characterization under Assumption 4.3.1 provides new insights on the different effects of the number of per-cell users, transmit beams, and receive antennas on the achievable rate in multi-cell MIMO RBF. The notations $\mathcal{D}_{\text{MIMO}}(\boldsymbol{\alpha})$ and $\mathcal{D}_{\text{RBF-Rx}}(\boldsymbol{\alpha})$ will be used in the sequel to denote the DoF regions under Assumption 4.3.1 with $K_c = \Theta(\rho^{\alpha_c})$, $c = 1, \cdots, C$, and $\boldsymbol{\alpha} = [\alpha_1, \cdots, \alpha_C]^T$. It is worth noting that our high-SNR approach is along the same line of those recently reported in [41] [69] [79], where the authors obtain the achievable DoF of their studied systems assuming that the number of users/links scales in a certain polynomial order with the SNR as the SNR goes to infinity.

5.2 SINR Distribution

To characterize the achievable rates of the proposed RBF schemes with different spatial receivers, it is necessary to investigate the receiver SINRs given in (5.3), (5.5), and (5.8). In this section, we derive the (exact) distribution of the SINR in each receiver case.

5.2.1 RBF-MMSE

To obtain the SINR distribution for the RBF-MMSE scheme, we first prove a more general result in MVA, which is given as follows.

Theorem 5.2.1 *Given* $\boldsymbol{h} \sim \mathcal{CN}(\mathbf{0}_{p\times 1}, \boldsymbol{I}_p)$, $\boldsymbol{X} \sim \mathcal{CN}(\mathbf{0}_{p\times n}, \boldsymbol{I}_p \otimes \boldsymbol{I}_n)$[1], $n \geq p \geq 1$, *where* $\boldsymbol{h}$ *is independent of* $\boldsymbol{X}$, *and* $\boldsymbol{\Psi} = diag(\psi_1, \ldots, \psi_n)$, *with* $\psi_i > 0$, $i = 1, \ldots, n$, *being constants, the CDF of the random variable* $S := \boldsymbol{h}^H(\boldsymbol{X}\boldsymbol{\Psi}\boldsymbol{X}^H)^{-1}\boldsymbol{h}$ *is given by*

$$F_S(s) = \frac{\sum_{i=p}^{n} \beta_i s^i}{\prod_{i=1}^{n}(1+\psi_i s)}, \tag{5.12}$$

where β_i *is the coefficient of* s^i *after expanding the polynomial* $\prod_{j=1}^{n}(1+\psi_j s)$.

Proof 8 *Please refer to Appendix A.3.*[2]

[1] $\boldsymbol{X}$ is said to have a matrix-variate complex Gaussian distribution with mean matrix $\mathbf{0} \in \mathbb{C}^{p\times n}$ and covariance matrix $\boldsymbol{I}_p \otimes \boldsymbol{I}_n$, where $\otimes$ denotes the Kronecker product.

[2] Note that a similar result of Theorem 5.2.1 has been reported in [16], but via a different proof method. Specifically, the authors in [16] applied a "top-down" approach, whereby they used a more general result [33, Theorem 3 and (59)] to derive the explicit expression (5.12) for the case in Theorem 5.2.1. In Appendix A.3, we propose an alternative more direct approach, which uses only fundamental properties in MVA and thus leads to a more compact proof.

It is worth noting that extensions of Theorem 5.2.1 to the case of Rician-fading and/or correlated channels can be found in subsequent studies, e.g., [32] [46] [61], where the moment generating function and distribution of the output SINR have been derived. These results are then applied to find the closed-form expressions of the capacity and/or bit error rate for the investigated systems. Under such cases, the SINR distribution in general possesses a complicated form and is often expressed in terms of determinants of certain matrices.

Next, we observe that (5.12) can be equivalently expressed as

$$F_S(s) = 1 - \frac{\sum_{i=0}^{p-1} \beta_i s^i}{\prod_{i=1}^{n}(1+\psi_i s)}. \tag{5.13}$$

We are now ready to obtain the SINR distribution with RBF-MMSE, based on Theorem 5.2.1.

Corollary 5.2.1 *Given* $N_R \leq \sum_{l=1}^{C} M_l - 1$, *the CDF of the random variable* $S := SINR_{k,m}^{(MMSE,c)}$ *defined in (5.3) is given by*

$$F_S(s) = 1 - \frac{e^{-s/\eta_c}\left(\sum_{i=0}^{N_R-1}\zeta_i s^i\right)}{(1+s)^{M_c-1}\prod_{l=1,l\neq c}^{\sum M_c-1}(1+\frac{\mu_{l,c}}{\eta_c}s)^{M_l}}, \tag{5.14}$$

where ζ_i *is the coefficient of* s^i *in the polynomial expansion of* $(1+s)^{M_c-1}\prod_{l=1,l\neq c}^{\sum M_c-1}(1+\frac{\mu_{l,c}}{\eta_c}s)^{M_l}$.

Proof 9 *Please refer to Appendix C.1.*

5.2.2 RBF-MF

The interference-plus-noise covariance matrix $\boldsymbol{W}_k^{(c)}$ given in (5.2) can be alternatively expressed as

$$\boldsymbol{W}_k^{(c)} = \left(\tilde{\boldsymbol{H}}_{k,m}^{(c)}\right)^H diag\Bigg(\underbrace{\frac{P_T}{M_c},\cdots,\frac{P_T}{M_c}}_{M_c-1},\cdots,\underbrace{\frac{P_T\gamma_{l,c}}{M_l},\cdots,\frac{P_T\gamma_{l,c}}{M_l}}_{M_l},\cdots\Bigg)\tilde{\boldsymbol{H}}_{k,m}^{(c)} + \sigma^2\boldsymbol{I}, \tag{5.15}$$

where $\tilde{\boldsymbol{H}}_{k,m}^{(c)} = \left[\tilde{\boldsymbol{H}}_{k,-m}^{(c,c)}, \tilde{\boldsymbol{H}}_k^{(1,c)},\cdots,\tilde{\boldsymbol{H}}_k^{(l,c)},\cdots,\tilde{\boldsymbol{H}}_k^{(C,c)}\right]$; $\tilde{\boldsymbol{H}}_{k,-m}^{(c,c)}$ and $\tilde{\boldsymbol{H}}_k^{(l,c)}$ are defined in (5.2), $l,c \in \{1,\ldots,C\}$, $l \neq c$. Define

$$\hat{\boldsymbol{h}}_{k,m}^{(c)} = \frac{\tilde{\boldsymbol{h}}_{k,m}^{(c,c)}}{\|\tilde{\boldsymbol{h}}_{k,m}^{(c,c)}\|}\tilde{\boldsymbol{H}}_{k,m}^{(c)}. \tag{5.16}$$

Note that $\hat{\boldsymbol{h}}_{k,m}^{(c)} \in \mathbb{C}^{(\sum_{l=1}^{C} M_l - 1)\times 1}$ is independent of $\tilde{\boldsymbol{h}}_{k,m}^{(c,c)}$ and all the elements of $\hat{\boldsymbol{h}}_{k,m}^{(c)}$ are i.i.d. CSCG random variables each distributed as $\mathcal{CN}(0,1)$. For RBF-MF, the SINR in (5.5) is thus expressed as

$$\text{SINR}_{k,m}^{(\text{MF},c)} = \frac{||\tilde{\boldsymbol{h}}_{k,m}^{(c,c)}||^2}{\left(\hat{\boldsymbol{h}}_{k,m}^{(c)}\right)^H \boldsymbol{G}\hat{\boldsymbol{h}}_{k,m}^{(c)} + \frac{1}{\eta_c}}, \tag{5.17}$$

where $\boldsymbol{G} = diag\Bigg(\underbrace{1,\cdots,1}_{M_c-1},\cdots,\underbrace{\frac{\mu_{l,c}}{\eta_c},\cdots,\frac{\mu_{l,c}}{\eta_c}}_{M_l},\cdots\Bigg)$, with $l,c \in \{1,\ldots,C\}$, $l \neq c$.

By applying the *characteristic function* approach, we obtain the CDF of the SINR with RBF-MF in the following theorem.

Theorem 5.2.2 *The CDF of the random variable $S := SINR_{k,m}^{(MF,c)}$ in (5.17) is given by*

$$F_S(s) = 1 - e^{-s/\eta_c}\sum_{k=0}^{N_R-1}\sum_{m=0}^{k}\frac{(-1)^m s^k}{(k-m)!m!\eta_c^{k-m}}\frac{d^m T_0(s)}{ds^m}, \tag{5.18}$$

where

$$T_0(s) = \frac{1}{(1+s)^{M_c-1}\prod_{l=1,l\neq c}^{C}(1+\frac{\mu_{l,c}}{\eta_c}s)^{M_l}}. \tag{5.19}$$

Proof 10 *Please refer to Appendix C.2.*

5.2.3 RBF-AS

First, we investigate the distribution of the $\text{SINR}_{k,n,m}$ given in (5.7). Note that $\left|\boldsymbol{h}_{k,n}^{(l,c)}\boldsymbol{\phi}_i^{(l)}\right|^2$, $\forall k,n,l,c,i$, are i.i.d. chi-square random variables with 2 degrees of freedom, denoted by $\chi^2(2)$ [64]. From Corollary 5.2.1 or Theorem 5.2.2, we can easily obtain the same distribution for $\text{SINR}_{k,n,m}$ and thereby $\text{SINR}_{k,m}^{(\text{AS},c)}$ in (5.8), as given in the following corollary.

Corollary 5.2.2 *The CDF of the random variable $S := SINR_{k,m}^{(AS,c)}$ defined in (5.8) is given by*

$$F_S(s) = \left(1 - \frac{e^{-s/\eta_c}}{(s+1)^{M_c-1}\prod\limits_{l=1,l\neq c}^{C}\left(\frac{\mu_{l,c}}{\eta_c}s+1\right)^{M_l}}\right)^{N_R}. \tag{5.20}$$

In Fig. 5.1, we show the SINR CDFs of the RBF-MMSE, RBF-MF, and RBF-AS schemes under the following setup: $C = 4$, $\eta_1 = 20$ dB, $N_R = 3$, $M_1 = 3$, $[\mu_{2,1}, \mu_{3,1}, \mu_{4,1}] = [0, -3, 3]$ dB, and $[M_2, M_3, M_4] = [3, 2, 4]$ (see Section 5.1 for the implementation of these schemes). The CDFs obtained by Monte-Carlo simulations (with 10^4 channel realizations) are compared to our analytical results from Corollary 5.2.1,

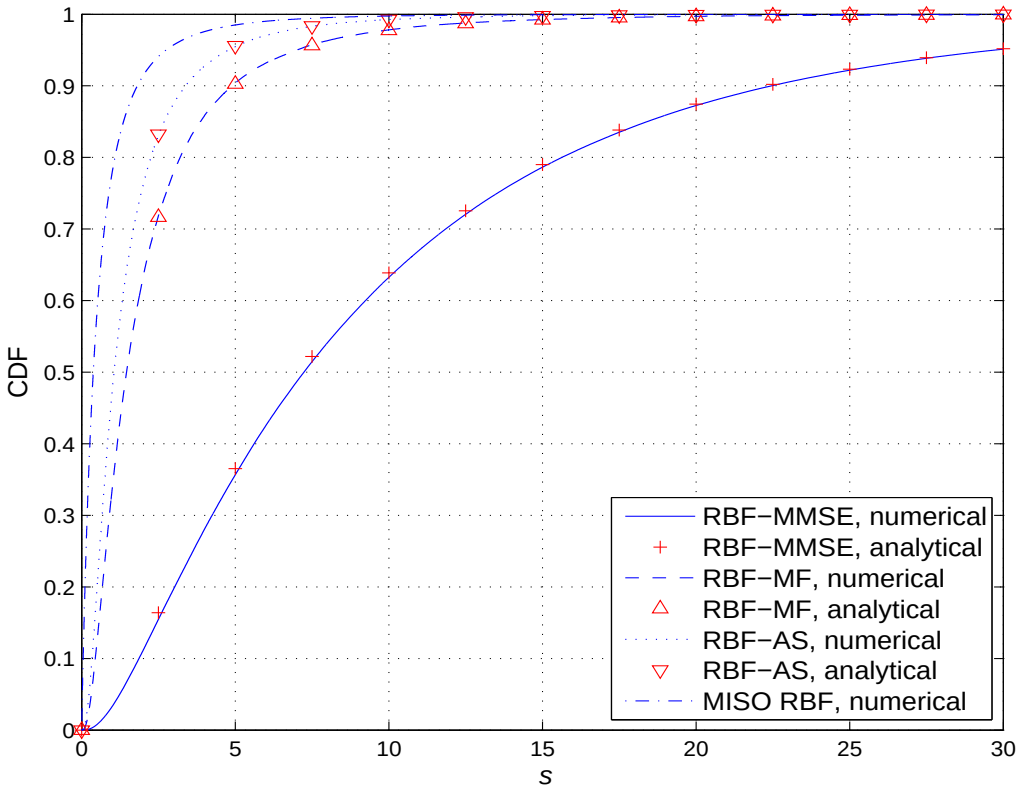

Figure 5.1: Comparison of the simulated and analytical CDFs of the SINR with different spatial receiver schemes.

Theorem 5.2.2, and Corollary 5.2.2. It is observed that the simulation results follows closely the analytical results. For comparison, we also plot the SINR CDF in the case with $N_R = 1$, i.e., the MISO RBF scheme that was given in Lemma 4.2.2. It is observed that receive spatial diversity helps enhance the SINR performance substantially. In particular, with RBF-MMSE, the SINR distribution is most significantly improved. It is thus expected that RBF-MMSE should also provide the best rate performance, as will be shown next.

5.3 DoF Analysis

In this section, we first study the DoF for the achievable sum-rate in the single-cell MIMO RBF case. Then, we extend the DoF analysis for the single-cell RBF to the more general multi-cell RBF subject to the ICI. Finally, we investigate the optimality of RBF in terms of achievable DoF region.

5.3.1 Single-Cell Case

First, we consider the single-cell case without the ICI to draw some useful insights. For brevity, we drop the cell index c in this subsection. We define the achievable DoF for the sum-rate in one single cell with a given pair of user density α and number of transmit beams M as

$$d_{\text{RBF-Rx}}(\alpha, M) = \lim_{\rho\to\infty} \frac{R_{\text{RBF-Rx}}}{\log_2 \rho}. \tag{5.21}$$

We first obtain the following lemma on the achievable DoF in one single cell.

Lemma 5.3.1 *In the single-cell case, given $K = \Theta(\rho^\alpha)$, the achievable DoF of RBF-MMSE, RBF-MF, and RBF-AS schemes are given by*

$$d_{RBF\text{-}MMSE}(\alpha, M) = \begin{cases} \dfrac{\alpha M}{M - N_R}, & 0 \le \alpha \le M - N_R \quad (5.22a) \\ M, & \alpha > M - N_R. \quad (5.22b) \end{cases}$$

$$d_{RBF\text{-}MF/AS}(\alpha, M) = \begin{cases} \dfrac{\alpha M}{M - 1}, & 0 \le \alpha \le M - 1 \quad (5.23a) \\ M, & \alpha > M - 1. \quad (5.23b) \end{cases}$$

Proof 11 *Please refer to Appendix C.3.*

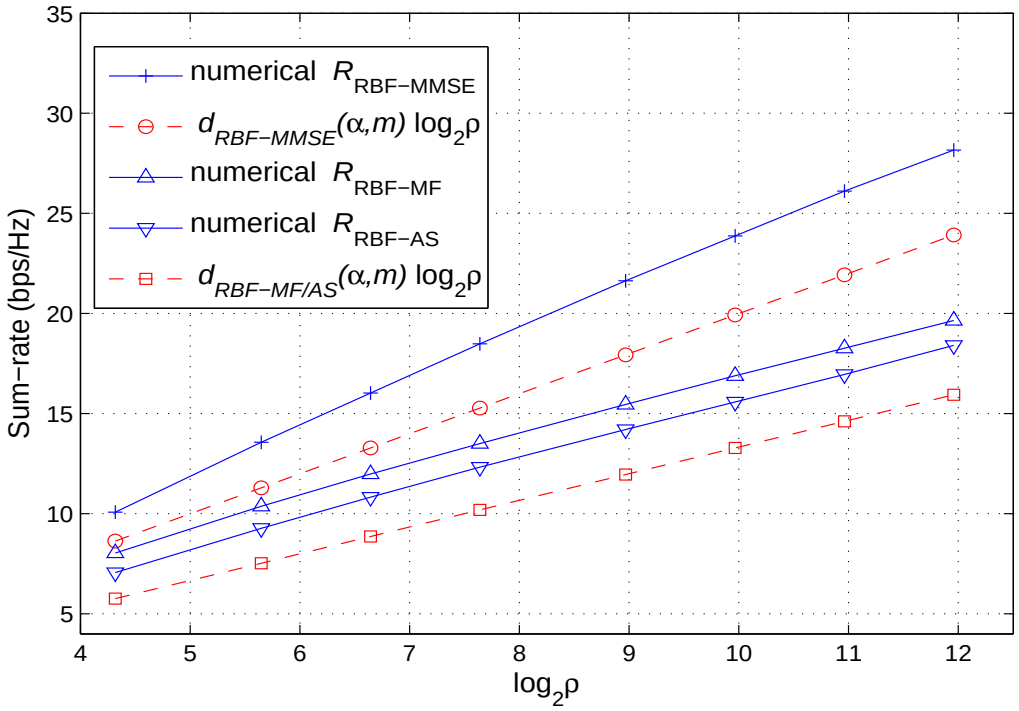

Figure 5.2: Comparison of the numerical sum-rate and sum-rate scaling law in the single-cell MIMO RBF with different spatial receivers.

In Fig. 5.2, we compare the sum-rate scaling laws $d_{\text{RBF-MMSE}}(\alpha, M)\log_2\rho$ and $d_{\text{RBF-MF/AS}}(\alpha, M)\log_2\rho$ with the actual sum-rates achievable by RBF-MMSE, RBF-MF, and RBF-AS schemes obtained by simulation. The system parameters are set as $M = 4$, $N_R = 2$, $\alpha = 1$, and $K = \lfloor \rho^{\alpha} \rfloor$. It is observed that the numerical sum-rate results follow quite closely the theoretical rate scaling laws, even with moderate SNR values of ρ.

From Lemma 5.3.1, we observe an interesting interplay among the available multi-user diversity (specified by the user density α), the level of the intra-cell interference (specified by $M-1$), the receive diversity gain (specified by the number of receive antennas N_R), and the achievable spatial multiplexing gain (specified by the

DoF $d_{RBF}(\alpha, M)$), which is elaborated as follows.

First, note that in a single-cell RBF system, transmitting M beams simultaneously results in $M-1$ intra-cell interfering beams for each received beam. The term $M-1$ in the denominator of (5.23a) is exactly the number of interfering beams to one particular received beam in RBF-MF/AS. However, there exist only $M-N_R$ effective interference beams in RBF-MMSE, as shown in (5.22a), since MMSE receiver achieves an additional *interference mitigation* gain of N_R-1. Specifically, with the total N_R spatial DoF, the MMSE receiver effectively uses one DoF for receiving signal and the other N_R-1 DoF for suppressing the interference. Furthermore, in terms of achievable sum-rate DoF, the performance of either RBF-MF or RBF-AS is the same as that of MISO RBF system without receive spatial diversity [50], and is thus poorer as compared to RBF-MMSE with $N_R > 1$. The DoF gain by receive spatial diversity therefore clearly depends on the availability of the interference covariance matrix at each MS. In the case of RBF-MMSE, the interference-plus-noise covariance matrix $\boldsymbol{W}_k^{(c)}$ in (5.2) needs to be estimated at the receiver, while this operation is not required in RBF-MF or RBF-AS.

Another interpretation of Lemma 5.3.1 is that it gives the *user scaling law* with SNR required to achieve d DoF, similarly to [41] [69] [79]. Specifically, the number of users should scale as $K = \Theta\left(\rho^{d\frac{M-N_R}{M}}\right)$ and $\Theta\left(\rho^{d\frac{M-1}{M}}\right)$ for RBF-MMSE and RBF-MF/AS, respectively. Thus, significantly less number of users is required in RBF-MMSE as compared to RBF-MF/AS for achieving the same DoF. With RBF and under the assumption $K = \Theta(\rho^{\alpha})$, it is also interesting to observe from Lemma

5.3.1 that the achievable DoF can be a non-negative real number (as compared to the conventional integer DoF in the literature with finite K). This comes from our (quite general) assumption that α can take any arbitrary real value.

Next, we obtain the maximum achievable DoF of RBF-MMSE for a given α by searching over all possible values of M. We note that for any $M < \lfloor\alpha\rfloor + N_R$, $d_{RBF}(\alpha, M) < d_{RBF}(\alpha, \lfloor\alpha\rfloor + N_R)$, while for any $M > \lfloor\alpha\rfloor + N_R + 1$, $d_{RBF}(\alpha, M) < d_{RBF}(\alpha, \lfloor\alpha\rfloor + N_R + 1)$. Thus we only need to compare $d_{RBF}(\alpha, \lfloor\alpha\rfloor + N_R)$ and $d_{RBF}(\alpha, \lfloor\alpha\rfloor + N_R + 1)$ in searching for the optimal M. The maximum achievable DoF of RBF-MF/AS can be obtained similarly.

Theorem 5.3.1 *For a single-cell MIMO RBF system with N_T transmit antennas, N_R receive antennas, and user density coefficient α, the maximum achievable DoF and the corresponding optimal number of transmit beams with MMSE, MF, or AS based receivers are*[3]

$$d^*_{\textit{RBF-MMSE}}(\alpha) = \begin{cases} \lfloor\alpha\rfloor + N_R, & \alpha \le N_T - N_R, N_R \ge \{\alpha\}(\lfloor\alpha\rfloor + N_R + 1), \\ \frac{\alpha(\lfloor\alpha\rfloor + N_R + 1)}{\lfloor\alpha\rfloor + 1}, & \alpha \le N_T - N_R, \{\alpha\}(\lfloor\alpha\rfloor + N_R + 1) > N_R, \\ N_T, & \alpha > N_T - N_R. \end{cases} \tag{5.24}$$

$$M^*_{\textit{RBF-MMSE}}(\alpha) = \begin{cases} \lfloor\alpha\rfloor + N_R, & \alpha \le N_T - N_R, N_R \ge \{\alpha\}(\lfloor\alpha\rfloor + N_R + 1), \\ \lfloor\alpha\rfloor + N_R + 1, & \alpha \le N_T - N_R, \{\alpha\}(\lfloor\alpha\rfloor + N_R + 1) > N_R, \\ N_T, & \alpha > N_T - N_R. \end{cases} \tag{5.25}$$

[3]The notations $\lfloor\alpha\rfloor$ and $\{\alpha\}$ denote the integer and fractional parts of a real number α, respectively.

$$d^*_{RBF\text{-}MF/AS}(\alpha) = \begin{cases} \lfloor \alpha \rfloor + 1, & \alpha \leq N_T - 1, 1 \geq \{\alpha\}(\lfloor \alpha \rfloor + 2), \\ \frac{\alpha(\lfloor \alpha \rfloor + 2)}{\lfloor \alpha \rfloor + 1}, & \alpha \leq N_T - 1, \{\alpha\}(\lfloor \alpha \rfloor + 2) > 1, \\ N_T, & \alpha > N_T - 1. \end{cases} \tag{5.26}$$

$$M^*_{RBF\text{-}MF/AS}(\alpha) = \begin{cases} \lfloor \alpha \rfloor + 1, & \alpha \leq N_T - 1, 1 \geq \{\alpha\}(\lfloor \alpha \rfloor + 2), \\ \lfloor \alpha \rfloor + 2, & \alpha \leq N_T - 1, \{\alpha\}(\lfloor \alpha \rfloor + 2) > 1, \\ N_T, & \alpha > N_T - 1. \end{cases} \tag{5.27}$$

In Fig. 5.3, we show the maximum DoF and the corresponding optimal number of transmit beams versus the user density coefficient α with $N_T = 5$ and $N_R = 3$ for each single-cell RBF scheme, according to Theorem 5.3.1. It is observed that in general, RBF-MMSE achieves a higher maximum DoF by transmitting more data beams as compared to RBF-MF or RBF-AS. As a result, RBF-MMSE system can serve more users with better rate performance than RBF-MF/AS. However, the improvement in the achievable rate and coverage comes at the cost of higher complexity by employing MMSE receivers.

One important question is how the RBF schemes perform as compared to the optimal DPC-based transmission scheme assuming the full transmitter-side CSI in single-cell MIMO BCs. In the following, we answer this question in terms of achievable sum-rate DoF. First, we obtain an upper bound on the single-cell achievable DoF with arbitrary transmission schemes.

Proposition 5.3.1 *Assuming $K = \Theta(\rho^\alpha)$ with $\alpha \geq 0$, the DoF of a single-cell MIMO*

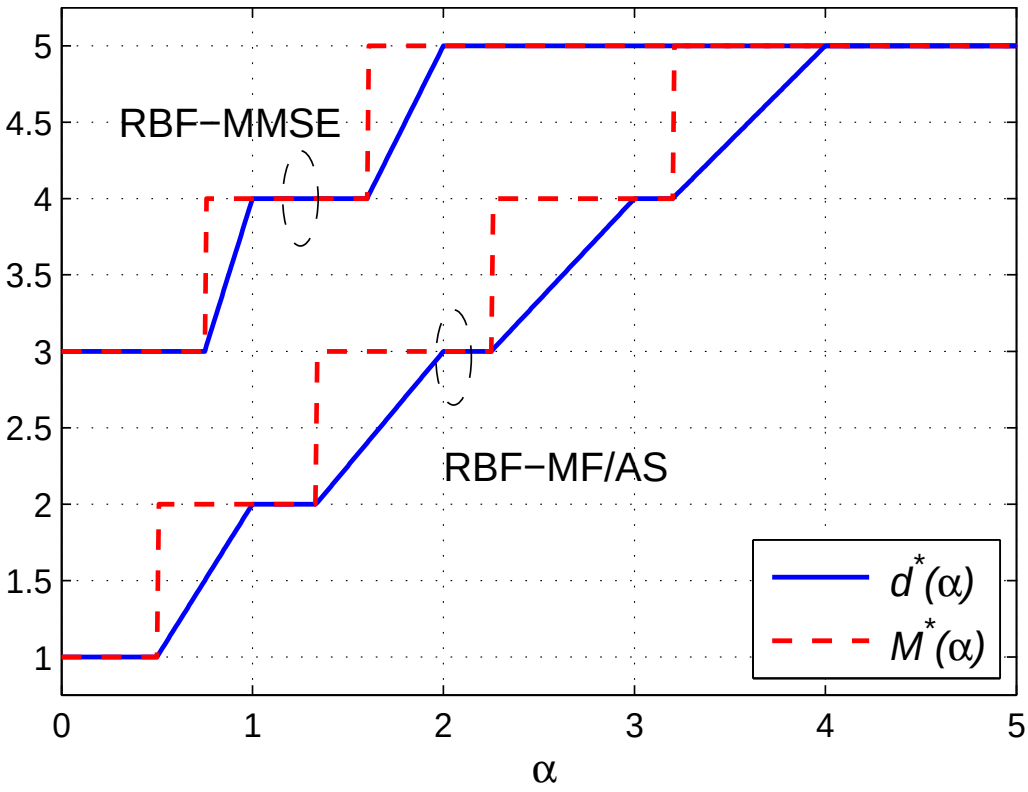

Figure 5.3: The maximum sum-rate DoF $d^*_{\text{RBF-Rx}}(\alpha)$ and optimal number of transmit beams $M^*_{\text{RBF-Rx}}(\alpha)$ with $N_T = 5$ and $N_R = 3$, where "Rx" denotes MMSE, MF, or AS.

BC with N_T transmit antennas at the BS and N_R receive antennas at each MS is upper-bounded by N_T as $\rho \to \infty$.

Proof 12 *Please refer to Appendix C.4.*

Proposition 5.3.1 states that the maximum DoF of the single-cell MIMO BC is always N_T, even with asymptotically large number of users that scales with the increasing SNR. Next, applying Theorem 5.3.1 and Proposition 5.3.1 yields the following proposition.

Proposition 5.3.2 *Assuming $K = \Theta(\rho^\alpha)$, the single-cell RBF schemes are DoF-optimal, i.e., $d^*_{RBF\text{-}MMSE}(\alpha) = N_T$ and $d^*_{RBF\text{-}MF/AS}(\alpha) = N_T$, if and only if*

- *RBF-MMSE: $\alpha \geq N_T - N_R$;*
- *RBF-MF/AS: $\alpha \geq N_T - 1$.*

It thus follows that the single-cell RBF schemes achieve the maximum DoF with $M = N_T$ if the number of users per-cell is sufficiently large, thanks to the multiuser diversity and/or spatial diversity that completely eliminates the intra-cell interference. However, spatial diversity gain in the achievable DoF is available only in the case of MMSE based receiver.

As an example for illustration, we compare the numerical sum-rates and the DoF scaling law in Fig. 5.4, in which the DPC, RBF-MMSE, RBF-MF, and RBF-AS are employed, and $N_T - 1 > \alpha \geq N_T - N_R$. We consider two single-cell systems with the following parameters: (a) $M = N_T = 3$, $N_R = 2$, $\alpha = 1$, $K = \lfloor \rho^\alpha \rfloor$; and (b) $M = N_T = 4$, $N_R = 3$, $\alpha = 1.2$, $K = \lfloor \rho^\alpha \rfloor$. The rates and scaling law of system (a) and (b) are denoted as the solid and dash lines, respectively. Note that in both cases, the DPC and RBF-MMSE sum-rates follow the (same) DoF scaling law quite closely. This example clearly demonstrates the DoF optimality of the RBF-MMSE given that $\alpha \geq N_T - N_R$. Furthermore, since $\alpha < N_T - 1$, the RBF-MF, RBF-AS, and consequently MISO RBF schemes are DoF sub-optimal as clearly shown in Fig. 5.4. It is important to note that the values of the SNR and the numbers of users are only moderate in this example. This thus shows the practical usefulness of our

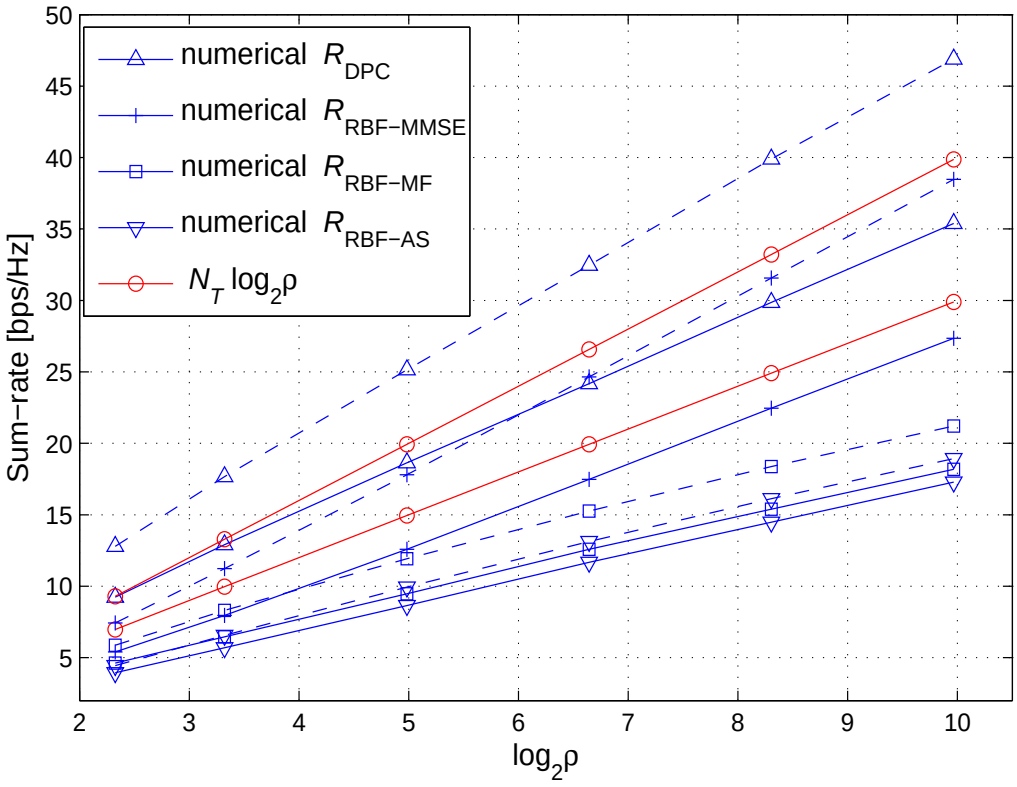

Figure 5.4: Comparison of the numerical DPC, RBF-MMSE, RBF-MF, and RBF-AS sum-rates, and the DoF scaling law with $N_T - 1 \geq \alpha \geq N_T - N_R$. The rates and scaling law of system (a) and (b) are denoted as the solid and dash lines, respectively.

optimality conditions for RBF schemes given in Proposition 5.3.2.

Next, we compare our new asymptotic result to the conventional one in [64] and [65] with finite per-cell SNR, which states that for any given $M \leq N_T$ and $N_R \geq 1$, the sum-rate achievable by single-cell RBF satisfies

$$\lim_{K\to\infty} \frac{R_{\text{RBF-Rx}}}{M \log_2 \log K} = 1, \tag{5.28}$$

where "Rx" denotes any of MMSE, MF, and AS.

We observe a notable difference between the conclusions drawn from our high-SNR analysis and the conventional finite-SNR analysis both with the number of per-cell users increasing to infinity. In the finite-SNR case, from (5.28) it follows that there is no asymptotic sum-rate gain by RBF-MMSE over RBF-MF or RBF-AS, and the asymptotic sum-rate is independent of N_R. This thus leads to an improper conclusion that using only one single antenna at each receiver is sufficient to capture the asymptotic rate of RBF. As a result, the benefit of receive spatial diversity is neglected, which in turn severely degrades the RBF rate performance especially for interference-limited multi-cell systems. However, with our high-SNR analysis, the effects of the number of receive antennas as well as the spatial diversity technique used (MMSE versus MF/AS) on the DoF performance are clearly shown. This demonstrates the advantage of our new approach for designing practical multi-cell systems employing RBF.

5.3.2 Multi-Cell Case

In this subsection, we extend the DoF analysis for the single-cell case to the more general multi-cell RBF. For convenience, we define the achievable sum-rate DoF of the c-th cell as $d_{\text{RBF-Rx},c}(\alpha_c, \boldsymbol{m}) = \lim_{\rho\to\infty} \frac{R^{(c)}_{\text{RBF-Rx}}}{\log_2 \rho}$, where $\boldsymbol{m} = [M_1,\cdots,M_C]^T$ is a given set of numbers of transmit beams at different BSs. We then state the following result on the achieve DoF of the c-th cell.

Lemma 5.3.2 *In the multi-cell case, given $K_c = \Theta(\rho^{\alpha_c})$ and $\boldsymbol{m}$, the achievable DoF of the c-th cell with RBF-MMSE, RBF-MF, and RBF-AS schemes are given by*

$$d_{RBF\text{-}MMSE,c}(\alpha_c, \boldsymbol{m}) = \begin{cases} \dfrac{\alpha_c M_c}{\sum_{l=1}^{C} M_l - N_R}, & 0 \le \alpha_c \le \sum_{l=1}^{C} M_l - N_R \quad (5.29a) \\ M_c, & \alpha_c > \sum_{l=1}^{C} M_l - N_R. \quad (5.29b) \end{cases}$$

$$d_{RBF\text{-}MF/AS,c}(\alpha_c, \boldsymbol{m}) = \begin{cases} \dfrac{\alpha_c M_c}{\sum_{l=1}^{C} M_l - 1}, & 0 \le \alpha_c \le \sum_{l=1}^{C} M_l - 1 \quad (5.30a) \\ M_c, & \alpha_c > \sum_{l=1}^{C} M_l - 1. \quad (5.30b) \end{cases}$$

The proof of the above lemma can be obtained by similar arguments as for Lemma 5.3.1, and is thus omitted for brevity. Compared to the single-cell case, in the multi-cell case there are not only $M_c - 1$ intra-cell interfering beams, but also $\sum_{l=1, l\neq c}^{C} M_l$ inter-cell interfering beams for any received beam in the c-th cell, as observed from the denominators in (5.29a) and (5.30a), which results in a decrease in the achievable DoF per cell.

We again compare our new asymptotic result to that obtained from the conventional asymptotic analysis with finite per-cell SNR [64], [65]. We first note the following result, which states that for any given $M_c \le N_T$ and $N_R \ge 1$, the sum-rate achievable by the c-th cell RBF satisfies

$$\lim_{K_c \to \infty} \frac{R^{(c)}_{\text{RBF-Rx}}}{M_c \log_2 \log K_c} = 1, \quad (5.31)$$

where "Rx" denotes any of MMSE, MF, and AS. Thus (5.28) and (5.31) imply that the rate performance of each cell with any given number of receive antennas at the users in a multi-cell RBF system is equivalent to that of a single-cell RBF with *one antenna at each user*. Such a conclusion may be misleading in a practical multi-cell system with non-negligible ICI where receive spatial diversity can help significantly improve the rate performance based on our new DoF analysis. Furthermore, (5.31) implies

that even in multi-cell RBF systems, each BS should use *all* available orthogonal beams for transmission, i.e., $M_c = N_T$, $\forall\ c = 1, \ldots, C$. This conclusion can severely degrade the rate performance of RBF systems, as illustrated in the next example.

In Fig. 5.5, we depict the (total) achievable sum-rates of two RBF-MMSE systems with the following parameters: (a) $C = 2$, $M_1 = M_2 = M \leq N_T = 4$, $N_R = 2$, $\gamma_{1,2} = \gamma_{2,1} = 0.8$, and $K_1 = K_2 = K = 200$; and (b) $C = 3$, $M_1 = M_2 = M_3 = M \leq N_T = 4$, $N_R = 2$, $\gamma_{l,c} = 0.8$, l, $c = 1, 2, 3$, $l \neq c$, and $K_1 = K_2 = K_3 = K = 200$. Thus, with $\rho = [5\ 10\ 15\ 20]$ dB, we have $K \approx \lfloor \rho^{\alpha} \rfloor$, where $\alpha = [4.6021\ 2.3010\ 1.5340\ 1.1505]$. Consider first system (a). From (5.31), the conventional asymptotic analysis implies that the optimal rate performance is achieved with $M_1 = M_2 = 4$. However, given the constraint $M_1 = M_2 = M$, Lemma 5.3.2 suggests that the best rate performance is achieved with $M = 3$ when $\rho = 5$ dB and $M = 2$ for the other cases. The reason is that the discrete function $\frac{\alpha M}{2M - N_R}$, under $M \leq 4$, is maximized at $M = 3$ when $\alpha = 4.6021$ and $M = 2$ for the other values of α. A similar argument can be applied to system (b), where the best rate performance is achieved with $M = 2$ when $\rho = 5$ dB and $M = 1$ for the other cases. Figs. 5.5a and 5.5b thus clearly confirm the conclusions inferred from Lemma 5.3.2. Note that the setting $M = 4$ almost gives the worst rate performance in all cases.

For convenience, let $\boldsymbol{d}_{\text{RBF-Rx}}(\boldsymbol{\alpha}, \boldsymbol{m}) = \left[d_{\text{RBF-Rx},1}(\alpha_1, \boldsymbol{m}), \cdots, d_{\text{RBF-Rx},C}(\alpha_C, \boldsymbol{m})\right]^T$ be the DoF vector, with $d_{\text{RBF-Rx},c}(\alpha_c, \boldsymbol{m})$, $c = 1, \ldots, C$, obtained from Lemma 5.3.2. The characterization of the DoF region for the multi-cell RBF scheme with different receive spatial diversity techniques is then given in the following proposition.

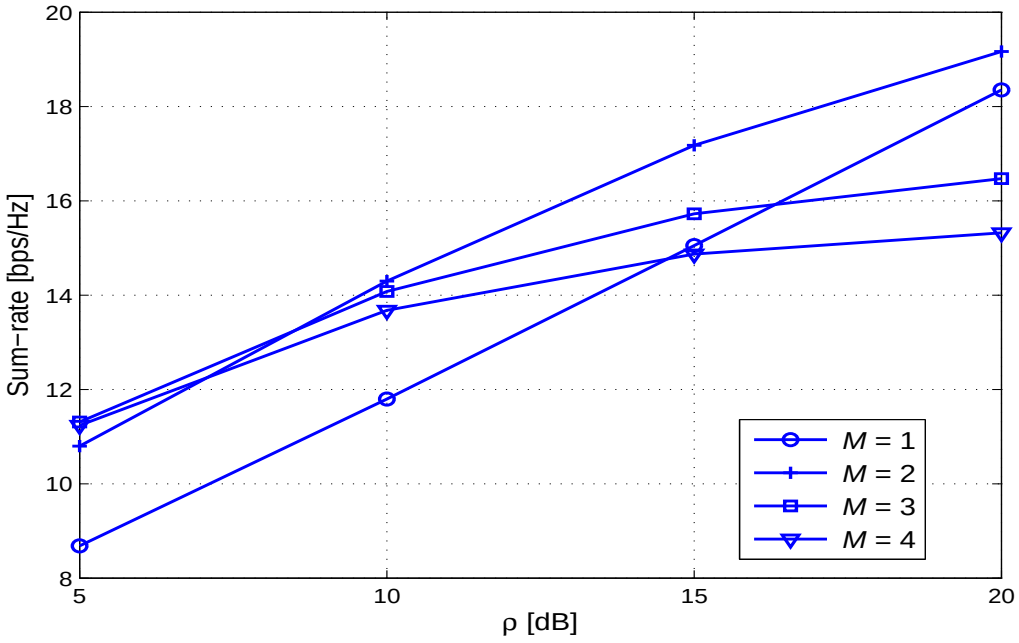

(a) Two-cell

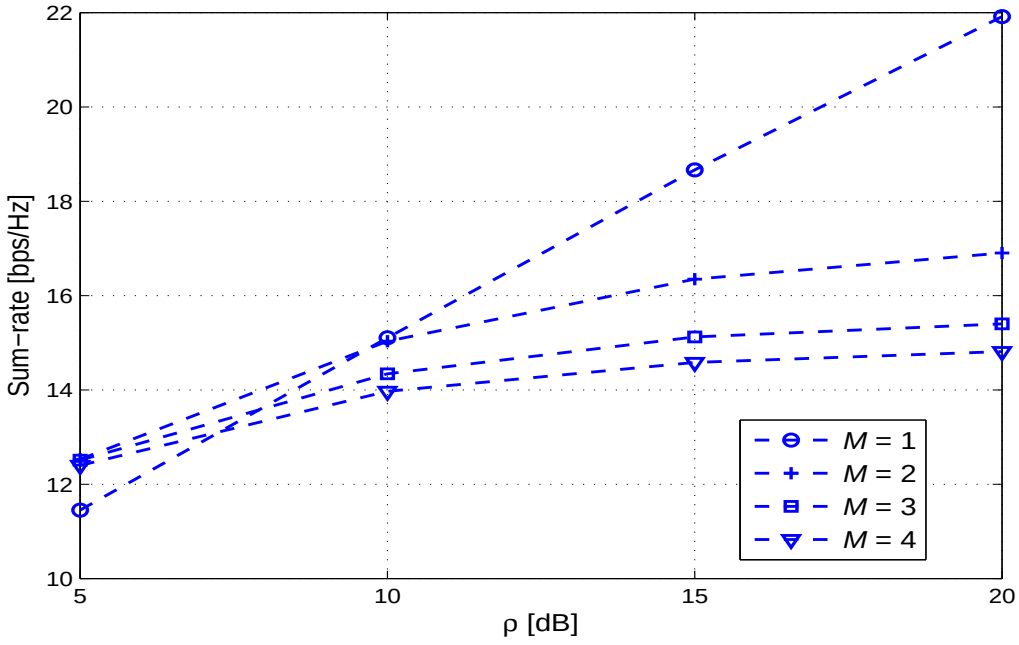

(b) Three-cell

Figure 5.5: Sum-rates of RBF-MMSE systems as a function of the SNR.

Proposition 5.3.3 *Given $K_c = \Theta\left(\rho^{\alpha_c}\right), c = 1, \ldots, C$, the achievable DoF region of a C-cell MIMO RBF system is given by*

$$\mathcal{D}_{RBF\text{-}Rx}(\boldsymbol{\alpha}) = \boldsymbol{conv}\left\{\boldsymbol{d}_{RBF\text{-}Rx}(\boldsymbol{\alpha}, \boldsymbol{m}), M_c \in \{0, \cdots, N_T\}, c = 1, \cdots, C\right\}, \quad (5.32)$$

where $\boldsymbol{conv}$ *denotes the convex hull operation over all DoF vectors obtained with different values of* $\boldsymbol{m}$ *and "Rx" stands for MMSE, MF, or AS.*

Fig. 5.6 shows the DoF region of a two-cell system employing either RBF-MMSE or RBF-MF/AS. We assume $N_T = 4$ and $N_R = 2$. It is observed that when α_1 and α_2 are small, the DoF region is more notably expanded by using MMSE receiver over MF/AS receiver. We conclude that receive spatial diversity is more beneficial when the numbers of users are relatively small. Note that to obtain d_c DoF, the number of users in the c-th cell are at least in the order of $\Theta\left(\rho^{d_c \frac{\sum_{l=1}^{C} M_l - N_R}{M_c}}\right)$ and $\Theta\left(\rho^{d_c \frac{\sum_{l=1}^{C} M_l - 1}{M_c}}\right)$ with RBF-MMSE and RBF-MF/AS, respectively (cf. Lemmas 5.3.2). Thus, significantly less number of users per cell is required in RBF-MMSE as compared to RBF-MF/AS for achieving the same DoF.

In practice, each cell can set different numbers of transmit beams at the BS. In general, the optimal DoF tradeoffs or the boundary DoF points are achieved when all the MSs apply the MMSE receiver and all the BSs cooperatively assign their numbers of transmit beams based on per-cell user densities and number of transmit/receive antennas. However, it is worth noting that there exists an underlying tradeoff between the achievable DoF and the receiver complexity, which determines the most desirable operating configuration of the system in consideration.

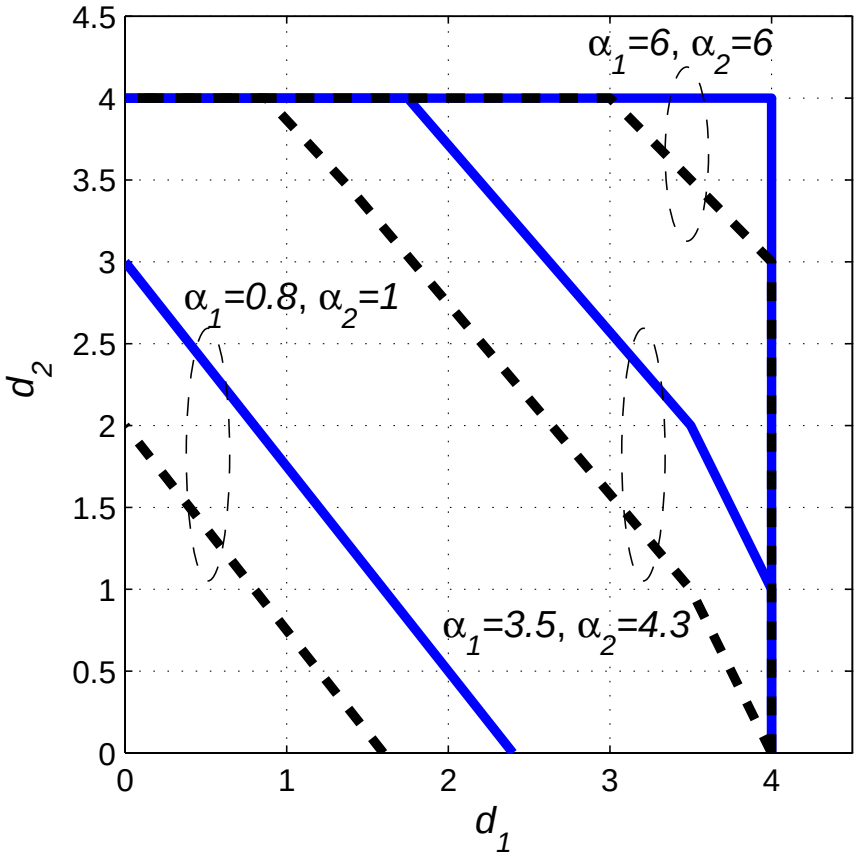

Figure 5.6: DoF regions of two-cell MIMO RBF with different types of diversity receivers. The region boundaries for RBF-MMSE and RBF-MF/AS are denoted by solid and dashed lines, respectively.

5.3.3 Optimality of Multi-Cell RBF

It can be inferred from Lemma 5.3.2 and observed from Fig. 5.6 that the DoF regions of RBF-MMSE and RBF-MF/AS both converge to the same region if the per-cell user densities are sufficiently large, in which all cells attain their maximum DoF N_T by setting $M_c = N_T$, $\forall c$. The converged region is thus the "interference-free" DoF region as if there was no ICI such that each cell can be treated as an independent

single-cell system. The above result implies that the multi-cell RBF is conceivably DoF-optimal given a sufficiently large number of users per cell, which is an extension of Proposition 5.3.2 to the multi-cell case. In this subsection, we rigorously develop this result. First, we present a (crude) DoF region upper bound for the C-cell MIMO downlink system with arbitrary transmission schemes. The proof follows directly from Proposition 5.3.1 and is thus omitted for brevity.

Proposition 5.3.4 *Given $K_c = \Theta(\rho^{\alpha_c})$, $c = 1, \cdots, C$, an upper bound of the DoF region defined in (1.2.1) for a C-cell MIMO downlink system is*

$$\mathcal{D}_{\text{UB}}(\boldsymbol{\alpha}) = \left\{(d_1, d_2, \cdots d_C) \in \mathbb{R}_+^C : d_c \leq N_T, c = 1, \cdots, C\right\}. \tag{5.33}$$

The DoF optimality of multi-cell RBF schemes is then obtained in the following proposition.

Proposition 5.3.5 *Given $K_c = \Theta(\rho^{\alpha_c})$, $c = 1, \cdots, C$, the multi-cell RBF schemes with different receive spatial diversity techniques achieve the "interference-free" DoF region upper bound of a C-cell MIMO downlink system, i.e., $\mathcal{D}_{RBF\text{-}Rx}(\boldsymbol{\alpha}) = \mathcal{D}_{\text{UB}}(\boldsymbol{\alpha})$, if*

- *RBF-MMSE: $\alpha_c \geq CN_T - N_R$, $\forall c \in \{1, \cdots, C\}$.*
- *RBF-MF/AS: $\alpha_c \geq CN_T - 1$, $\forall c \in \{1, \cdots, C\}$.*

A direct consequence of Proposition 5.3.5 is thus $\mathcal{D}_{\text{RBF-Rx}}(\boldsymbol{\alpha}) = \mathcal{D}_{\text{MIMO}}(\boldsymbol{\alpha})$, i.e., each RBF scheme is indeed DoF-optimal when the numbers of users in all cells are sufficiently large. Due to the dominant multi-user diversity gain, RBF compensates

the lack of full CSI at transmitters without any DoF loss. Furthermore, to achieve the interference-free DoF region, we infer from Proposition 5.3.5 that RBF-MMSE requires a much less number of users per cell, with a difference of $N_R - 1$ in the scaling order with respect to the SNR, as compared to RBF-MF or RBF-AS.

5.4 Conclusion

In this chapter, we study the achievable sum-rate in multi-cell MIMO RBF systems for the regime of both high SNR and large number of users per cell. We propose three RBF schemes for spatial diversity receivers with multiple antennas, namely, RBF-MMSE, RBF-MF, and RBF-AS. The SINR distributions in the multi-cell RBF with different types of spatial receiver are obtained in closed-form at any given finite SNR. Based on these results, we characterize the DoF region achievable by different multi-cell MIMO RBF schemes under the assumption that the number of users per cell scales in a polynomial order with the SNR as the SNR goes to infinity. Our investigation reveals significant gains by using MMSE-based spatial receiver in the achievable sum-rate and DoF region in multi-cell RBF, which considerably differs from the existing result based on the conventional asymptotic analysis with fixed per-cell SNR. The results of this chapter thus provide new insights on the optimal design of interference-limited multi-cell MIMO systems with only partial CSI at transmitters.

Chapter 6

Conclusions and Future Works

6.1 Summary of Contributions and Insights

Single-cell RBF is an important topic which has attracted a lot of attention. There is, however, virtually no investigation on cellular systems with RBF employed at each BS. Furthermore, how receive spatial diversity affects the performance of RBF systems has not been fully understood. In this thesis, we studied the multi-cell MISO and MIMO RBF systems with different types of receiver. The aim is to characterize the interplays among the receive spatial diversity, multi-user diversity, spatial multiplexing gain, inter-/intra-cell interferences, and BSs collaborative transmission.

In summary, the main contributions of this thesis are as follows.

- We presented an exact analytic investigation on fundamental performance measures of multi-cell MISO and MIMO RBF systems. Particularly, we studied the SINR and the sum-rate of the systems given a finite SNR. This was done in the

context of probability and multivariate analysis, by leveraging newly obtained results.

  - Multi-cell MISO RBF systems: The SINR distribution at each user was derived. Based on that, we presented an exact expression for the sum-rate of the systems (see Section 4.2.2).

  - Multi-cell MIMO RBF systems: We provided another proof of an important theorem in multivariate analysis. Furthermore, the SINR distributions of multi-cell MIMO RBF systems with different receive spatial diversity techniques were obtained (see Section 5.2).

- We investigated the rate performance of multi-cell RBF schemes under the regime of large number of users. We showed that the asymptotic rate scaling law of a single-cell MISO RBF system still holds for multi-cell RBF even with ICI and with or without receive spatial diversity (see Sections 4.2.3 and 5.3.1). This suggests that the large-number-of-user asymptotic analysis is not suitable for studying multi-cell RBF systems, where the ICI becomes a dominant factor, and a new approach should be considered.

- We proposed a new asymptotic investigation on the rate performance of multi-cell RBF systems under high-SNR regime. By using the notion of DoF region, we investigated the throughput trade-offs between all the cells. This approach effectively provides a unified view on the rate performance of multi-cell RBF systems under different setups (see Sections 4.3 and 5.3).

Based on these results, we have explored the performance of multi-cell RBF systems. In summary, the key insights obtained in this thesis are as follows.

- Collaboration among the BSs in assigning their respective numbers of data beams based on different per-cell user densities is essential to achieve the optimal throughput trade-offs among different cells. This is in sharp contrast with the result obtained in the regime of large number of users but fixed SNR per cell, which suggests that transmitting all beams is the optimal solution for multi-cell RBF systems (see Sections 4.3.2 and 5.3.2).

- The benefit of receive spatial diversity is significant for multi-cell RBF schemes. This insight also contrasts with the existing result that spatial diversity receivers only yield marginal sum-rate gain, which was obtained in the regime of large number of users but fixed SNR per cell. However, we note that there exists a trade-off between the rate/DoF performance and the complexity/delay time of RBF systems with different receivers (see Section 5.3).

- Multi-cell RBF schemes are optimal in terms of the rate performance albeit requiring only partial CSI at transmitters as compared to other full-CSI transmission schemes, such as IA. However, this only holds when the numbers of users in all cells are sufficiently large compared with the SNR (see Sections 4.3.3 and 5.3.3).

6.2 Proposals for the Future Research

Since multi-cell RBF systems have not been investigated extensively, there are many interesting topics which we can consider. In this section, we discuss several possible future works.

This thesis has focused only on the rate performance of multi-cell RBF systems, assuming perfect and analog CSI feedback. An interesting topic for future work is to investigate the multi-cell RBF schemes with reduced and quantized feedback. It is intuitive that more feedback bits might be necessary to capture the gain from multi-user diversity rather than only one bit in the single-cell case. However, more rigorous works are required before any conclusion is drawn.

The application of non-orthogonal RBF to cellular networks is also another promising direction. The first study needs to fully characterize the performance of non-orthogonal RBF in single-cell case. Further work might consider the problem of designing non-orthogonal RBF in all cells so that the intra-/inter-cell interference is kept small. The problem will essentially be related to the GLPP.

In this thesis, we mostly assume that the user is homogeneous, i.e., the large-scale fading is the same across all users. However, a multi-cell RBF system with heterogeneous users under diverse large-scale fading channels is a more realistic setup. An important topic is to examine the problem of user scheduling and investigate the rate performance with different scheduling schemes under heterogeneous multi-cell RBF systems.

Bibliography

[1] Abramowitz, M. and Stegun, I. A. (eds) [1972]. *Handbook of Mathematical Functions with Formulas, Graphs, and Mathematical Tables, 10th ed.*, New York: Dover.

[2] Andrews, M. [2004]. Instability of the proportional dair scheduling algorithm for hdr, *IEEE Trans. on Wireless Commun.,* **3**: 1422–1426.

[3] Andrews, M., Kumaran, K., Ramanan, K., Stoyar, A. and Whitting, P. [2001]. Providing quality of service over a shared wireless link, *IEEE Communications Mag.,* **39**: 150–154.

[4] Barg, A. and Nogin, D. Y. [2002]. Bounds on packings of spheres in the grassmann manifold, *IEEE Trans. Inf. Theory,* **48**: 2450–2454.

[5] Biglieri, E., Constantinides, A., Calderbank, R., Goldsmith, A., Paulraj, A. and Poor, V. [2006]. *Introduction to MIMO Wireless Communications*, Cambridge Univ. Press.

[6] Bjornson, E., Zakhour, R., Gesbert, D. and Ottersten, B. [2010]. Cooperative

multicell precoding: rate region characterization and distributed strategies with instantaneous and statistical csi, *IEEE Trans. Signal Process.,* **58**: 4298–4310.

[7] Brown, J. W. and Churchill, R. V. [2009]. *Complex Variables and Applications, 8th ed.*, Singapore: McGraw-Hill.

[8] Cadambe, V. R. and Jafar, S. A. [2008]. Interference alignment and degrees of freedom of the k-user interference channel, *IEEE Trans. Inf. Theory,* **54**: 3425–3441.

[9] Caire, G. and Shamai, S. [2003]. On the achievalbe throughput of a multi-antenna gaussian broadcast channel, *IEEE Trans. Inf. Theory,* **49**: 1691–1706.

[10] Costa, M. [1983]. Writing on dirty paper, *IEEE Trans. Inf. Theory,* **29**: 439–441.

[11] Couillet, R., Hoydis, J. and Debbah, M. [2012]. Random beamforming over quasi-static and fading channels: a deterministic equivalent approach, *IEEE Trans. Inf. Theory* **58**: 6392–6425.

[12] Dahrouj, H. and Yu, W. [2010]. Coordinated beamforming for the multicell multi-antenna wireless systems, *IEEE Trans. Wireless Commun.,* **9**: 1748–1795.

[13] David, H. and Nagaraja, H. [2003]. *Order statistics*, 3rd edn, New York: Wiley.

[14] Etkin, R., Tse, D. and Wang, H. [2008]. Gaussian interference channel capacity to within one bit, *IEEE Trans. Inf. Theory,* **54**: 5534–5562.

[15] Foschini, G. J. and Gans, M. [1998]. On limits of wireless communications in a fading environment when using multiple antennas, *Wireless Pers. Commun.,* **6**: 311355.

[16] Gao, H. and Smith, P. J. [1998]. Exact sinr calculations for optimum linear combining in wireless systems, *Prob. Eng. Inf. Sci.,* **40**: 261–281.

[17] Gershman, A. B. and Sidiropoulos, N. (eds) [2005]. *Space-Time Processing for MIMO Communications*, John Wiley & Sons.

[18] Gomadam, K., Cadambe, V. and Jafar, S. [2011]. A distributed numerical approach to interference alignment and applications to wireless interference networks, *IEEE Trans. Inf. Theory,* **57**: 3309–3322.

[19] Gou, T. and Jafar, S. A. [2010]. Degrees of freedom of the k user $m \times n$ mimo interference channel, *IEEE Trans. Inf. Theory,* **56**: 6040–6057.

[20] Gradshteyn, I. S. and Ryzhik, I. M. [2007]. *Table of Integrals, Series and Products*, 7th edn, Jeffrey, A. & Zwillinger, D. (eds), Academic Press.

[21] Gross, K. I. and Richards, D. S. P. [1989]. Total positivity, spherical series, and hyper-geometric functions of matrix argument, *J. Approx. Theory,* **59**: 224–246.

[22] Han, T. S. and Kobayashi, K. [1981]. A new achievable rate region for the interference channel, *IEEE Trans. Inf. Theory,* **27**: 49–60.

[23] Hochwald, B. M., Marzetta, T. L., Richardson, T. J., Sweldens, W. and Urbanke,

R. [2000]. Systematic design of unitary space-time constellations, *IEEE Trans. Inf. Theory,* **46**: 1962–1973.

[24] Huang, K., Andrews, J. G. and Heath, R. W. [2009]. Performance of orthogonal beamforming for sdma with limited feedback, *IEEE Trans. Veh. Tech.,* **58**: 152–164.

[25] Huang, K., Heath, R. W. and Andrews, J. G. [2007]. Space division multiple access with a sum feedback rate constraint, *IEEE Trans. Veh. Tech.,* **58**: 3879–3891.

[26] Huang, Y. and Rao, B. D. [2012]. Closed form sum rate of random beamforming, *IEEE Commun. Lett.,* **16**: 630–633.

[27] Huang, Y. and Rao, B. D. [2013]. Random beamforming with heterogeneous users and selective feedback: individual sum rate and individual scaling laws, *IEEE Trans. Wireless Commun.,* **12**: 2080–2090.

[28] Jafar, S. A. [2011]. *Interference alignment: a new look at signal dimensions in a communication network*, Foundations and Trends in Communications and Information Theory.

[29] James, A. T. [1964]. *Distributions of matrix variates and latent roots derived from normal samples*, Vol. 35.

[30] Jindal, N. [2006]. Mimo broadcast channels with finite-rate feedback, *IEEE Trans. Inf. Theory,* **52**: 5045–5060.

[31] Jindal, N., Rhee, W., Vishwanath, S., Jafar, S. A. and Goldsmith, A. [2005]. Sum power iterative water-filling for multi-antenna gaussian broadcast channels, *IEEE Trans. Inf. Theory,* **51**: 1570–1580.

[32] Kang, M., Yang, L. and Alouini, M. S. [2006]. Outage probability of mimo optimum combining in presence of unbalanced co-channel interferences and noise, *IEEE Trans. Wireless Commun.,* **5**: 1661–1668.

[33] Khatri, C. G. [1966]. On certain distribution problems based on positive definite quadratic functions in normal vectors, *Ann. Inst. Statist. Math.,* **37**: 468–479.

[34] Kim, C., Lee, S. and Lee, J. [2013]. Sinr and throughput analysis for random beamforming systems with adaptive modulation, *IEEE Trans. Wireless Commun.,* **12**: 1460–1471.

[35] Kim, I. H., Park, S. Y., Love, D. J. and Kim, S. J. [2009]. Improved multi-user mimo unitary precoding using partial channel state information and insights from the reimannian manifold, *IEEE Trans. Wireless Commun.,* **8**: 4014–4022.

[36] Kim, Y., Yang, J. and Kim, D. K. [2008]. A closed form approximation of the sum-rate upper bound of random beamforming, *IEEE Commun. Lett.,* **12**: 365–367.

[37] Ko, Y.-C., Yang, H.-C., Eom, S.-S. and Alouini, M.-S. [2007]. Adaptive modulation with diversity combining based on output-threshold mrc, *IEEE Trans. Wireless Commun.,* **6**: 3728–3737.

[38] Kountouris, M., Gesbert, D. and Salzer, T. [2008]. Enhanced multiuser random beamforming: dealing with the not-so-large number of users case, *IEEE Trans. Wireless Commun.,* **26**: 1536–1545.

[39] Kushner, H. and Whiting, P. A. [2004]. Convergence of proportional-fair sharing algorithms under general conditions, *IEEE Trans. Wireless Commun.,* **3**: 1250–1259.

[40] Kwon, H., Jang, E. W. and Cioffi, J. M. [2011]. Predetermined power allocation for opportunistic beamforming with limited feedback, *IEEE Trans. Wireless Commun.,* **10**: 84–90.

[41] Lee, J. H. and Choi, W. [2013]. On the achievable dof and user scaling law of opportunistic interference alignment in 3-transmitter mimo interference channels, *to appear in IEEE Trans. Wireless Commun., (available on-line at arXiv:1109.6541)* .

[42] Lee, J. and Jindal, N. [2007]. High snr analysis for mimo broadcast channels: dirty paper coding vs. linear precoding, *IEEE Trans. Inf. Theory* **53**: 4787–4792.

[43] Liu, Y.-F., Dai, Y.-H. and Luo, Z.-Q. [2011]. Coordinated beamforming for miso interference channel: complexity analysis and efficient algorithms, *IEEE Trans. Signal Process.,* **59**: 1142–1157.

[44] Louie, R. H. Y., McKay, M. R. and Collings, I. B. [2009]. Maximum sum-rate

of mimo multi-user scheduling with linear receivers, *IEEE Trans. Commun.,* **57**: 3500–3510.

[45] Love, D. J. and Heath, R. W. [2003]. Grassmannian beamforming for multiple-input multiple-ouput wireless systems, *IEEE Trans. Inf. Theory,* **49**: 2735–2747.

[46] McKay, M. R., Zanella, A., Collings, I. B. and Chiani, M. [2009]. Error probability and sinr analysis of optimum combining in rician fading, *IEEE Trans. Commun.,* **57**: 676–687.

[47] Moon, S.-H., Lee, S.-R. and Lee, I. [2011]. Sum-rate capacity of random beamforming for multi-antenna broadcast channels with other cell interference, *IEEE Trans. Wireless Commun.,* **10**: 2440–2444.

[48] Ng, B., Evans, J., Hanly, S. and Aktas, D. [2008]. Distributed downlink beamforming with cooperative base stations, *IEEE Trans. Inf. Theory,* **54**: 5491–5499.

[49] Nguyen, H. D., Zhang, R. and Hui, H. T. [2013a]. Effect of spatial receive diversity on the dof region of multi-cell random beamforming, *submitted to IEEE Trans. Wireless Commun.* .

[50] Nguyen, H. D., Zhang, R. and Hui, H. T. [2013b]. Multi-cell random beamforming: achievable rate and degree of freedom region, *IEEE Trans. Sig. Proc.,* **61**: 3532–3544.

[51] Ozdemir, O. and Torlak, M. [2010]. Optimum feedback quantization for an

opportunistic beamforming scheme, *IEEE Trans. Wireless Commun.,* **9**: 1584–1593.

[52] Papailiopoulos, D. S. and Dimakis, A. G. [2012]. Interference alignment as a rank constrained rank minimization, *IEEE Trans. Inf. Theory,* **60**: 4278–4288.

[53] Park, D. and Park, S. Y. [2008]. Performance analysis of multiuser diversity under transmit antenna correlation, *IEEE Trans. Commun.,* **56**: 666–674.

[54] Park, S. H. and Lee, I. [2011]. Degrees of freedom of multiple broadcast channels in the presence of inter-cell interference, *IEEE Trans. Commun.,* **59**: 1481–1487.

[55] Paulraj, A., Nabar, R. and Gore, D. [2003]. *Introduction to Space-Time Wireless Communications*, Cambridge Univ. Press.

[56] Peters, S. W. and Heath, R. W. [2011]. Cooperative algorithms for mimo interference channels, *IEEE Trans. Vel. Tech.,* **60**: 206218.

[57] Qiu, J., Zhang, R., Luo, Z. Q. and Cui, S. [2011]. Optimal distributed beamforming for miso interference channels, *IEEE Trans. Signal Process.,* **59**: 5638–5643.

[58] Rajanna, A. and Jindal, N. [2012]. Multi-user diversity in downlink channels: when does the feedback cost outweigh the spectral efficiency benefit, *IEEE Trans. Wireless Commun.,* **11**: 408–418.

[59] Razaviyayn, M., Sanjabi, M. and Luo, Z. Q. [2012]. Linear transceiver design for interference alignment: complexity and computation, *IEEE Trans. Inf. Theory,* **58**: 2896–2910.

[60] Sanayei, S. and Nosratinia, A. [2007]. Opportunistic beamforming with limited feedback, *IEEE Trans. Wireless Commun.,* **6**: 2765–2770.

[61] Shah, A. and Haimovich, A. M. [2000]. Performance analysis of maximum ratio combining and comparison with optimum combining for mobile radio communications with cochannel interference, *IEEE Trans. Veh. Tech.,* **49**: 1454–1463.

[62] Shang, X., Chen, B. and Poor, H. V. [2011]. Multiuser miso interference channels with single-user detection: optimality of beamforming and the achievable rate region, *IEEE Trans. Inf. Theory,* **57**: 4255–4273.

[63] Shannon, C. E. and Weaver, W. [1949]. *A Mathematical Theory of Communication*, Univ. of Illinois Press.

[64] Sharif, M. and Hassibi, B. [2005]. On the capacity of mimo broadcast channel with partial side information, *IEEE Trans. Inf. Theory,* **51**: 506–522.

[65] Sharif, M. and Hassibi, B. [2007]. A comparison of time-sharing, beamforming, and dpc for mimo broadcast channels with many users, *IEEE Trans. Commun.,* **55**: 11–15.

[66] So, J. and Cioffi, J. M. [2009]. Feedback reduction scheme for downlink multiuser diversity, *IEEE Trans. Wireless Commun.,* **8**: 668–672.

[67] Spencer, Q. H., Swindlehurst, A. L. and Haardt, M. [2004]. Zero-forcing methods for downlink spatial multiplexing in multiuser mimo channels, *IEEE Trans. Sig Proc.* **52**: 461–471.

[68] Sun, L. and McKay, M. R. [2010]. Eigen-based transceivers for the mimo broadcast channel with semi-orthogonal user selection, *IEEE Trans. Sig. Proc.,* **58**: 5246–5261.

[69] Tajer, A. and Wang, X. [2012]. (n,k)-user interference channel: degrees of freedom, *IEEE Trans. Inf. Theory,* **58**: 5338–5353.

[70] Telatar, E. [1999]. Capacity of multi-antenna gaussian channels, *European Trans. on Telecomm.,* **10**: 585596.

[71] Vicario, J. L., Bosisio, R., Anton-Haro, C. and Spagnolini, U. [2008]. Beam selection strategies for orthogonal random beamforming in sparse networks, *IEEE Trans. Wireless Commun.,* **7**: 3385–3396.

[72] Viswanath, P., Tse, D. N. C. and Laroia, R. [2002]. Opportunistic beamforming using dumb antennas, *IEEE Trans. Inf. Theory,* **48**: 1277–1294.

[73] Wagner, J., Liang, Y. C. and Zhang, R. [2008]. On the balance of multiuser diversity and spatial multiplexing gain in random beamforming, *IEEE Trans. Wireless Commun.,* **7**: 2512–2525.

[74] Weingarten, H., Steinberg, Y. and Shamai, S. [2006]. The capacity region of the gaussian multiple-input multiple-output broadcast channel, *IEEE Trans. Inf. Theory,* **52**: 3936–3964.

[75] Westphal, C. [2004]. Monitoring proportional fairness in cdma2000 high data rate networks, *Proc. Globecom,* **6**: 3866–3871.

[76] Winters, J. [1987]. On the capacity of radio communication systems with diversity in a rayleigh fading environment, *IEEE J. Sel. Areas Commun.,* **5**: 871878.

[77] Xia, M., Wu, Y.-C. and Aissa, S. [2012]. Non-orthogonal opportunistic beamforming: performance analysis and implementation, *IEEE Trans. Wireless Commun.,* **11**: 1424–1433.

[78] Xue, Y. and Kaiser, T. [2007]. Exploiting multiuser diversity with imperfect one-bit channel state feedback, *IEEE Trans. Veh. Tech.,* **56**: 183–193.

[79] Yang, H.-C., Lu, P., Sung, H.-K. and Ko, Y.-C. [2011]. Exact sum-rate analysis of mimo broadcast channels with random unitary beamforming, *IEEE Trans. Commun.,* **59**: 2982–2986.

[80] Yoo, T. and Goldsmith, A. [2006]. On the optimality of multi-antenna broadcast scheduling using zero-forcing beamforming, *IEEE J. Sel. Areas Commun.,* **24**: 528–541.

[81] Zhang, L., Zhang, R., Liang, Y. C., Xin, Y. and Poor, H. V. [2012]. On the gaussian mimo bc-mac duality with multiple transmit covariance constraints, *IEEE Trans. Inf. Theory,* **58**: 2064–2078.

[82] Zhang, R. [2010]. Cooperative multi-cell block diagonalization with per-base-station power constraints, *IEEE J. Sel. Areas Commun.,* **28**: 1435–1445.

[83] Zhang, R. and Cui, S. [2010]. Cooperative interference management with miso beamforming, *IEEE Trans. Sig. Proc.,* **58**: 5450–5458.

[84] Zhou, H., Fan, P. and Li, J. [2011]. Global proportional fair scheduling for networks with multiple base stations, *IEEE Trans. Veh. Tech.,* **60**: 1867–1879.

[85] Zorba, N. and Perez-Neira, A. I. [2008]. Opportunistic grassmannian beamforming for multi-user and multi-antenna downlink communications, *IEEE Trans. Wireless Commun.,* **7**: 1174–1178.

Appendix A

Multivariate Analysis

A.1 Preliminaries

The proof of Theorem 5.2.1 requires knowledge on finite-dimensional complex random matrices. In this section, we present a brief overview on random matrix theory. The objective is to provide necessary preliminary results and definitions.

In this appendix as well as the subsequent Appendices A.2, A.3, we use $\{a_{i,j}\}_{i,j}$ to denote a matrix $\boldsymbol{A}$ having $a_{i,j}$ as the (i,j)-th component. $O(n)$ denotes the set of all orthogonal matrix with dimension n, and $[d\boldsymbol{U}]$ is the normalized Haar invariant probability measure on $O(n)$, normalized to make the total measure unity [29]. $\text{etr}(\boldsymbol{X})$ is the short-hand notation for $\text{e}^{\boldsymbol{Tr}(\boldsymbol{X})}$.

Definition A.1.1 *The real and complex multivariate gamma function* $\tilde{\Gamma}_m(n)$ *are defined as*

$$\Gamma_m(n) = \prod_{j=1}^{n} \Gamma(m-j+1) = \prod_{j=1}^{n} (m-j)!, \tag{A.1}$$

$$\tilde{\Gamma}_m(n) = \int_{\boldsymbol{X}=\boldsymbol{X}^H \succ \mathbf{0}} etr(-\boldsymbol{X}) |\boldsymbol{X}|^{m-n} d\boldsymbol{X}. \tag{A.2}$$

Definition A.1.2 *The Vandermonde determinants of a diagonal matrix* $\boldsymbol{A} = diag($ $a_1, \ldots, a_n$ $)$ *are defined as*

$$V(\boldsymbol{A}) = |\{a_i^{j-1}\}_{i,j=1,\ldots,n}| = \prod_{1 \le i \le j \le n} (a_j - a_i), \tag{A.3}$$

$$\Delta(\boldsymbol{A}) = |\{a_i^{n-j}\}_{i,j=1,\ldots,n}| = \prod_{1 \le i \le j \le n} (a_i - a_j), \tag{A.4}$$

Clearly, $\Delta(\boldsymbol{A}) = (-1)^{n(n-1)/2} V(\boldsymbol{A})$.

Definition A.1.3 *Suppose that* k *is a positive integer. A partition of* k *into* p *parts, denoted as* $\mathcal{K} = ($ $k_1, k_2, \ldots, k_p$ $)$*, is a division such that* $\sum_{m=1}^{p} k_m = k$, $k_1 \ge \ldots \ge k_p \ge 0$.

The scalar hyper-geometric functions are defined as

$${}_pF_q(a_1, \ldots, a_p; b_1, \ldots, b_q; x) = \sum_{k=0}^{\infty} \frac{(a_1)_k \ldots (a_p)_k}{(b_1)_k \ldots (b_p)_k} \frac{x^k}{k!}, \tag{A.5}$$

where $(a)_k = a(a+1)\ldots(a+k-1)$. Hyper-geometric functions of matrix arguments are generalizations of these classical hyper-geometric functions.

Definition A.1.4 *(Hyper-geometric functions of one and two matrix arguments) Let* $\boldsymbol{A}$ *and* $\boldsymbol{B}$ *be Hermitian* $n \times n$ *matrices. The hyper-geometric functions of one and*

two matrix arguments are defined as

$$ {}_pF_q^{(n)}(a_1,\ldots,a_p;b_1,\ldots,b_q;\boldsymbol{A}) = \sum_{k=0}^{\infty}\sum_{\mathcal{K}} \frac{(a_1)_{\mathcal{K}}\ldots(a_p)_{\mathcal{K}}}{(b_1)_{\mathcal{K}}\ldots(b_p)_{\mathcal{K}}}\frac{\tilde{C}_{\mathcal{K}}(\boldsymbol{A})}{k!}, \tag{A.6} $$

$$ {}_pF_q^{(n)}(a_1,\ldots,a_p;b_1,\ldots,b_q;\boldsymbol{A},\boldsymbol{B}) = \sum_{k=0}^{\infty}\sum_{\mathcal{K}} \frac{(a_1)_{\mathcal{K}}\ldots(a_p)_{\mathcal{K}}}{(b_1)_{\mathcal{K}}\ldots(b_p)_{\mathcal{K}}}\frac{\tilde{C}_{\mathcal{K}}(\boldsymbol{A})\tilde{C}_{\mathcal{K}}(\boldsymbol{B})}{\tilde{C}_{\mathcal{K}}(\boldsymbol{I}_n)k!}, \tag{A.7} $$

where $\mathcal{K} = (\ k_1,\ k_2,\ \ldots,\ k_n\ )$ *is a partition of* k; $(a)_{\mathcal{K}} = \prod_{m=1}^{n}(a-m+1)_{k_m}$; *and* $\tilde{C}_{\mathcal{K}}(\boldsymbol{X})$ *is the complex zonal polynomial of a Hermitian matrix* $\boldsymbol{X}$, *which takes origins from group representation theory [29].*

The following lemmas state the most useful properties for the hyper-geometric functions

Lemma A.1.1 ([29]) *(Splitting Property) Suppose that* $\boldsymbol{A} \in \mathbb{C}^{n\times n}$, $\boldsymbol{A} \succ \boldsymbol{0}$, *and* $\boldsymbol{B} \in \mathbb{C}^{n\times n}$ *is a Hermitian matrix. Then we have*

$$ \int_{\boldsymbol{U}\in O(n)} {}_pF_q^{(n)}(a_1,\cdots,a_p;b_1,\cdots,b_q;\boldsymbol{A}\boldsymbol{U}\boldsymbol{B}\boldsymbol{U}^H)[d\boldsymbol{U}] = {}_pF_q^{(n)}(a_1,\cdots,a_p;b_1,\cdots,b_q;\boldsymbol{A},\boldsymbol{B}). \tag{A.8} $$

Lemma A.1.2 ([29]) *(Reproductive Property) Suppose that* $\boldsymbol{A} \in \mathbb{C}^{n\times n}$, $\boldsymbol{A} \succ \boldsymbol{0}$, *and* $\boldsymbol{B}$, $\boldsymbol{C} \in \mathbb{C}^{n\times n}$ *are Hermitian matrices. Then, for any complex number* a *with the real part* $Re(a) > n-1$, *we have*

$$ \begin{aligned} &\int_{\boldsymbol{X}\succ\boldsymbol{0}} etr(-\boldsymbol{A}\boldsymbol{X})|\boldsymbol{X}|^{a-n}\,{}_pF_q^{(n)}(a_1,\cdots,a_p;b_1,\cdots,b_q;\boldsymbol{X}\boldsymbol{B},\boldsymbol{C})d\boldsymbol{X} \\ &\qquad = \tilde{\Gamma}_n(a)|\boldsymbol{A}|^{-a}\,{}_{p+1}F_q^{(n)}(a_1,\cdots,a_p,a;b_1,\cdots,b_q;\boldsymbol{A}^{-1}\boldsymbol{B},\boldsymbol{C}). \end{aligned} \tag{A.9} $$

Lemma A.1.3 ([29]) *(Eigenvalue Transformation) Suppose that* $\boldsymbol{A} \in \mathbb{C}^{n\times n}$, $\boldsymbol{A} \succ \boldsymbol{0}$, *is a Hermitian matrix with the joint distribution* $f(\boldsymbol{A})$. *The joint PDF of the eigenvalues* $\lambda_n > \ldots > \lambda_1 > 0$ *of* $\boldsymbol{A}$ *is*

$$g(\boldsymbol{\Lambda}) = \frac{\pi^{n(n-1)}}{\tilde{\Gamma}_n(n)} V^2(\boldsymbol{\Lambda}) \int_{\boldsymbol{U}\in O(n)} f(\boldsymbol{U}\boldsymbol{\Lambda}\boldsymbol{U}^H)[d\boldsymbol{U}], \tag{A.10}$$

where $\boldsymbol{\Lambda} = diag(\lambda_1, \ldots, \lambda_n)$ *and* $\boldsymbol{U}\boldsymbol{\Lambda}\boldsymbol{U}^H$ *is the eigenvalue decomposition of the matrix* $\boldsymbol{A}$.

Lemma A.1.4 ([33]) *(Quadratic Distribution) Suppose that* $\boldsymbol{X} \sim \mathcal{CN}(\boldsymbol{0}_{p\times n}, \boldsymbol{\Sigma}\otimes\boldsymbol{\Omega})$, $n \geq p$, *and* $\boldsymbol{M} \succ \boldsymbol{0}$. *The distribution of* $\boldsymbol{V} = \boldsymbol{X}\boldsymbol{M}\boldsymbol{X}^H$ *is*

$$f_{\boldsymbol{V}}(\boldsymbol{V}) = \frac{1}{\tilde{\Gamma}_p(n)|\boldsymbol{\Sigma}|^n|\boldsymbol{M}\boldsymbol{\Omega}|^p} |\boldsymbol{V}|^{n-p}{}_0F_0^{(n)}(\boldsymbol{M}^{-1/2}\boldsymbol{\Omega}^{-1}\boldsymbol{M}^{-1/2}, -\boldsymbol{\Sigma}^{-1}\boldsymbol{V}). \tag{A.11}$$

A.2 Additional Lemmas for the Proof of Theorem 5.2.1

Next, we present two lemmas that will be used to prove Theorem 5.2.1 in Appendix A.3.

Lemma A.2.1 *Suppose that* $\psi_j \neq \psi_i$, $i \neq j \in \{1, \ldots, n\}$, *and* $A_i = 1/\prod_{j\neq i}^n (1 - \psi_j/\psi_i)$. *Then we have*

$$1 - \left(\prod_{i=1}^n \psi_i\right) \sum_{i=1}^n \frac{(-1)^{n+1} A_i}{\psi_i^n (1+\psi_i s)} = \frac{\prod_{i=1}^n \psi_i s^n}{\prod_{i=1}^n (1+\psi_i s)}. \tag{A.12}$$

Proof 13 *Multiplying both sides of (A.12) with* $\prod_{i=1}^n (1+\psi_i s)$ *and subtracting them, we obtain a polynomial in* s *of degree* n. *However, since this polynomial has* $n+1$

zeros: $s \in \{0, -1/\psi_1, \ldots, -1/\psi_n\}$*, it should be equal to 0. This completes the proof of Lemma A.2.1.*

Lemma A.2.2 *Suppose that* $\mathbf{\Psi} = diag(\psi_1, \ldots, \psi_p)$*,* $\psi_i > 0$*,* $\psi_j \neq \psi_i$*,* $i, j \in \{1, \ldots, n\}$*,* $i \neq j$*, and*

$$f_S(s) = \frac{s^{p-1}\tilde{\Gamma}_p(p+1)}{\tilde{\Gamma}_p(p)\tilde{\Gamma}(p)}|\mathbf{\Psi}|_1 F_0^{(p)}(p+1; \mathbf{\Psi}, -s). \tag{A.13}$$

The function $F_S(s) = \int_0^s f_S(x)dx$ *is then in the form of*

$$F_S(s) = \frac{\prod_{i=1}^n \psi_i s^n}{\prod_{i=1}^n (1+\psi_i s)}. \tag{A.14}$$

Proof 14 *Note that* ${}_1F_0^{(p)}(p+1; \mathbf{\Psi}, -s) = \lim_{\epsilon_1, \ldots, \epsilon_{p-2} \to 0} {}_1F_0^{(p)}(p+1; \mathbf{\Psi}, -\boldsymbol{S}_1)$*, where* $\boldsymbol{S}_1 = diag(s, 0, \epsilon_1, \ldots, \epsilon_{p-2})$*. From [21, (4.7)], we have*

$${}_1F_0^{(p)}(p+1; \mathbf{\Psi}, -\boldsymbol{S}_1) = \frac{|{}_1F_0(2; -\psi_i s_j)|}{p!\Delta(\mathbf{\Psi})\Delta(-\boldsymbol{S}_1)} = (-1)^{\frac{p(p-1)}{2}} \frac{|{}_1F_0(2; -\psi_i s_j)|}{p!V(\mathbf{\Psi})V(\boldsymbol{S}_1)}, \tag{A.15}$$

where $|{}_1F_0(2; -\psi_i s_j)|$ *denotes the determinant of a matrix with* (i, j)*-th component being* ${}_1F_0(2; -\psi_i s_j) = 1/(1+\psi_i s_j)^2$*, and* $[s_1, \ldots, s_p] := [s, 0, \epsilon_1, \ldots, \epsilon_{p-2}]$*. Denote*

$$|{}_1F_0(2; -\psi_i s_j)| = \begin{vmatrix} \frac{1}{(1+\psi_1 s)^2} & 1 & \frac{1}{(1+\psi_1\epsilon_1)^2} & \cdots & \frac{1}{(1+\psi_1\epsilon_{p-2})^2} \\ \vdots & \vdots & \vdots & \vdots & \vdots \\ \frac{1}{(1+\psi_p s)^2} & 1 & \frac{1}{(1+\psi_p\epsilon_1)^2} & \cdots & \frac{1}{(1+\psi_p\epsilon_{p-2})^2} \end{vmatrix}$$

$$:= |\boldsymbol{c}_0, \boldsymbol{c}_1, \boldsymbol{g}(\epsilon_1), \ldots, \boldsymbol{g}(\epsilon_{p-2})|, \tag{A.16}$$

where $\boldsymbol{c}_0 = \left[\frac{1}{(1+\psi_1 s)^2}, \ldots, \frac{1}{(1+\psi_p s)^2} \right]^T$*;* $\boldsymbol{c}_1 = \left[1, \ldots, 1 \right]^T$*; and* $\boldsymbol{g}(\epsilon_k) = \left[\frac{1}{(1+\psi_1\epsilon_k)^2}, \ldots, \frac{1}{(1+\psi_p\epsilon_k)^2} \right]^T$*,* $k = 1, \ldots, p-2$*.*

Similarly, we define determinant of the Vandermonde matrix of the matrix $\boldsymbol{S}_1$ *as a function of* $\epsilon_1, \ldots, \epsilon_{p-2}$ *as follows*

$$V(\boldsymbol{S}_1) = \begin{vmatrix} 1 & 1 & 1 & \cdots & 1 \\ s & 0 & \epsilon_1 & \cdots & \epsilon_{p-2} \\ \vdots & \vdots & \vdots & \vdots & \vdots \\ s^{p-1} & 0 & \epsilon_1^{p-1} & \cdots & \epsilon_{p-2}^{p-1} \end{vmatrix} := |\boldsymbol{c}_2, \boldsymbol{c}_3, \boldsymbol{h}(\epsilon_1), \ldots, \boldsymbol{h}(\epsilon_{p-2})|, \tag{A.17}$$

where $\boldsymbol{c}_2 = 1, \ldots, s^{p-1} \,\big]^T$; $\boldsymbol{c}_1 = \big[\, 1, 0, \ldots, 0 \,\big]^T$; *and* $\boldsymbol{h}(\epsilon_k) = \big[\, 1, \epsilon_k, \ldots, \epsilon_k^{p-1} \,\big]^T$, $k = 1, \ldots, p-2$.

Using the L' Hospital rule *[1, 3.4.1], we then have*

$$\begin{aligned} \frac{|{}_1F_0(2; -\psi_i s_j)|}{V(\boldsymbol{S}_1)} &= \frac{|\boldsymbol{c}_0, \boldsymbol{c}_1, \boldsymbol{g}(\epsilon_1), \ldots, \boldsymbol{g}(\epsilon_{p-2})|}{|\boldsymbol{c}_2, \boldsymbol{c}_3, \boldsymbol{h}(\epsilon_1), \ldots, \boldsymbol{h}(\epsilon_{p-2})|} \\ &= \frac{\left| \boldsymbol{c}_0, \boldsymbol{c}_1, \frac{d\boldsymbol{g}(x)}{dx}\Big|_{x=\epsilon_1}, \ldots, \frac{d^{p-2}\boldsymbol{g}(x)}{dx^{p-2}}\Big|_{x=\epsilon_{p-2}} \right|}{\left| \boldsymbol{c}_2, \boldsymbol{c}_3, \frac{d\boldsymbol{h}(x)}{dx}\Big|_{x=\epsilon_1}, \ldots, \frac{d^{p-2}\boldsymbol{h}(x)}{dx^{p-2}}\Big|_{x=\epsilon_{p-2}} \right|}. \end{aligned} \tag{A.18}$$

After some manipulations, we obtain

$$\begin{aligned} &\left| \boldsymbol{c}_0, \boldsymbol{c}_1, \frac{d\boldsymbol{g}(x)}{dx}\Big|_{x=\epsilon_1}, \ldots, \frac{d^{p-2}\boldsymbol{g}(x)}{dx^{p-2}}\Big|_{x=\epsilon_{p-2}} \right| \xrightarrow{\epsilon_1, \ldots, \epsilon_{p-2} \to 0} \\ &\qquad (-1)^{\frac{(p-1)(p-2)}{2}} \left(\prod_{i=1}^{p} \Gamma(i) \right) \begin{vmatrix} \frac{1}{(1+\psi_1 s)^2} & 1 & \psi_1 & \cdots & \psi_1^{p-2} \\ \vdots & \vdots & \vdots & \vdots & \vdots \\ \frac{1}{(1+\psi_p s)^2} & 1 & \psi_p & \cdots & \psi_p^{p-2} \end{vmatrix}, \end{aligned} \tag{A.19}$$

$$\left|\boldsymbol{c}_2, \boldsymbol{c}_3, \frac{d\boldsymbol{h}(x)}{dx}\Big|_{x=\epsilon_1}, \ldots, \frac{d^{p-2}\boldsymbol{h}(x)}{dx^{p-2}}\Big|_{x=\epsilon_{p-2}}\right|$$

$$\xrightarrow{\epsilon_1,\ldots,\epsilon_{p-2}\to 0} \begin{vmatrix} 1 & 1 & 0 & \cdots & 0 \\ s & 0 & 1 & \cdots & 0 \\ \vdots & \vdots & \vdots & \vdots & \vdots \\ s^{p-2} & 0 & 0 & \cdots & (p-2)! \\ s^{p-1} & 0 & 0 & \cdots & 0 \end{vmatrix} = (-1)^{p-1}\left(\prod_{i=1}^{p-1}\Gamma(i)\right)s^{p-1}. \tag{A.20}$$

Now, we are ready to derive a closed-form expression for the function $F_S(s)$. First note that by combining (A.15), (A.18), (A.19), and (A.20), $f_S(s)$ can be expressed as

$$f_S(s) = \frac{1}{V(\boldsymbol{\Psi})}\begin{vmatrix} \frac{\psi_1}{(1+\psi_1 s)^2} & \psi_1 & \cdots & \psi_1^{p-1} \\ \vdots & \vdots & \vdots & \vdots \\ \frac{\psi_p}{(1+\psi_p s)^2} & \psi_p & \cdots & \psi_p^{p-1} \end{vmatrix}. \tag{A.21}$$

Hence, we have

$$F_S(s) = \int_0^s f_S(x)dx = \frac{1}{V(\boldsymbol{\Psi})}\begin{vmatrix} 1-\frac{1}{1+\psi_1 s} & \psi_1 & \cdots & \psi_1^{p-1} \\ \vdots & \vdots & \vdots & \vdots \\ 1-\frac{1}{1+\psi_p s} & \psi_p & \cdots & \psi_p^{p-1} \end{vmatrix}$$

$$= 1 - \frac{1}{V(\boldsymbol{\Psi})}\begin{vmatrix} \frac{1}{1+\psi_1 s} & \psi_1 & \cdots & \psi_1^{p-1} \\ \vdots & \vdots & \vdots & \vdots \\ \frac{1}{1+\psi_p s} & \psi_p & \cdots & \psi_p^{p-1} \end{vmatrix}. \tag{A.22}$$

Using the Laplace's cofactor expansion *[20, 14.15], we obtain*

$$\begin{aligned} F_S(s) &= 1 - \sum_{i=1}^{p} \frac{(-1)^{i+1} \prod_{j\neq i} \psi_j}{1+\psi_i s} \frac{V(\boldsymbol{\Psi}_{-\boldsymbol{i}})}{V(\boldsymbol{\Psi})} \\ &= 1 - \sum_{i=1}^{p} \frac{(-1)^{i+1} \prod_{j\neq i} \psi_j}{1+\psi_i s} \frac{1}{\prod_{j<i}(\psi_i - \psi_j) \prod_{j>i}(\psi_j - \psi_i)} \\ &= 1 - \left(\prod_{i=1}^{p} \psi_i\right) \sum_{i=1}^{p} \frac{(-1)^{p+1} A_i}{\psi_i^p (1+\psi_i s)} = \frac{\prod_{i=1}^{p} \psi_i s^p}{\prod_{i=1}^{p}(1+\psi_i s)}, \end{aligned} \tag{A.23}$$

where $A_i = 1/\prod_{j\neq i}^{p}(1-\psi_j/\psi_i)$, $\boldsymbol{\Psi}_{-i} = diag(\psi_1, \ldots, \psi_{i-1}, \psi_{i+1}, \ldots, \psi_p)$, *and the last equality is obtained from Lemma A.2.1. This completes the proof of Lemma A.2.2.*

A.3 Proof of Theorem 5.2.1

Denoting $\boldsymbol{V} = \boldsymbol{X}\boldsymbol{\Psi}\boldsymbol{X}^H$, the PDF of $\boldsymbol{V}$ can then be obtained from Lemma A.1.4 as

$$f_{\boldsymbol{V}}(\boldsymbol{V}) = \frac{|\boldsymbol{V}|^{n-p}}{\tilde{\Gamma}_p(n)|\boldsymbol{\Psi}|^p} {}_0F_0^{(n)}(\boldsymbol{\Psi}^{-1}, -\boldsymbol{V}) d\boldsymbol{V}. \tag{A.24}$$

From Lemma A.1.4, given $\boldsymbol{V}$, the conditional PDF of the random variable $S := \boldsymbol{h}^H \boldsymbol{V}^{-1} \boldsymbol{h}$ can be expressed as

$$f_{S|\boldsymbol{V}}(s|\boldsymbol{V}) = \frac{|\boldsymbol{V}| s^{p-1}}{\Gamma(p)} {}_0F_0^{(p)}(\boldsymbol{V}, -s). \tag{A.25}$$

From (A.24) and (A.25), we have

$$\begin{aligned} f_S(s) &= \int_{\boldsymbol{V}\succ\boldsymbol{0}} f_{S|\boldsymbol{V}}(s|\boldsymbol{V}) f_{\boldsymbol{V}}(\boldsymbol{V}) d\boldsymbol{V} \\ &= \frac{s^{p-1}}{\Gamma(p)\tilde{\Gamma}_p(n)|\boldsymbol{\Psi}|^p} \int_{\boldsymbol{V}\succ\boldsymbol{0}} |\boldsymbol{V}|^{n+1-p} {}_0F_0^{(p)}(\boldsymbol{V}, -s) {}_0F_0^{(n)}(\boldsymbol{\Psi}^{-1}, -\boldsymbol{V}) d\boldsymbol{V}. \end{aligned} \tag{A.26}$$

Next, we prove Theorem 5.2.1 by induction. We first prove that Theorem 5.2.1 is true for $n = p$, and then given that it is true for $n = m - 1 \geq p$, we show that it is also true for $n = m$. Note that for convenience, we assume $\psi_j \neq \psi_i$, $i \neq j \in \{1, \ldots, n\}$.

A.3.1 The Case of $n = p$

From (A.26) with $n = p$, we first express the function $f_S(s)$ as

$$\begin{aligned} f_S(s) &= \frac{s^{p-1}}{\Gamma(p)\tilde{\Gamma}_p(p)|\boldsymbol{\Psi}|^p} \int_{\boldsymbol{V}\succ\boldsymbol{0}} |\boldsymbol{V}|_0 F_0^{(p)}(\boldsymbol{V}, -s)_0 F_0^{(p)}(\boldsymbol{\Psi}^{-1}, -\boldsymbol{V}) d\boldsymbol{V} \\ &= \frac{s^{p-1}}{\Gamma(p)\tilde{\Gamma}_p(p)|\boldsymbol{\Psi}|^p} \int_{\boldsymbol{V}\succ\boldsymbol{0}} \int_{\boldsymbol{U}\in O(p)} |\boldsymbol{V}| \mathrm{etr}(-\boldsymbol{U}\boldsymbol{\Psi}^{-1}\boldsymbol{U}^H\boldsymbol{V})_0 F_0^{(p)}(\boldsymbol{V}, -s)[d\boldsymbol{U}]d\boldsymbol{V}, \end{aligned} \tag{A.27}$$

where (A.27) follows from Lemma A.1.2. Now by applying again Lemma A.1.2, we obtain

$$\begin{aligned} f_S(s) &= \frac{s^{p-1}\tilde{\Gamma}_p(p+1)}{\Gamma(p)\tilde{\Gamma}_p(p)|\boldsymbol{\Psi}|^p} \int_{\boldsymbol{U}\in O(p)} |\boldsymbol{U}\boldsymbol{\Psi}^{-1}\boldsymbol{U}^H|^{-(n+1)}{}_1 F_0^{(p)}(p+1; \left(\boldsymbol{U}\boldsymbol{\Psi}^{-1}\boldsymbol{U}^H\right)^{-1}, -s)[d\boldsymbol{U}] \\ &= \frac{s^{p-1}\tilde{\Gamma}_p(p+1)}{\Gamma(p)\tilde{\Gamma}_p(p)} |\boldsymbol{\Psi}|_1 F_0^{(p)}(p+1; \boldsymbol{\Psi}, -s), \end{aligned} \tag{A.28}$$

where we have used Lemma A.1.1. Combining (A.28) and Lemma A.2.2, it follows that Theorem 5.2.1 is true for $n = p$.

A.3.2 The Case of $n > p$

Suppose that Theorem 5.2.1 is true for $n = m - 1 > p$. We will show in the following that it is also true for $n = m$. Applying Lemma A.1.3 to (A.26) with any pair of n and m with $n = m - 1 > p$, we can express the function $f_S(s)$ as in the following form

$$\begin{aligned} &f_S(s) = \\ &\frac{s^{p-1}}{\Gamma(p)\tilde{\Gamma}_p(m)|\boldsymbol{\Psi}|^p} \frac{\pi^{p(p-1)}}{\tilde{\Gamma}_p(p)} \int_{\infty>\lambda_p>\ldots>\lambda_1>0} V^2(\boldsymbol{\Lambda})|\boldsymbol{\Lambda}|^{m+1-p}{}_0 F_0^{(p)}(\boldsymbol{\Lambda}, -s)_0 F_0^{(m)}(\boldsymbol{\Psi}^{-1}, -\boldsymbol{\Lambda}) d\boldsymbol{\Lambda}, \end{aligned} \tag{A.29}$$

where $\mathbf{\Lambda} = diag(\lambda_1, \ldots, \lambda_p)$. We then find an alternative form for ${}_0F_0^{(m)}(\mathbf{\Psi}^{-1}, -\mathbf{\Lambda})$ by using [21, (4.6)] as follows:

$$\begin{aligned} {}_0F_0^{(m)}(\mathbf{\Psi}^{-1}, -\mathbf{\Lambda}) &= \lim_{\delta_1,\ldots,\delta_{m-p-1}\to 0} {}_0F_0^{(m)}(\mathbf{\Psi}^{-1}, -\mathbf{\Lambda_1}) \\ &= (-1)^{\frac{m(m-1)}{2}} \prod_{k=1}^{m} \Gamma(k) \lim_{\delta_1,\ldots,\delta_{m-p-1}\to 0} \frac{|{}_0F_0(-\psi_i^{-1}\lambda_j)|}{V(\mathbf{\Psi}^{-1})V(\mathbf{\Lambda}_1)}, \end{aligned} \tag{A.30}$$

where $\mathbf{\Lambda}_1 = diag(\lambda_1, \ldots, \lambda_m) := diag(\lambda_1, \ldots, \lambda_p, 0, \delta_1, \ldots, \delta_{m-p-1})$. Denote

$$\begin{aligned} &\left|{}_0F_0(-\frac{\lambda_j}{\psi_i})\right| \\ &= \begin{vmatrix} \exp(-\lambda_1/\psi_1) & \cdots & \exp(-\lambda_p/\psi_1) & 1 & \exp(-\delta_1/\psi_1) & \cdots & \exp(-\delta_{m-p-1}/\psi_1) \\ \exp(-\lambda_1/\psi_2) & \cdots & \exp(-\lambda_p/\psi_2) & 1 & \exp(-\delta_1/\psi_2) & \cdots & \exp(-\delta_{m-p-1}/\psi_2) \\ \vdots & \vdots & \vdots & \vdots & \vdots & \vdots & \vdots \\ \exp(-\lambda_1/\psi_m) & \cdots & \exp(-\lambda_p/\psi_m) & 1 & \exp(-\delta_1/\psi_m) & \cdots & \exp(-\delta_{m-p-1}/\psi_m) \end{vmatrix} \\ &:= |\boldsymbol{d}_0, \ldots, \boldsymbol{d}_p, \boldsymbol{g}_1(\delta_1), \ldots, \boldsymbol{g}_1(\delta_{m-p-1})|, \end{aligned} \tag{A.31}$$

where $\boldsymbol{d}_{k-1} = \left[\, \exp(-\lambda_k/\psi_1), \ldots, \exp(-\lambda_k/\psi_m) \,\right]^T$, $k = 1, \ldots, p$; $\boldsymbol{d}_p = \left[\, 1, \ldots, 1 \,\right]^T$; $\boldsymbol{g}_1(\delta_j) = \left[\, \exp(-\delta_j/\psi_1), \ldots, \exp(-\delta_j/\psi_m) \,\right]^T$, $j = 1, \ldots, m-p-1$. Furthermore, we denote

$$\begin{aligned} V(\mathbf{\Lambda}_1) &= \begin{vmatrix} 1 & \cdots & 1 & 1 & 1 & \cdots & 1 \\ \lambda_1 & \cdots & \lambda_p & 0 & \delta_1 & \cdots & \delta_{m-p-1} \\ \vdots & \vdots & \vdots & \vdots & \vdots & \vdots & \vdots \\ \lambda_1^{m-1} & \cdots & \lambda_p^{m-1} & 0 & \delta_1^{m-1} & \cdots & \delta_{m-p-1}^{m-1} \end{vmatrix} \\ &:= |\boldsymbol{d}_{p+1}, \ldots, \boldsymbol{d}_{2p+1}, \boldsymbol{h}_1(\delta_1), \ldots, \boldsymbol{h}_1(\delta_{m-p-1})|, \end{aligned} \tag{A.32}$$

where $\boldsymbol{d}_{p+k} = \left[\ 1,\ \lambda_k,\ \ldots,\ \lambda_k^{m-1}\ \right]^T$, $k = 1, \ldots, p$; $\boldsymbol{d}_{2p+1} = \left[\ 1,\ 0,\ \ldots,\ 0\ \right]^T$; $\boldsymbol{h}_1(\delta_j) = \left[\ 1,\ \delta_j,\ \ldots,\ \delta_j^{m-1}\ \right]^T$, $j = 1, \ldots, m-p-1$. Using the *L' Hospital rule* [1, 3.4.1], we obtain

$$\begin{aligned}\frac{|{}_0F_0(-\frac{\lambda_j}{\psi_i})|}{V(\boldsymbol{\Lambda}_1)} &= \frac{|\boldsymbol{d}_0, \ldots, \boldsymbol{d}_p, \boldsymbol{g}_1(\delta_1), \ldots, \boldsymbol{g}_1(\delta_{m-p-1})|}{|\boldsymbol{d}_{p+1}, \ldots, \boldsymbol{d}_{2p+1}, \boldsymbol{h}_1(\delta_1), \ldots, \boldsymbol{h}_1(\delta_{m-p-1})|} \\ &= \frac{\left|\boldsymbol{d}_0, \ldots, \boldsymbol{d}_p, \frac{d\boldsymbol{g}_1(x)}{dx}\Big|_{x=\delta_1}, \ldots, \frac{d^{m-p-1}\boldsymbol{g}_1(x)}{dx^{m-p-1}}\Big|_{x=\delta_{m-p-1}}\right|}{\left|\boldsymbol{d}_{p+1}, \ldots, \boldsymbol{d}_{2p+1}, \frac{d\boldsymbol{h}_1(x)}{dx}\Big|_{x=\delta_1}, \ldots, \frac{d^{m-p-1}\boldsymbol{h}_1(x)}{dx^{m-p-1}}\Big|_{x=\delta_{m-p-1}}\right|}. \qquad \text{(A.33)}\end{aligned}$$

Now, we consider the nominator and the denominator of (A.33). After some manipulations, we can compute the denominator as follows

$$\begin{aligned}&\left|\boldsymbol{d}_{p+1}, \ldots, \boldsymbol{d}_{2p+1}, \frac{d\boldsymbol{h}_1(x)}{dx}\Big|_{x=\delta_1}, \ldots, \frac{d^{m-p-1}\boldsymbol{h}_1(x)}{dx^{m-p-1}}\Big|_{x=\delta_{m-p-1}}\right| \\ &\xrightarrow{\delta_1, \ldots, \delta_{m-p-1} \to 0} \begin{vmatrix} 1 & \cdots & 1 & 1 & 0 & \cdots & 0 & 0 \\ \lambda_1 & \cdots & \lambda_p & 0 & 1 & \cdots & 0 & 0 \\ \vdots & \vdots & \vdots & \vdots & \vdots & \vdots & \vdots & \vdots \\ \lambda_1^{m-p-2} & \cdots & \lambda_p^{m-p-2} & 0 & 0 & \cdots & (m-p-2)! & 0 \\ \lambda_1^{m-p-1} & \cdots & \lambda_p^{m-p-1} & 0 & 0 & \cdots & 0 & (m-p-1)! \\ \lambda_1^{m-p} & \cdots & \lambda_p^{m-p} & 0 & 0 & \cdots & 0 & 0 \\ \vdots & \vdots & \vdots & \vdots & \vdots & \vdots & \vdots & \vdots \\ \lambda_1^{m-1} & \cdots & \lambda_p^{m-1} & 0 & 0 & \cdots & 0 & 0 \end{vmatrix} \\ &= (-1)^{(p+2)(m-p)} \prod_{k=1}^{m-p} \Gamma(k) |\Lambda|^{m-p} V(\boldsymbol{\Lambda}). \qquad \text{(A.34)}\end{aligned}$$

The nominator of (A.33) can be given as

$$\left|\boldsymbol{d}_0,\ldots,\boldsymbol{d}_p,\left.\frac{d\boldsymbol{g}_1(x)}{dx}\right|_{x=\delta_1},\ldots,\left.\frac{d^{m-p-1}\boldsymbol{g}_1(x)}{dx^{m-p-1}}\right|_{x=\delta_{m-p-1}}\right| \xrightarrow{\delta_1,\ldots,\delta_{m-p-1}\to 0}$$

$$(-1)^{\frac{(m-p)(m-p-1)}{2}}\begin{vmatrix} \exp(-\lambda_1/\psi_1) & \cdots & \exp(-\lambda_p/\psi_1) & 1 & 1/\psi_1 & \cdots & 1/\psi_1^{m-p-1} \\ \vdots & & \vdots & \vdots & \vdots & & \\ \exp(-\lambda_1/\psi_m) & \cdots & \exp(-\lambda_p/\psi_m) & 1 & 1/\psi_m & \cdots & 1/\psi_m^{m-p-1} \end{vmatrix}$$

$$:= (-1)^{\frac{(m-p)(m-p-1)}{2}} T(p,m,\lambda_1,\ldots,\lambda_p,\psi_1,\ldots,\psi_m), \tag{A.35}$$

where the function $T(p,m,\lambda_1,\ldots,\lambda_p,\psi_1,\ldots,\psi_m)$ is defined for the sake of brevity. The PDF $f_S(s)$ in (A.29) can thus be expressed as

$$f_S(s) = \frac{(-1)^{\frac{p(p-1)}{2}} s^{p-1}}{\Gamma(p)\prod_{k=1}^{p}\Gamma(k) V(\boldsymbol{\Psi}^{-1})|\boldsymbol{\Psi}|^p} \times \\ \times \int_{\infty>\lambda_p>\cdots>\lambda_1>0} V(\boldsymbol{\Lambda})|\boldsymbol{\Lambda}|_0 F_0^{(p)}(\boldsymbol{\Lambda},-s) T(p,m,\lambda_1,\ldots,\lambda_p,\psi_1,\ldots,\psi_m) d\boldsymbol{\Lambda}. \tag{A.36}$$

Now using the Laplace's cofactor expansion [20, 14.15], we can rewrite $T(p,\, m,\, \lambda_1,\, \ldots,\, \lambda_p,\, \psi_1,\, \ldots,\, \psi_m)$ as

$$T(p,m,\lambda_1,\ldots,\lambda_p,\psi_1,\ldots,\psi_m) \\ = \sum_{i=1}^{m} \frac{(-1)^{m+i}}{\psi_i^{m-p-1}} T(p,m-1,\lambda_1,\ldots,\lambda_p,\psi_1,\ldots,\psi_{i-1},\psi_{i+1},\ldots,\psi_m). \tag{A.37}$$

Therefore, we have

$$F_S(s) = \sum_{i=1}^{m} \frac{(-1)^{m+i}}{\psi_i^{m-p-1}} \frac{V(\boldsymbol{\Psi}_{-i}^{-1})|\boldsymbol{\Psi}_{-i}|^p}{V(\boldsymbol{\Psi}^{-1})|\boldsymbol{\Psi}|^p} \frac{(-1)^{\frac{p(p-1)}{2}} s^{p-1}}{\Gamma(p)\prod_{k=1}^{p}\Gamma(k) V(\boldsymbol{\Psi}_{-i}^{-1})|\boldsymbol{\Psi}_{-i}|^p} \times \\ \times \int_0^s \int_{\infty>\lambda_p>\cdots>\lambda_1>0} V(\boldsymbol{\Lambda})|\boldsymbol{\Lambda}|_0 F_0^{(p)}(\boldsymbol{\Lambda},-x) \times \\ \times T(p,m-1,\lambda_1,\ldots,\lambda_p,\psi_1,\ldots,\psi_{i-1},\psi_{i+1},\ldots,\psi_m) \tag{A.38}$$

where we have used the fact that $F_S(s) = \int_{x=0}^{s} f_S(x)$, (A.36), and (A.37). Now using the inductive assumption that Theorem 5.2.1 is true for $n = m - 1 \geq p$, we can express (A.38) as follows

$$\begin{aligned} F_S(s) &= \sum_{i=1}^{m} \frac{(-1)^{m+i}}{\psi_i^{m-p-1}} \frac{V(\boldsymbol{\Psi}_{-i}^{-1})|\boldsymbol{\Psi}_{-i}|^p}{V(\boldsymbol{\Psi}^{-1})|\boldsymbol{\Psi}|^p} \left[\frac{\sum_{k=p}^{m-1} \beta_{k,-i} s^k}{\prod_{j=1,j\neq i}^{m}(1+\psi_j s)} \right] \\ &= \prod_{k=1}^{m} \psi_k \sum_{i=1}^{m} \frac{(-1)^{m+1} A_i}{\psi_i^m} \left[\frac{\sum_{k=p}^{m-1} \beta_{k,-i} s^k}{\prod_{j=1,j\neq i}^{m}(1+\psi_j s)} \right] \\ &= \frac{1}{\prod_{j=1}^{m}(1+\psi_j s)} \prod_{k=1}^{m} \psi_k \sum_{i=1}^{m} \frac{(-1)^{m+1} A_i}{\psi_i^m} \left[\left(\sum_{k=p}^{m-1} \beta_{k,-i} s^k \right) (1+\psi_i s) \right], \end{aligned} \tag{A.39}$$

Furthermore, from Lemma A.2.1, we have

$$\begin{aligned} \frac{\prod_{i=1}^{m}(1+\psi_i s)}{\prod_{i=1}^{m}(1+\psi_i s)} = 1 &= \prod_{k=1}^{m} \psi_k \sum_{i=1}^{m} \frac{(-1)^{m+1} A_i}{\psi_i^m} \\ &= \prod_{k=1}^{m} \psi_k \sum_{i=1}^{m} \frac{(-1)^{m+1} A_i}{\psi_i^m} \frac{\prod_{j=1,j\neq i}^{m}(1+\psi_j s)}{\prod_{j=1,j\neq i}^{m}(1+\psi_j s)} \\ &= \frac{1}{\prod_{j=1}^{m}(1+\psi_j s)} \prod_{k=1}^{m} \psi_k \sum_{i=1}^{m} \frac{(-1)^{m+1} A_i}{\psi_i^m} \left[\left(\sum_{k=0}^{m-1} \beta_{k,-i} s^k \right) (1+\psi_i s) \right]. \end{aligned} \tag{A.40}$$

By comparing (A.39) and (A.40), it follows that

$$F_S(s) = \frac{\sum_{k=p}^{m} \beta_k s^k}{\prod_{i=1}^{m}(1+\psi_i s)}. \tag{A.41}$$

Therefore, given that Theorem 5.2.1 is true for $n = m - 1 \geq p$, it is also true for $n = m$. By combining the results in the above two cases, the proof of Theorem 5.2.1 is thus completed.

Appendix B

Proofs of Chapter 4

B.1 Proof of Lemma 4.2.1

It is easy to see that

$$\mathbb{E}\left[\log_2\left(1+\max_{k\in\{1,\cdots,K\}}\text{SINR}_{k,1}\right)\right]=\int_0^\infty \log_2(1+x)Kf_S(x)F_S^{K-1}(x)dx, \qquad \text{(B.1)}$$

where $f_S(s)$ and $F_S(s)$ are given in (4.7) and (4.8). Therefore, the RBF sum-rate can be obtained as follows.

$$\begin{aligned}
R_{\text{RBF}} &= M\int_0^\infty \log_2(1+x)Kf_S(x)F_S^{K-1}(x)dx = \frac{M}{\log 2}\int_0^\infty \log(1+x)d\big(F_S^K(x)\big)\\
&= \frac{M}{\log 2}F_S^K(x)\log(1+x)\Big|_0^\infty - \frac{M}{\log 2}\int_0^\infty \frac{1}{1+x}\left(1-\frac{\exp(-x/\eta)}{(1+x)^{M-1}}\right)^K dx\\
&= \frac{M}{\log 2}\lim_{x\to\infty}\big(F_S^K(x)-1\big)\log(1+x) + \frac{M}{\log 2}\sum_{n=1}^K(-1)^n\binom{K}{n}\int_0^\infty \frac{\exp(-nx/\eta)dx}{(1+x)^{n(M-1)+1}}\\
&= \frac{M}{\log 2}\sum_{n=1}^K(-1)^n\binom{K}{n}e^{-n/\eta}\int_1^\infty \frac{\exp(-ny/\eta)dy}{y^{n(M-1)+1}}. \qquad \text{(B.2)}
\end{aligned}$$

Now by using [20, 2.324.2], (4.9) can be obtained. This completes the proof of Lemma 4.2.1.

B.2 Proof of Lemma 4.2.2

Denote $X = \left|\boldsymbol{h}_k^{(c,c)}\boldsymbol{\phi}_m^{(c)}\right|^2$, and

$$V = \sum_{i=1,i\neq m}^{M_c}\left|\boldsymbol{h}_k^{(c,c)}\boldsymbol{\phi}_i^{(c)}\right|^2 + \sum_{l=1,l\neq c}^{M_l}\frac{\mu_{l,c}}{\eta_c}\sum_{i=1}^{M_l}\left|\boldsymbol{h}_k^{(l,c)}\boldsymbol{\phi}_i^{(l)}\right|^2. \tag{B.3}$$

We note that the terms $\left|\boldsymbol{h}_k^{(l,c)}\boldsymbol{\phi}_i^{(l)}\right|^2$, $\forall k,l,c,i$, are independent chi-square random variables with two degrees of freedom, denoted by $\chi^2(2)$. Using the characteristic function, we can express the PDF of V as follows.

$$f_V(v) = \frac{1}{2\pi}\int_{-\infty}^{\infty}\frac{e^{-j\omega v}d\omega}{(1-j\omega)^{M_c-1}\prod_{l=1,l\neq c}^{C}\left(1-j\frac{\mu_{l,c}}{\eta_c}\omega\right)^{M_l}}, \tag{B.4}$$

where $j=\sqrt{-1}$. Since $S=\frac{X}{1/\eta_c+V}$, the PDF of S is

$$f_S^{(c)}(s) = \int_0^{\infty} f_{S|V}(s|v)f_V(v)dv = A + B, \tag{B.5}$$

in which,

$$A = \frac{e^{-s/\eta_c}}{2\pi\eta_c}\int_{-\infty}^{\infty}\frac{d\omega}{(s+j\omega)(1-j\omega)^{M_c-1}\prod_{l=1,l\neq c}^{C}\left(1-j\frac{\mu_{l,c}}{\eta_c}\omega\right)^{M_l}}, \tag{B.6}$$

$$B = \frac{e^{-s/\eta_c}}{2\pi}\int_{-\infty}^{\infty}\frac{d\omega}{(s+j\omega)^2(1-j\omega)^{M_c-1}\prod_{l=1,l\neq c}^{C}\left(1-j\frac{\mu_{l,c}}{\eta_c}\omega\right)^{M_l}}. \tag{B.7}$$

We first use the following partial fraction expansion to decompose A,

$$\frac{1}{(s+j\omega)\,(1-j\omega)^{M_c-1}\prod_{l=1,l\neq c}^{C}\left(1-j\frac{\mu_{l,c}}{\eta_c}\omega\right)^{M_l}} = \frac{A_0}{s+j\omega}+\frac{A_c}{1-j\omega}+\sum_{l=1,l\neq c}^{C}\frac{A_l}{1-j\frac{\mu_{l,c}}{\eta_c}\omega}+A', \tag{B.8}$$

where A' is the sum of all terms with order greater than 1.

We then apply the *Cauchy integral formula* [7] to obtain

$$\begin{aligned} A &= \frac{e^{-s/\eta_c}}{2\pi\eta_c}\int_{-\infty}^{\infty}\left[\frac{A_0}{s+j\omega}+\frac{A_c}{1-j\omega}+\sum_{l=1,l\neq c}^{C}\frac{A_l}{1-j\frac{\mu_{l,c}}{\eta_c}\omega}+A'\right]d\omega \\ &= \frac{e^{-s/\eta_c}}{2\eta_c}\left(A_0+A_c+\sum_{l=1,l\neq c}^{C}\frac{\eta_c}{\mu_{l,c}}A_l\right). \end{aligned} \tag{B.9}$$

Now from (B.8) we note that

$$\begin{aligned} 1 &= A_0(1-j\omega)^{M_c-1}\prod_{l=1,l\neq c}^{C}\left(1-j\frac{\mu_{l,c}}{\eta_c}\omega\right)^{M_l} \\ &+ A_c(s+j\omega)(1-j\omega)^{(M_c-2)^+}\prod_{l=1,l\neq c}^{C}\left(1-j\frac{\mu_{l,c}}{\eta_c}\omega\right)^{M_l} \\ &+ (s+j\omega)(1-j\omega)^{M_c-1}\sum_{l=1,l\neq c}^{C}\left[A_l\left(1-j\frac{\mu_{l,c}}{\eta_c}\omega\right)^{M_l-1}\prod_{n=1,n\neq l,c}^{C}\left(1-j\frac{\mu_{n,c}}{\eta_c}\omega\right)^{M_n}\right] \\ &+ A'(s+j\omega)\,(1-j\omega)^{M_c-1}\prod_{l=1,l\neq c}^{C}\left(1-j\frac{\mu_{l,c}}{\eta_c}\omega\right)^{M_l}. \end{aligned} \tag{B.10}$$

where the notation $(x)^+$ represents $\max(x,0)$. Substituting $\omega=-s/j$, we have

$$A_0 = \frac{1}{(1+s)^{M_c-1}\prod_{l=1,l\neq c}^{C}(1+\frac{\mu_{l,c}}{\eta_c}s)^{M_l}}. \tag{B.11}$$

Also, by observing the coefficient of $\omega^{(\sum_{l=1}^{C}M_l-1)}$, (B.10) leads to

$$A_0 = A_c+\sum_{l=1,l\neq c}^{C}\frac{\eta_c}{\mu_{l,c}}A_l. \tag{B.12}$$

Therefore, from (B.9), we conclude

$$A = \frac{e^{-s/\eta_c}}{\eta_c} A_0 = \frac{e^{-s/\eta_c}}{\eta_c (1+s)^{M_c - 1} \prod_{l=1, l\neq c}^{C} (1 + \frac{\mu_{l,c}}{\eta_c} s)^{M_l}}. \tag{B.13}$$

By differentiating A in (B.9) with respect to s, we obtain $\frac{dA}{ds} = -\frac{A}{\eta_c} - \frac{B}{\eta_c}$, i.e., $f_S^{(c)}(s) = A + B = -\eta_c \frac{dA}{ds}$. Combining this result and (B.13), (4.10) and (4.11) are obtained. This completes the proof of Lemma 4.2.2.

B.3 Proof of Theorem 4.2.1

Using the similar derivation as in Appendix B.1, we obtain

$$\begin{aligned} R_{\text{RBF}}^{(c)} &= \frac{M_c}{\log 2} \sum_{n=1}^{K_c} (-1)^n \binom{K_c}{n} \int_0^\infty \frac{\exp(-nx/\eta) dx}{(1+x)^{n(M_c-1)+1} \prod_{l=1, l\neq c}^{C} \left(\frac{\mu_{l,c}}{\eta_c} x + 1 \right)^{nM_l}} \\ &= \frac{M_c}{\log 2} \sum_{n=1}^{K_c} (-1)^n \binom{K_c}{n} \prod_{l=1, l\neq c}^{C} \left(\frac{\eta_c}{\mu_l} \right)^{nM_l} \times \\ &\qquad \times \int_0^\infty \frac{\exp(-nx/\eta) dx}{(x+1)^{n(M_c-1)+1} \prod_{l=1, l\neq c}^{C} \left(x + \frac{\eta_c}{\mu_{l,c}} \right)^{nM_l}}. \end{aligned} \tag{B.14}$$

By applying the partial fractional decomposition given in (4.13) and using [20, 2.234.2] for each term therein, we arrive at (4.12). This completes the proof of Theorem 4.2.1.

B.4 Proof of Proposition 4.2.1

Due to the similarity between (4.8) and (4.11), the original approach in [64, Theorem 1] can be applied to prove this proposition with minor modifications. For the completeness, only a sketch proof is presented here.

To show that $R_{\text{RBF}}^{(c)} \xrightarrow{K_c \to \infty} M_c \log_2 \log K_c$, we first note that $f_S^{(c)}(s)$ and $F_S^{(c)}(s)$ satisfy the *von Mises condition* for the Gumbel-type limiting distributions (see, e.g., [13, Theorem 10.5.2.c]). Therefore, as $K_c \to \infty$, there exist constants a_{K_c} and b_{K_c} such that $\left[F_S^{(c)}(a_{K_c}x + b_{K_c})\right]^{K_c} \to \exp\left(-e^{-x}\right)$. The value of b_{K_c} can be found to be[1]

$$b_{K_c} = \eta_c \log K_c - \eta_c \left(\sum_{l=1}^{C} M_l - 1\right) \log\log K_c + O(\log\log\log K_c). \tag{B.15}$$

Furthermore, the growth function, defined as $g_S^{(c)}(s) = \left(1 - F_S^{(c)}(s)\right) / f_S^{(c)}(s)$ for $s \geq 0$, is given by

$$g_S^{(c)}(s) = \frac{1}{\frac{1}{\eta_c} + \frac{M_c - 1}{s+1} + \sum_{l=1, l\neq c}^{C} \frac{M_l}{s + \frac{\eta_c}{\mu_{l,c}}}}. \tag{B.16}$$

It is easy to verify the followings:

- $\lim_{s\to\infty} g_S^{(c)}(s) = \eta_c > 0$,
- $b_{K_c} = O(\log K_c)$ as $K_c \to \infty$, and
- The derivative of $g_S^{(c)}(s)$ satisfies

$$\left.\frac{d^n g_S^{(c)}(s)}{ds^n}\right|_{s=b_{K_c}} = O\left(\frac{1}{b_{K_c}^{n+1}}\right). \tag{B.17}$$

Hence, by applying [64, Corollary A.1], we have

$$\Pr\left\{\eta_c \log K_c - \eta_c \left(\sum_{l=1}^{C} M_l\right) \log\log K_c + O(\log\log\log K_c) \leq \max_{k\in\{1,\cdots,K_c\}} \text{SINR}_{k,m}^{(c)} \right.$$
$$\left. \leq \eta_c \log K_c - \eta_c \left(\sum_{l=1}^{C} M_l - 2\right) \log\log K_c + O(\log\log\log K_c)\right\} \geq 1 - O\left(\frac{1}{\log K_c}\right). \tag{B.18}$$

This completes the proof of Proposition 4.2.1.

[1]Let $f(K_c)$ be a function of K_c. $f(K_c) = O(\log\log\log K_c)$ means that $f(K_c)/\log\log\log K_c < \infty$ as $K_c \to \infty$.

B.5 Proof of Lemma 4.3.1

For convenience, we denote the following auxiliary random variable

$$R_{k,m} = \log_2 (1 + \mathrm{SINR}_{k,m}) . \tag{B.19}$$

From(4.8), the CDF of $R_{k,m}$ is obtained as

$$F_R(r) = 1 - \frac{e^{-(2^r-1)/\eta}}{2^{r(M-1)}}.$$

To prove Lemma 4.3.1, we first show that

$$\Pr\left\{ \frac{\alpha}{M-1} \log_2 \eta + \log_2 \log \eta \geq \max_{k\in\{1,\cdots,K\}} R_{k,1} \geq \frac{\alpha}{M-1} \log_2 \eta - \log_2 \log \eta \right\}$$
$$\xrightarrow{\eta\to\infty} 1, \text{ if } 0 < \alpha \leq M-1, \tag{B.20}$$

$$\Pr\left\{ \log_2 \eta + \log_2 \log \eta + \log_2 \alpha \geq \max_{k\in\{1,\cdots,K\}} R_{k,1} \geq \log_2 \eta + \log_2 \log \eta + \log_2 \beta \right\}$$
$$\xrightarrow{\eta\to\infty} 1, \text{ if } \alpha > M-1, \tag{B.21}$$

in which the constant β is define as $\beta = \frac{\alpha-M+1}{2}$; hence $\alpha > \beta > 0$ when $\alpha > M-1$. Considering (B.20), the upper-bound probability can be expressed as

$$\Pr\left\{ \frac{\alpha}{M-1} \log_2 \eta + \log_2 \log \eta \geq \max_{k\in\{1,\cdots,K\}} R_{k,1} \right\}$$
$$= \left[F_R\left(\frac{\alpha}{M-1} \log_2 \eta + \log_2 \log \eta \right) \right]^K = \left(1 - \frac{\exp\left(-\eta^{\frac{\alpha}{M-1}-1} \log \eta\right) \exp\left(\eta^{-1}\right)}{\eta^{\alpha} (\log \eta)^{M-1}} \right)^K . \tag{B.22}$$

Using the asymptotic relation $\log(1-x) = -x + O(x^2)$ when x is small, we get

$$\begin{aligned}
&K \log\left(1 - \frac{\exp\left(-\eta^{\frac{\alpha}{M-1}-1}\log\eta\right)\exp\left(\eta^{-1}\right)}{\eta^{\alpha}(\log\eta)^{M-1}}\right) \\
&= -\frac{K}{\eta^{\alpha}(\log\eta)^{M-1}}\exp\left(-\eta^{\frac{\alpha}{M-1}-1}\log\eta\right)\exp\left(\eta^{-1}\right) \\
&+ O\left(\frac{K}{\eta^{2\alpha}(\log\eta)^{2(M-1)}}\exp\left(-2\eta^{\frac{\alpha}{M-1}-1}\log\eta\right)\exp\left(2\eta^{-1}\right)\right) \xrightarrow{\eta\to\infty} 0, \qquad \text{(B.23)}
\end{aligned}$$

in which we have used the assumptions $K = \Theta(\eta^{\alpha})$, and $0 < \alpha \leq M-1$. As a consequence, the upper-bound probability converges to 1 when $\eta \to \infty$. To show the convergence of the lower-bound probability in (B.20), we can utilize the same technique described above by showing

$$\begin{aligned}
&\Pr\left\{\frac{\alpha}{M-1}\log_2\eta - \log_2\log\eta \geq \max_{k\in\{1,\cdots,K\}} R_{k,1}\right\} \\
&= \left[F_R\left(\frac{\alpha}{M-1}\log_2\eta - \log_2\log\eta\right)\right]^K \\
&= \left(1 - \frac{\exp\left(-\frac{1}{\log\eta}\eta^{\frac{\alpha}{M-1}-1}\right)\exp\left(\eta^{-1}\right)(\log\eta)^{M-1}}{\eta^{\alpha}}\right)^K. \qquad \text{(B.24)}
\end{aligned}$$

Note that

$$\begin{aligned}
&K \log\left(1 - \frac{\exp\left(-\frac{1}{\log\eta}\eta^{\frac{\alpha}{M-1}-1}\right)\exp\left(\eta^{-1}\right)(\log\eta)^{M-1}}{\eta^{\alpha}}\right) \\
&= -\frac{K}{\eta^{\alpha}}(\log\eta)^{M-1}\exp\left(-\frac{1}{\log\eta}\eta^{\frac{\alpha}{M-1}-1}\right)\exp\left(\eta^{-1}\right) \\
&\qquad + O\left(\frac{K}{\eta^{2\alpha}}(\log\eta)^{2(M-1)}\exp\left(-\frac{2}{\log\eta}\eta^{\frac{\alpha}{M-1}-1}\right)\exp\left(2\eta^{-1}\right)\right) \xrightarrow{\eta\to\infty} -\infty, \qquad \text{(B.25)}
\end{aligned}$$

since, when $\eta \to \infty$, the first term in (B.25) goes to $-\infty$, while the second term goes to 0. (B.24) thus converges to 0 and the lower-bound probability is confirmed. The

proof of (B.21) follows similar arguments as the above, and is omitted for brevity. This completes the proof of Lemma 4.3.1.

B.6 Proof of Proposition 4.3.1

According to the main text, it is sufficient to show the DoF upper bound to be N_T as follows. Note that in a single-cell MISO-BC, the DPC yields the optimal sum-rate, denoted by R_{DPC}. Therefore, $d^*(\alpha) = \lim_{\rho\to\infty} \frac{R_{\mathrm{DPC}}}{\log_2 \rho}$. From [30, Theorem 1], we have

$$R_{\mathrm{DPC}} \leq N_T \mathbb{E}\left[\log_2\left[1 + \eta \max_{k\in\{1,\cdots,K\}} ||\boldsymbol{h}_k||^2\right]\right]. \tag{B.26}$$

Note that $\eta = P_T/(N_T\sigma^2)$ is the SNR per beam, and $||\boldsymbol{h}_k||^2$'s are i.i.d. chi-square random variables with $2N_T$ degrees of freedom, denoted by $\chi^2(2N_T)$. Thus, if we denote $R_k = \log_2(1+\eta||\boldsymbol{h}_k||^2)$, the CDF of $R = R_k$ is $F_R(r) = \frac{1}{\Gamma(N_T)}\gamma\left(N_T, \frac{2^r-1}{\eta}\right)$, where $\Gamma(\cdot)$ and $\gamma(\cdot,\cdot)$ are the gamma and the incomplete gamma function, respectively. The same reasoning as in the proof of Lemma 4.3.1 can be reused here to show that

$$\Pr\left\{\log_2\eta + \log_2\log\eta + \log_2(\alpha+1) \geq \max_{k\in\{1,\cdots,K\}} R_k\right\} \xrightarrow{\eta\to\infty} 1. \tag{B.27}$$

This completes the proof of Proposition 4.3.1.

Appendix C

Proofs of Chapter 5

C.1 Proof of Corollary 5.2.1

The interference-plus-noise covariance matrix $\boldsymbol{W}_k^{(c)}$ given in (5.2) can be written as

$$\boldsymbol{W}_k^{(c)} = \lim_{N\to\infty}\left(\frac{P_T}{M_c}\tilde{\boldsymbol{H}}_{k,-m}^{(c,c)}\Big(\tilde{\boldsymbol{H}}_{k,-m}^{(c,c)}\Big)^H + \sum_{l=1,l\neq c}^{C}\frac{P_T\gamma_{l,c}}{M_l}\tilde{\boldsymbol{H}}_k^{(l,c)}\Big(\tilde{\boldsymbol{H}}_k^{(l,c)}\Big)^H + \frac{\sigma^2}{N}\boldsymbol{H}_N\boldsymbol{H}_N^H\right), \tag{C.1}$$

where $\boldsymbol{H}_N \in \mathbb{C}^{N_R\times N}$ consists of i.i.d. random variables each distributed as $\sim \mathcal{CN}(0,1)$. To find the PDF of $\mathrm{SINR}_{k,m}^{(\mathrm{MMSE},c)}$ in (5.3), we apply Theorem 5.2.1 with $\boldsymbol{h} := \tilde{\boldsymbol{h}}_{k,m}^{(c,c)}$,

$$\boldsymbol{X} := \Big[\tilde{\boldsymbol{H}}_{k,-m}^{(c,c)}, \tilde{\boldsymbol{H}}_k^{(1,c)}, \cdots, \tilde{\boldsymbol{H}}_k^{(l,c)}, \cdots, \tilde{\boldsymbol{H}}_k^{(C,c)}, \boldsymbol{H}_N\Big], \tag{C.2}$$

and

$$\mathbf{\Psi} := diag\left(\underbrace{1,\cdots,1}_{M_c-1},\cdots,\underbrace{\frac{\mu_{l,c}}{\eta_c},\cdots,\frac{\mu_{l,c}}{\eta_c}}_{M_l},\cdots,\underbrace{\frac{\mu_{C,c}}{\eta_c},\cdots,\frac{\mu_{C,c}}{\eta_c}}_{M_C},\underbrace{\frac{1}{N\eta_c},\cdots,\frac{1}{N\eta_c}}_{N}\right). \tag{C.3}$$

The PDF of $S := \mathrm{SINR}_{k,m}^{(\mathrm{MMSE},c)}$ can thus be expressed as

$$F_S(s) = 1 - \lim_{N\to\infty} \frac{\left(\sum_{i=0}^{N_R-1}\theta_i s^i\right)}{\left(1+\frac{s}{N\eta_c}\right)^N (1+s)^{M_c-1}\prod_{l=1,l\neq c}^{\sum M_c-1}(1+\frac{\mu_{l,c}}{\eta_c}s)^{M_l}}, \tag{C.4}$$

where θ_i is the coefficient of s^i in the polynomial expansion of $\left(1+\frac{s}{N\eta_c}\right)^N (1+s)^{M_c-1}\prod_{l=1,l\neq c}^{\sum M_c-1}(1+\frac{\mu_{l,c}}{\eta_c}s)^{M_l}$.

Next, by letting $N\to\infty$, in the denominator in (C.4), the term $(1+\frac{s}{N\eta_c})^N$ converges to e^{s/η_c}, while the nominator converges to $\sum_{i=0}^{N_R-1}\zeta_i s^i$, where ζ_i's are defined in Corollary 5.2.1. We thus obtain (5.14). This completes the proof of Corollary 5.2.1.

C.2 Proof of Theorem 5.2.2

We first note that

$$\begin{aligned} f_S^{(c)}(s) &= \int_0^\infty f_{S|V}(s|v)f_V(v)dv \\ &= \int_{-\infty}^{\infty}\int_0^\infty \frac{s^{N_R-1}}{2\pi\Gamma(N_R)} \frac{(v+\frac{1}{\eta_c})^{N_R}e^{-(v+\frac{1}{\eta_c})s}e^{-j\omega v}}{(1-j\omega)^{M_c-1}\prod_{l=1,l\neq c}^{C}\left(1-j\frac{\mu_{l,c}}{\eta_c}\omega\right)^{M_l}}dvd\omega, \end{aligned} \tag{C.5}$$

where $j=\sqrt{-1}$.

Therefore,

$$F_S(s) = \int_{-\infty}^{\infty}\int_{0}^{\infty}\int_{0}^{s} \frac{(v+\frac{1}{\eta_c})^{N_R} e^{-j\omega v} x^{N_R-1} e^{-(v+\frac{1}{\eta_c})x}}{2\pi\Gamma(N_R)\left(1-j\omega\right)^{M_c-1}\prod\limits_{l=1,l\neq c}^{C}\left(1-j\frac{\mu_{l,c}}{\eta_c}\omega\right)^{M_l}} dx dv d\omega. \quad \text{(C.6)}$$

Now by using [20, (3.351.1)], we can write (C.6) as

$$F_S(s) = 1 - \sum_{k=0}^{N_R-1}\frac{e^{-s/\eta_c}s^k}{2\pi k!}\int_{-\infty}^{\infty}\int_{0}^{\infty}\frac{(v+\frac{1}{\eta_c})^k e^{-(s+j\omega)}}{\left(1-j\omega\right)^{M_c-1}\prod\limits_{l=1,l\neq c}^{C}\left(1-j\frac{\mu_{l,c}}{\eta_c}\omega\right)^{M_l}} dv d\omega \quad \text{(C.7)}$$

$$= 1 - \sum_{k=0}^{N_R-1}\sum_{m=0}^{k}\frac{e^{-s/\eta_c}s^k}{(k-m)!\eta_c^{k-m}}\times \underbrace{\times\frac{1}{2\pi}\int_{-\infty}^{\infty}\frac{d\omega}{(s+j\omega)^{m+1}\left(1-j\omega\right)^{M_c-1}\prod\limits_{l=1,l\neq c}^{C}\left(1-j\frac{\mu_{l,c}}{\eta_c}\omega\right)^{M_l}}}_{T_m(s)}, \quad \text{(C.8)}$$

where we have used the binomial expansion and the result in [20, (3.351.3)] to obtain (C.7). From (B.6)-(B.13), we see that $T_0(s)$ can be expressed as in (5.19). It is also easy to show that $T_m(s) = \frac{(-1)^m}{m!}\frac{d^m T_0(s)}{ds^m}$. Combining this result, (5.19), and (C.8), we obtain (5.18). This completes the proof of Theorem 5.2.2.

C.3 Proof of Lemma 5.3.1

C.3.1 RBF-MMSE

We first investigate the DoF with RBF-MMSE. Consider the following two cases.

C.3.1.1 Case 1, $N_R \leq M-1$

Denote $R_{k,m}^{(\mathrm{MMSE})} := \log_2\left(1+\mathrm{SINR}_{k,m}^{(\mathrm{MMSE})}\right)$. We first show that the following two probabilities are true

$$\Pr\left\{\frac{\alpha}{M-N_R}\log_2\eta+\log_2\log\eta \geq \max_{k\in\{1,\cdots,K\}} R_{k,1}^{(\mathrm{MMSE})} \geq \frac{\alpha}{M-N_R}\log_2\eta-\log_2\log\eta\right\}$$
$$\xrightarrow{\eta\to\infty} 1, \text{ if } 0<\alpha\leq M-N_R, \tag{C.9}$$

$$\Pr\left\{\log_2\eta+\log_2\log\eta+\log_2\alpha \geq \max_{k\in\{1,\cdots,K\}} R_{k,1}^{(\mathrm{MMSE})} \geq \log_2\eta+\log_2\log\eta+\log_2\beta_1\right\}$$
$$\xrightarrow{\eta\to\infty} 1, \text{ if } \alpha>M-N_R, \tag{C.10}$$

where $\beta_1=\frac{\alpha-M+N_R}{2}$; hence, $\alpha>\beta_1>0$ when $\alpha>M-N_R$.

From Corollary 5.2.1, the CDF of the single-cell RBF-MMSE $S := \mathrm{SINR}_{k,1}^{(\mathrm{MMSE})}$ can be expressed as

$$\begin{aligned}F_S(s) &= 1-e^{-s/\eta}\frac{\sum_{i=1}^{N_R-1}\frac{(M-1)!}{i!(M-1-i)!}s^i}{(1+s)^{M-1}}\\ &= 1-e^{-s/\eta}\left(\Theta\left(\frac{1}{(s+1)^{M-N_R}}\right)+O\left(\frac{1}{(s+1)^{M-N_R+1}}\right)\right),\end{aligned} \tag{C.11}$$

as s and/or $\eta\to\infty$. Therefore, the CDF of $Y_k := R_{k,1}^{(\mathrm{MMSE})}$ has the following asymptotic form

$$F_{Y_k}(y) = 1-e^{-(2^y-1)/\eta}\left(\Theta\left(\frac{1}{2^{(M-N_R)y}}\right)+O\left(\frac{1}{2^{(M-N_R+1)y}}\right)\right),$$

as y and/or $\eta \to \infty$. In (C.9), the upper-bound probability can thus be given as

$$\begin{aligned}
&\Pr\left\{\frac{\alpha}{M-N_R}\log_2\eta+\log_2\log\eta \geq \max_{k\in\{1,\cdots,K\}} Y_k\right\} \\
&= \left[F_{Y_k}\left(\frac{\alpha}{M-N_R}\log_2\eta+\log_2\log\eta\right)\right]^K \\
&= \Bigg(1-\exp\left(-\eta^{\frac{\alpha}{M-N_R}-1}\log\eta+\frac{1}{\eta}\right)\times \\
&\qquad \times\left(\Theta\left(\frac{1}{\eta^\alpha\left(\log\eta\right)^{M-N_R}}\right)+O\left(\frac{1}{\left(\eta^{\frac{\alpha}{M-N_R}}\log\eta\right)^{M-N_R+1}}\right)\right)\Bigg)^K, \quad \text{(C.12)}
\end{aligned}$$

as $\eta \to \infty$. Note that when x is small, we have the following asymptotic relation $\log(1-x) = -x + O(x^2)$. We thus have

$$\begin{aligned}
&K\log\Bigg(1-\exp\left(-\eta^{\frac{\alpha}{M-N_R}-1}\log\eta+\frac{1}{\eta}\right)\Bigg(\Theta\left(\frac{1}{\eta^\alpha\left(\log\eta\right)^{M-N_R}}\right) \\
&\qquad\qquad +O\left(\frac{1}{\left(\eta^{\frac{\alpha}{M-N_R}}\log\eta\right)^{M-N_R+1}}\right)\Bigg)\Bigg) \\
&= -\Theta\left(\frac{K}{\eta^\alpha(\log\eta)^{M-N_R}}\right)\exp\left(-\eta^{\frac{\alpha}{M-N_R}-1}\log\eta+\frac{1}{\eta}\right) \\
&\quad +O\left(\frac{K}{\left(\eta^{\frac{\alpha}{M-N_R}}\log\eta\right)^{M-N_R+1}}\right)\exp\left(-\eta^{\frac{\alpha}{M-N_R}-1}\log\eta+\frac{1}{\eta}\right) \\
&\quad +O\Bigg(\Theta\left(\frac{K}{\eta^{2\alpha}(\log\eta)^{2n}}\right)\exp\left(-2\eta^{\frac{\alpha}{n}-1}\log\eta+\frac{2}{\eta}\right) \\
&\quad +O\left(\frac{K}{\left(\eta^{\frac{\alpha}{n}}\log\eta\right)^{2(n+1)}}\right)\exp\left(-2\eta^{\frac{\alpha}{n}-1}\log\eta+\frac{2}{\eta}\right)\Bigg) \\
&\xrightarrow{\eta\to\infty} 0, \quad \text{(C.13)}
\end{aligned}$$

since $K = \Theta(\eta^\alpha)$, and $0 < \alpha \leq M - N_R$. As a consequence, the upper-bound

probability converges to 1 when $\eta \to \infty$. To prove the convergence to 1 of the lower-bound probability in (C.12), we observe that

$$\begin{aligned}
&\Pr\left\{\frac{\alpha}{M-N_R}\log_2\eta - \log_2\log\eta \geq \max_{k\in\{1,\cdots,K\}} Y_k\right\} \\
&= \left[F_{Y_k}\left(\frac{\alpha}{M-N_R}\log_2\eta - \log_2\log\eta\right)\right]^K \\
&= \left(1-\exp\left(-\eta^{\frac{\alpha}{M-N_R}-1}\frac{1}{\log\eta}+\frac{1}{\eta}\right)\times\right. \\
&\qquad\qquad \left.\times\left(\Theta\left(\frac{(\log\eta)^{M-N_R}}{\eta^\alpha}\right)+O\left(\frac{(\log\eta)^{M-N_R+1}}{\eta^{\frac{\alpha(M-N_R+1)}{M-N_R}}}\right)\right)\right)^K. \qquad \text{(C.14)}
\end{aligned}$$

Note that

$$\begin{aligned}
&K\log\left(1-\exp\left(-\eta^{\frac{\alpha}{M-N_R}-1}\frac{1}{\log\eta}+\frac{1}{\eta}\right)\times\right. \\
&\qquad\qquad \left.\times\left(\Theta\left(\frac{(\log\eta)^{M-N_R}}{\eta^\alpha}\right)+O\left(\frac{(\log\eta)^{M-N_R+1}}{\eta^{\frac{\alpha(M-N_R+1)}{M-N_R}}}\right)\right)\right) \\
&= -\Theta\left(\frac{K(\log\eta)^{M-N_R}}{\eta^\alpha}\right)\exp\left(-\eta^{\frac{\alpha}{M-N_R}-1}\frac{1}{\log\eta}+\frac{1}{\eta}\right) \\
&\quad + O\left(\frac{K\left(\log\eta\right)^{M-N_R+1}}{\eta^{\frac{\alpha(M-N_R+1)}{M-N_R}}}\right)\exp\left(-\eta^{\frac{\alpha}{M-N_R}-1}\frac{1}{\log\eta}+\frac{1}{\eta}\right) \\
&\quad + O\left(\Theta\left(\frac{K(\log\eta)^{2(M-N_R)}}{\eta^{2\alpha}}\right)\exp\left(-2\eta^{\frac{\alpha}{M-N_R}-1}\frac{1}{\log\eta}+\frac{2}{\eta}\right)\right. \\
&\quad \left. + O\left(\frac{K\left(\log\eta\right)^{2(M-N_R+1)}}{\eta^{\frac{2\alpha(M-N_R+1)}{M-N_R}}}\right)\exp\left(-2\eta^{\frac{\alpha}{M-N_R}-1}\frac{1}{\log\eta}+\frac{2}{\eta}\right)\right) \\
&\xrightarrow{\eta\to\infty} -\infty, \qquad \text{(C.15)}
\end{aligned}$$

since, when $\eta \to \infty$, the first term goes to $-\infty$, while the second term goes to 0. (C.14) thus converges to 0 and the lower-bound probability is confirmed. We omit the proof of (C.10) since it follows similar arguments. With (C.9) and (C.10), the results in (5.22a) and (5.22b) follow immediately.

C.3.1.2 Case 2, $N_R \geq M$

Suppose that M receive antennas are used. Then the DoF is M from Case 1 above. Therefore, $d_{\text{RBF-MMSE}}(\alpha, \boldsymbol{m}) \geq M$. Also note that in a single-cell MIMO RBF with M transmit beams, the BS can be considered as having M transmit antennas only. Proposition 5.3.1 thus leads to $d_{\text{RBF-MMSE}}(\alpha, \boldsymbol{m}) \leq M$. We thus conclude that $d_{\text{RBF-MMSE}}(\alpha, \boldsymbol{m}) = M$.

C.3.2 RBF-MF/AS

To obtain the DoF of RBF-MF/AS, we first show that

$$\Pr\left\{ \frac{\alpha}{M-1}\log_2\eta + \log_2\log\eta \geq \max_{k\in\{1,\cdots,K\}} R_{k,1}^{(\text{MF/AS})} \geq \frac{\alpha}{M-1}\log_2\eta - \log_2\log\eta \right\} \xrightarrow{\eta\to\infty} 1, \text{ if } 0 < \alpha \leq M-1, \tag{C.16}$$

$$\Pr\left\{ \log_2\eta + \log_2\log\eta + \log_2\alpha \geq \max_{k\in\{1,\cdots,K\}} R_{k,1}^{(\text{MF/AS})} \geq \log_2\eta + \log_2\log\eta + \log_2\beta \right\} \xrightarrow{\eta\to\infty} 1, \text{ if } \alpha > M-1, \tag{C.17}$$

where $\beta_2 = \frac{\alpha-M+1}{2}$; hence, $\alpha > \beta_2 > 0$ when $\alpha > M-1$. From Theorem 5.2.2, the CDF of the single-cell RBF-MF $S := \text{SINR}_{k,m}^{(\text{MF})}$ is

$$F_S(s) = 1 - e^{-s/\eta} \sum_{k=0}^{N_R-1} \sum_{m=0}^{k} \frac{s^k}{(k-m)!m!\eta^{k-m}} \frac{\frac{(M+m-2)!}{(M-2)!}}{(s+1)^{M+m-1}}. \tag{C.18}$$

Denote $Z_k := R_{k,1}^{(\text{MF})} := \log_2\left(1 + \text{SINR}_{k,1}^{(\text{MF})}\right)$. The CDF of Z_k is thus

$$F_{Z_k}(z) = 1 - e^{-z/\eta} \sum_{k=0}^{N_R-1} \sum_{m=0}^{k} \frac{(M+m-2)!}{(k-m)!m!(M-2)!} \frac{(2^z-1)^k}{\eta^{k-m}2^{(M+m-1)z}}. \tag{C.19}$$

In (C.16), the upper-bound probability can thus be given as

$$\begin{aligned}
&\Pr\left\{\frac{\alpha}{M-1}\log_2\eta+\log_2\log\eta\geq\max_{k\in\{1,\cdots,K\}}Z_k\right\}=\left[F_{Z_k}\left(\frac{\alpha}{M-1}\log_2\eta+\log_2\log\eta\right)\right]^K\\
&=\left(1-\exp\left(-\eta^{\frac{\alpha}{M-1}-1}\log\eta+\frac{1}{\eta}\right)\times\right.\\
&\qquad\left.\times\left(\sum_{k=0}^{N_R-1}\sum_{m=0}^{k}\frac{(M+m-2)!}{(k-m)!m!(M-2)!}\frac{(\eta^{\frac{\alpha}{M-1}}\log\eta-1)^k}{\eta^{k-m}\eta^{\frac{\alpha(M+m-1)}{M-1}}(\log\eta)^{(M+m-1)}}\right)\right)^K\\
&=\left(1-\exp\left(-\eta^{\frac{\alpha}{M-1}-1}\log\eta+\frac{1}{\eta}\right)\left(\Theta\left(\frac{1}{\eta^\alpha\left(\log\eta\right)^{M-1}}\right)+O\left(\frac{1}{\eta^{\frac{\alpha M}{M-1}}}\right)\right)\right)^K,
\end{aligned}\tag{C.20}$$

as $\eta\to\infty$, which is quite similar to (C.12) with $N_R=1$ in this case. Now following the same reasoning as in (C.13), we can prove that the upper-bound probability (C.20) $\to 1$ as $\eta\to\infty$. To prove the convergence of the lower-bound, we note that

$$\begin{aligned}
&\Pr\left\{\frac{\alpha}{M-1}\log_2\eta-\log_2\log\eta\geq\max_{k\in\{1,\cdots,K\}}Z_k\right\}=\left[F_{Z_k}\left(\frac{\alpha}{M-1}\log_2\eta-\log_2\log\eta\right)\right]^K\\
&=\left(1-\exp\left(-\eta^{\frac{\alpha}{M-1}-1}\frac{1}{\log\eta}+\frac{1}{\eta}\right)\times\right.\\
&\qquad\left.\times\left(\sum_{k=0}^{N_R-1}\sum_{m=0}^{k}\frac{(M+m-2)!}{(k-m)!m!(M-2)!}\frac{(\eta^{\frac{\alpha}{M-1}}\frac{1}{\log\eta}-1)^k(\log\eta)^{M+m-1}}{\eta^{k-m}\eta^{\frac{\alpha(M+m-1)}{M-1}}}\right)\right)^K\\
&=\left(1-\exp\left(-\eta^{\frac{\alpha}{M-1}-1}\frac{1}{\log\eta}+\frac{1}{\eta}\right)\left(\Theta\left(\frac{(\log\eta)^{M-1}}{\eta^\alpha}\right)+O\left(\frac{(\log\eta)^{M-1}}{\eta^{\frac{\alpha M}{M-1}}}\right)\right)\right)^K,
\end{aligned}\tag{C.21}$$

which is quite similar to (C.14). Now following the same reasoning as in (C.15), we can prove that (C.21) $\to 0$ as $\eta\to\infty$. Thus we confirm (C.16). The proof of (C.17) follows similarly and is thus omitted.

On the other hand, for the case of RBF-AS, note that RBF-AS scheme consists of two selection processes: antenna selection at each MS with N_R antennas and user

selection at the BS with K users. The rate performance of RBF-AS is therefore equivalent to that of MISO RBF with $N_R K$ single-antenna users in the cell. Thus, we obtain (C.16) and (C.17) for the case of RBF-AS. With (C.16) and (C.17), the results in (5.23a) and (5.23b) follow immediately.

This thus completes the proof of Lemma 5.3.1.

C.4 Proof of Proposition 5.3.1

In a single-cell MIMO-BC, DPC yields the maximum sum-rate, denoted by R_{DPC}. Therefore, the single-cell DoF can be bounded as $d \leq \lim\limits_{\rho\to\infty} \dfrac{R_{\text{DPC}}}{\log_2 \rho}$. From [30, Theorem 1], we have

$$\begin{aligned} R_{\text{DPC}} &\leq N_T \mathbb{E}\left[\log_2\left[1+\eta \max_{k\in\{1,\cdots,K\}} ||\boldsymbol{H}_k||_2^2\right]\right] \\ &\leq N_T \mathbb{E}\left[\log_2\left[1+\eta \max_{k\in\{1,\cdots,K\}} \boldsymbol{Tr}\left(\boldsymbol{H}_k^H \boldsymbol{H}_k\right)\right]\right]. \end{aligned} \tag{C.22}$$

Denote $R_k := \log_2\left[1+\eta \boldsymbol{Tr}\left(\boldsymbol{H}_k^H \boldsymbol{H}_k\right)\right]$. Note that $\boldsymbol{Tr}\left(\boldsymbol{H}_k^H \boldsymbol{H}_k\right)$ is distributed as $\chi^2(2N_T N_R)$. Similarly to (C.10) and (C.17), we can show that

$$\Pr\left\{\log_2\eta + \log_2\log\eta + \log_2(\alpha+1) \geq \max_{k\in\{1,\cdots,K\}} R_k\right\} \xrightarrow{\eta\to\infty} 1. \tag{C.23}$$

Combining (C.22) and (C.23), we obtain $d \leq N_T$, where the equality is achieved by, e.g., the DPC scheme. The proof of Proposition 5.3.1 is thus completed.